SYNTHESIS AND APPLICATIONS OF NANOPARTICLES IN BIOSENSING SYSTEMS

Sergio Marín Mancebo

Nanobioelectronics and Biosensors Group, Catalan Institute of Nanotecnology
Bellaterra, Barcelona, Spain

&

Grup de Sensors i Biosensors, Department de Química, Universitat Autònoma de Barcelona.

April 2009

The present thesis titled “Synthesis and applications of nanoparticles in biosensing systems” has been performed at the laboratories of Nanobioelectronics & Biosensors Group of Catalan Institute of Nanotechnology and Group of Sensors and Biosensors at Chemistry Department of Autonomous University of Barcelona under the direction of Arben Merkoçi Hyka, ICREA Professor and Salvador Alegret Sanromà, UAB Professor.

Arben Merkoçi Hyka

Salvador Alegret Sanromà

Bellaterra, April, 2009

This thesis is carried with the support of the following projects:

- "Desarrollo de nuevas bionanoestructuras inteligentes para biosensores moleculares de interés medioambiente, Fundación Ramón Areces, XIII Concurso nacional para la adjudicación de ayudas a la investigación científica y técnica". (Project reference: Bionanosensores).

- "Los Quantum Dots modificados biologicamente como bionanoestructuras inteligentes para el desarrollo de nuevos sistemas de detección incluyendo su integracion en un lab-on-a-chip". Grant by Ministerio de Ciencia e Innovación, Spain (Project reference: MEC, MAT2004-05164)

- "Development of novel nanomaterial based targeting approaches as emerging universal platforms with interest for biosensors". Grant by Ministerio de Ciencia e Innovación, Spain, (Project reference: MAT2008-03079).

- "Nanoparticulas modificadas para analisis proteomico rapido basado en inmunoensayos con tecnologias de codificacion electroquimica multiplex y lab-on-a-chip" Grant by Ministerio de Ciencia e Innovación, Spain, (Project reference: MEC, MAT2005-03553/)

- "Nanotechnologies in biomedicine". Grant by Ministerio de Ciencia e Innovación, Spain, (Project reference: CSD2006-00012 "NANOBIOMED", Consolider-Ingenio 2010).

- "Water Risk Management In Europe" (WARMER). EU grant, (Project reference: FP6-034472-2005-IST-5).

A la memoria de mi abuelo (el que siempre me ayudo, planteándome problemas matemáticos (nunca te olvidare))

Por mis compañeros de laboratorio que sin su ayuda ni colaboración esta tesis no se podría cumplir
Anna Puig, Gemma Aragay, Maria Teresa Castañeda, Briza Pérez, Adriano Ambrosi, Alfredo de la Escosura, Marisa Maltez, Maria Guix, Gina Alarcón

También si la inestimable ayuda de colaboradores
Martin Pumera, Ülkü Kirgöz, Luiz Humberto, Patrizia Moretti, Humberto Takeda, Melike Sahin, Claudio Parolo, Federico Airó

Y colaboraciones con otros grupos como son el caso de química inorgánica de la UAB: Josep Ros, Joan Sola, Ramón Yañez, Fraser Douglas y Leo Pérez. Otro colaboración importante se realizó en el grupo de péptidos y proteínas dirigido por Ernest Giralt, con la gran ayuda de Silvía Pujals.

A mis amigos de la universidad de los cuales he recibido un gran apoyo y amistad
Xavi Bagan, Julen de Mendizábal, Alessandra Bonani, Lisi Franch, Kepa Koldo, Xavi Pérez, Xavi Palmer, Adu Njie, Francisco Benarre, Leo Pérez, Sandra Pérez, Silvia Gómez, Susana, Raquel Enrech, entre otros
(en especial a los que me llevaron a realizar la tesis : Manuel Gutiérrez Capitán, Anabel Lermo Soria)

Al Grupo de Sensors i biosensors
En especial a Salvador Alegret por su colaboración y ayuda

Y por último, y más importante mi mayor agradecimiento a Arben Merkoçi por su dirección de tesis, por tener tanta paciencia, por ser tan buen maestro y persona, por su gran visión de la investigación y persistencia

Abstract

Abstract

The principal focus of this thesis is the synthesis of nanoparticles with electrochemical properties and their applications in affinity biosensors. The thesis is structured in nine chapters.

Chapter 1 contains a general introduction about nanotechnology. The two strategies, top-down and bottom-up, are briefly introduced followed by general description of nanoparticles, their properties, synthesis procedures, characterizations techniques and biological modifications. A general overview on the applications of nanoparticles in biosensors is also given in this part. General concepts related to affinity biosensors such as immunosensors, genosensors and cells sensors are also mentioned.

Chapter 2 describes the objectives of the thesis ranging from synthesis of nanoparticles to their applications in biosensing.

Chapter 3 is related to the synthesis of nanoparticles. Different methods of synthesis of electroactive quantum dots (QDs) are presented. In the first part They are based on two general ways of controlling the formation and growth of the nanoparticles: (a) physical restriction of the volume available for the growth of the individual nanoparticles by using templates such as reverse micelles; (b) arrested precipitation that depends on exhaustion of one of the reactants. The water dispersed QDs are characterized by optical or electrochemical techniques so as to evaluate the quality of the prepared QDs. A novel direct electrochemical stripping detection protocol that involves the use of a bismuth modified graphite epoxy composite electrode is also developed and applied to quantify the CdS QDs. The electrochemical study revealed a linear dependency of the stripping current upon the concentration of CdS QDs with a detection limit of around 10^{15} CdS QDs cm^{-3} showing that the obtained QDs are of great interest for future applications in electrochemical genosensors. The second part of this chapter is related to the synthesis of silver and gold nanoparticles (AgNP and AuNP) along with the corresponding core shell nanoparticles (Au–Ag and Ag–Au). The morphologies of the obtained nanoparticles are controlled by the order of reactants addition. The obtained NPs, with sizes in the range 3–40 nm, are characterized by transmission electronic microscopy (TEM) and UV–Vis spectroscopy, so as to evaluate their qualities. Moreover, a direct electrochemical detection protocol based on cyclic voltammetry in water solution and using a glassy carbon electrode is also applied to characterize the

prepared NPs. Although not applied in this thesis the developed Au and Ag NPs and the related electroanalytical method seems to be interesting for future sensing and biosensing applications including DNA sensors and immunosensors.

Chapter 4 describes a simple method for the detection of water soluble cadmium sulfide quantum dots(CdS QDs) modified with glutathione based on screen-printed electrodes and a handheld potentiostatic device. The detection method is based on the stripping of electrochemically reduced cadmium at pH 7.0 by using square wave voltammetry. Various parameters that affect the sensitivity of the method are optimized. QD suspension volumes of 20 μl and a number of around 2×10^{11} CdS quantum dots have been able to be detected. The proposed method is of special interest for bioanalytical assays, where CdS quantum dots can be used as electrochemical tracers (as seen at chapter 5).

Chapter 5 describes an electrochemical detection of a CdS quantum dots–DNA complex connected to paramagnetic microbeads (MB) without the need for chemical dissolving. The method is based on dropping 20 μl of CdS QD–DNA–MB suspension on the surface of a screen-printed electrode. It is followed by magnetic collection on the surface of the working electrode and electrochemical detection using square-wave voltammetry (SWV), giving a well-shaped and sensitive analytical signal. A cystic-fibrosis-related DNA sequence is sandwiched between the two DNA probes. One DNA probe is linked via biotin–streptavidin bonding with MB and the other one via thiol groups with the CdS QD used as tags. Nonspecific signals of DNA were minimized using a blocking agent and the results obtained are successfully employed in a model DNA sensor with an interest in future applications in the clinical field. The developed nanoparticle biosensing system may offer numerous opportunities in other fields where fast, low cost and efficient detection of small volume samples is required.

Chapter 6 describes the use of square wave voltammetry to monitor the cellular uptake, in HeLa cells, of Quantum Dots (QD) decorated with Sweet Arrow Peptide (SAP). A SAP derivative containing an additional *N*-terminal cysteine residue (C-SAP) is synthesized using the solid phase method and conjugated to QDs. The obtained results show that QDs-SAP either interacts with the extracellular cell membrane matrix or translocates the bilayer. The first situation, membrane adsorption, is probably a transient state before cellular uptake. Both confocal microscopy and SWV results support the detection of this cellular internalization process. The developed electrochemical interrogation technique can provide valuable insights into the study of peptide-mediated delivery as well as the design and

development of nanoparticle probes for intracellular imaging, diagnostic and therapeutic applications. In addition the described electrochemical interrogation is of low cost, is friendly-use and offers future interest for diagnosis including cell analysis.

Chapter 7 summarizes the general conclusions of the PhD thesis followed by some proposals for future studies in the field of the application of quantum dots in electrochemical biosensing approaches. **Chapter 8** and **9** include the publications that resulted from this PhD thesis research.

Chapter 8 Publications

I. Merkoçi A., Aldavert M., Marín S., Alegret S. *"New materials for electrochemical sensing V: Nanoparticles for DNA labeling"* **2005** *Trends in Analytical Chemistry* 24, 341-349.

II. Merkoçi A, Marín S., Castañeda M. T., Pumera M., Ros J., Alegret S. *"Crystal and electrochemical properties of water dispersed CdS nanocrystals obtained via reverse micelles and arrested precipitation"* **2006** *Nanotechnology* 17, 2553-2559.

III. Merkoçi A., Marcolino-Junior L. H., Marín S., Fatibello-Filho O., Alegret S. *"Detection of cadmium sulphide nanoparticles by using screen-printed electrodes and a handheld device"* **2007** *Nanotechnology* 18, 035502 (1-6).

IV. Douglas F., Yañez R., Ros J., Marín S., de la Escosura-Muñiz A., Alegret S., Merkoçi A. *"Silver, gold and the corresponding core shell nanoparticles: synthesis and characterization"* **2008** *J. Nanopart. Res.* 10, 9374-9384.

V. Marín S., Merkoçi A. *"Direct electrochemical stripping detection of cystic fibrosis related DNA linked through cadmium sulphide quantum dots"* **2009** *Nanotechnology* 20, 055101(1-6).

Chapter 9 Annex

I. Marín S., Pujals S., Giralt E., Merkoçi A. *"Electrochemical interrogation of cellular uptake of quantum dots decorated with a proline-rich cell penetrating peptide"* **2009,** Prepared manuscript (sent for publication).

Abbreviations

Abbreviations

A	Auxiliary electrode
AB	Antibody
AFM	Atomic Force Microscopy
AG	Antigen
AOT	Sodium dioctyl sulfosuccinate
BSA	Bovine serum albumin
C	Counter electrode
CF-A	Cystic fibrosis capture DNA
CF-B	Cystic fibrosis signaling DNA
CF-MX1	Cystic fibrosis one base mismatch
CF-MX3	Cystic fibrosis three base mismatch
CF-NC	Cystic fibrosis non complementary
CF-T	Cystic fibrosis target DNA
CLSM	Confocal laser scanning microscopy
CNT	Carbon nanotube
CPP	Cell-penetrating peptide
CV	Cyclic voltammetry
DCM	Dichloromethane
DIEA	N,N-diisopropylethylamine
DL	Detection limit
DMF	Dimethylformamide
DPASV	Differential Pulse Anodic Stripping Voltammetry
DPV	Differential Pulse Voltammetry
EDTA	Ethylenediaminetetraacetic acid
EIS	Electrochemical impedance spectroscopy
FCS	Fetal calf serum
FT	Fourier Transform
GECE	Graphite Epoxy Composite Electrode
HMSDT	Hexamethyldisilathiane
HOAt	1-hydroxy-7-azabenzotriazole
HQ	Hydroquinone
HRTEM	High Resolution Transmission Electron Microscopy
IUPAC	International Union of Pure and Applied Chemistry
LEDs	Light-emitting devices

MB	Magnetic beads
MWCNT	Multiwall carbon nanotubes
NCs	Nanocrystals
NP	Nanoparticle
PBS	Phosphate buffered saline
PCR	Polymerase chain reaction
PE	Polyethylene
PEG	Poly (ethylene glycol)
PSA	Potentiometric stripping analysis
PyAOP	7-azabenzotriazol-1-yloxytris(pyrrolidino)phosphonium hexafluorophosphate
PyBOP	benzotriazol-1-yloxytris(pyrrolidino)phosphonium hexafluorophosphate
QDs	Quantum Dots
R	Reference electrode
R_{et}	electron-transfer resistance
RSD	Relative standard deviation
S	Surfactant
SAMs	Self-assembled monolayers
SAP	Sweet arrow peptide
SFM	Scanning force microscopy
SPE	Screen-printed electrode
SWCNT	single wall carbon nanotube
SWV	Square wave voltammetry
TBTU	2-(1Hbenzotriazol-1-yl)-1,1,3,3-tetramethyluronium tetrafluoroborate
TEM	Transmission Electron Microscopy
TFA	Trifluoroacetic acid
THF	Tetrahydrofuran
TIS	Triisopropylsilane
TOP	Trioctylphosphine
TOPO	Trioctylphosphine oxide
TMAH	Tetramethylammoniumhydroxide
TRITC-WGA	Tetramethylrhodamine isothiocyanate
TT	Buffer: 250 mM Tris-HCl, pH 8.0; and 0.1% Tween 20
TTL	Buffer 100 mM Tris-HCl, pH 8.0; 0.1 % Tween 20; and 1 M LiCl
TTE	Buffer: 250 mM Tris-HCl, pH 8.0; 0.1% Tween 20; and 20 mM Na_2EDTA
W	Working electrode
XRD	X ray diffraction

Chapter 1

General Introduction

Chapter 1 General Introduction

1.1 Nanotechnology

We broadly define "nanotechnology" as the creation of objects or surfaces whose unique functions are a direct result of their nanoscale dimensions and/or organization. These unique properties may be mechanical, electrical, or photochemical, and are not seen in the bulk materials. "Nanoscale" generally refers to objects 1–100 nm in one or more dimensions. At its lower limit, this definition intentionally excludes individual molecules, which actually define the lower end of nanotechnology— i.e. nano-derived features are as much a function of larger bulk materials approaching the molecular scale as they are a selective change in molecules' properties as they aggregate[1].

Nanofabrication methods can be divided roughly into two groups: top down and bottom up methods. Top down methods start with patterns made on a large scale and reduce its lateral dimensions before forming nanostructures. On the other hand, bottom up methods begin with atoms or molecules to build up nanostructures, in some cases through smart use of self organization. (Figure 1.1)

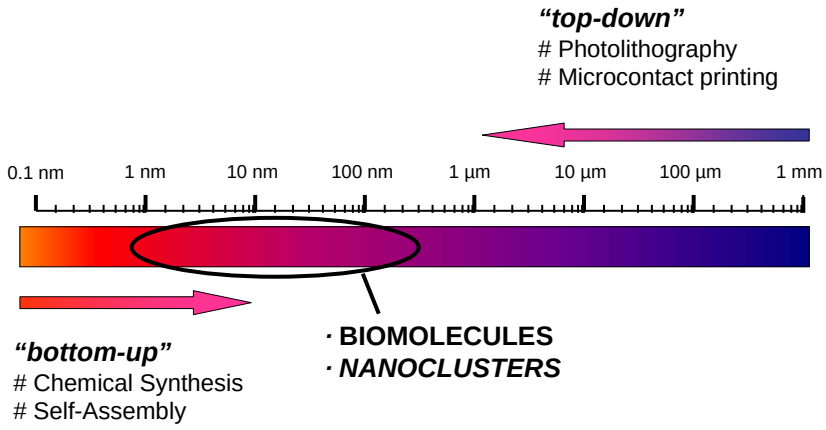

Figure 1.1 A gap currently exists in the engineering of small-scale devices. Whereas conventional top-down processes hardly allow the production of the smaller than about 200-100 nm, the limits of regular bottom-up processes are in the range of about 2-5 nm. As a result of their own dimension, two different types of compounds appear to be suited for addressing that gap: 1) biomolecular components, such as proteins and nucleic acids, and 2) colloidal nanoparticles comprised of metal and semiconductor materials.

1.1.1 Top down approaches

The top down approach has its foundation for example in lithographic techniques, in which a bulk material is selectively degraded to produce smaller, often patterned, features. For example, in the case of microlithography, light is shone through a mask to selectively etch either a positive or a negative pattern into a surface, yielding the desired microscopic topography. Size reductions to nanolithography are driven in large part by the computer industry, responding to the demand for smaller resistors and stronger computing power. To reach feature sizes <100 nm, researchers rely on shorter wavelengths of light, or even e-beam lithographic techniques. Top down processing can also be generated through selective chemical etching, although this relies much more on the initial properties of the bulk material.

1.1.2 Bottom up approaches

In bottom up methods, the atoms and molecules are assembled into the smallest nanostructures (dimensions of typically 2 to 10 nm) by carefully controlled chemical reactions, which make this technique cheaper as compared to the lithographical methods.

Self-assembly of atoms and molecules into nanostructures can be classified as a bottom up method. In nature selfassembly is often used to make complex structures. At present, the mastery of self-assembly is limited to relatively simple systems. To achieve complex systems hierarchical selfassembly can assist, where the products of one self-assembly step is a base for the next one. The formation of self-assembled monolayers (SAMs), that are produced when a substance spontaneously forms a molecular monolayer on a surface, could be successfully combined with standard lithographical methods to achieve large-scale and better controlled structures.

In one type of bottom up synthesis, individual molecules are triggered to self-assemble into larger objects with nanoscale dimension. The formation of micelles from individual charged lipids is a classic example of this method. In such systems, aggregate shape and size are pre-programmed through the specific features of the component molecules, often through the inclusion of selectively compatible and incompatible components. When we deliberately create molecules with such opposing segments (e.g.

hydrophilic and hydrophobic; rigid and flexible; directional hydrogen-bonding or π–π stacking; etc.), multiple molecules are forced to reduce their entropic/enthalpic balance through aggregation. Substantial advances have been made in this field of "supramolecular self-assembly" over the past 30 years, and researchers have a continual eye on advances in understanding nature's own methods for assembling proteins, nucleic acids, and other biomolecules.

Bottom up methods are also used, for instance, for the fabrication of carbon nanotubes (CNT) and nanoparticles. CNT are graphene cylindrical tubes of a few nanometers to some hundred nanometers in diameter. They can be produced by evaporation of solid carbon in an arc discharge, laser ablation, catalytic decomposition of fullerenes etc[2]. They can be used for studying the physics in one-dimensional solids as well as applied in various nanoscale devices and can be self assembled into hierarchical structures with controlled nanotube orientation[3]. Carbon nanotubes (CNTs) combine in a unique way high electrical conductivity, high chemical stability and extremely high mechanical strength. These special properties of both single-wall (SW) and multi-wall (MW) CNTs have attracted the interest of many researchers in the field of electrochemical sensors. CNTs have been integrated into the electrochemical systems[4 - 7]. As regards to the nanoparticles are described in the following sections.

1.2 Nanoparticles

Nanocrystals are crystalline clusters of a few hundred to a few thousand atoms with sizes of a few nanometres. Although more complex than individual atoms, their properties are different from bulk crystals. Due to their small size, much of their chemical and physical properties are dominated by their surfaces and not by their bulk volume[8]. Nanocrystals can be synthesized from metallic materials such as gold[9,10], silver[11,12] or cobalt[13,14], from semiconductor materials such as cadmium sulfide[15,16], cadmium selenide[17,18], cadmium telluride[19,20], gallium arsenide[21] or indium phosphide[22,23], and from insulators such as iron oxide[24,25] or titanium oxide[26].

Three properties are important for the quality of colloidal nanocrystals. Firstly, nanocrystals obviously should be crystalline and thus preferentially consist of only one domain. Secondly, their size distribution should be as narrow as possible and the third part,

there should be a unique, uniform shape to nanocrystals in a particular sample. Colloidal nanocrystals are dispersed in a solvent and should be stabilized in a way that prevents agglomeration. Besides spherical nanocrystals, more complex geometries such as rods[27,28], prisms[29] and tetrapods[30] can be synthesized in a controlled way.

1.2.1 Quantum dots

Quantum dots, also known as semiconductor particles, are crystalline clusters of nanometers[31]. One of the most important fields of their application is their use as labels in imaging as well as biosensing. Compared to existing labels, QDs are more stable and cheaper. They allow more flexibility, faster binding kinetics (similar to those in a homogeneous solution), high sensitivity and high reaction rates for many types of multiplexed assays, ranging from immunoassays to DNA analysis. A comparison of the size range of QD nanocrystals, that have been solubilized and conjugated using affinity molecules, with other species can be seen in figure 1.2.

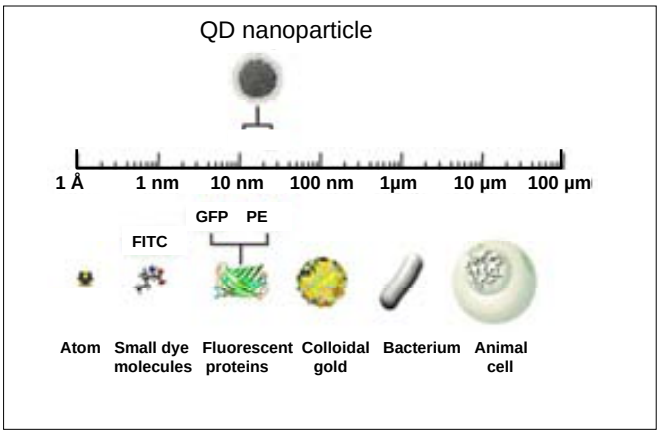

Figure 1.2 The size of a quantum dot (QD) compared to that of other materials. QD nanoparticle refers to quantum dots that have been solubilized and conjugated to affinity molecules. GFP, green fluorescent protein; PE, phycoerythrin; FITC, fluoresceineisothiocyanate.

QDs are emerging as a new class of fluorescent labels for molecular, cellular, and *in vivo* imaging applications, due to their special optical properties[32,33] such as a narrow and size-tuneable emission spectra[34], broad absorption profiles, superior photostability and

excellent resistance to chemical degradation or photodegradation compared to fluorescent dyes.

QDs are also interesting for electrochemical properties. QDs can be detected electrochemically either by dissolving HNO_3 and liberating the metal ions[35] or by a direct detection of the QDs[36]. QDs loaded with distinguishable electrochemical properties, can be used as a ‘‘barcode’’ DNA and proteins[37].

1.2.2 Gold nanoparticles

Colloidal gold has a long history and it was probably first described in the literature by the Florentine glass and alchemist Antonio Neri in 1612 in his treatise *L'Arte Vetraria*. Even earlier use of colloidal gold for decorative purposes is evidenced by Lycurgus cup, which was made by the Romans in the fourth century AD and is now exhibited in the British Museum. The first scientific studies of such materials were published much later by Michel Faraday in 1857[38]. He developed new physical as well as wet-chemical preparative methods for colloidal gold and, more important, was the first to recognize that the gold colloidal suspensions are present in the metallic state. This conclusion was drawn from the observation that red or purple colored thin films of the dry material on a quartz surface could be compressed mechanically so that they would exhibit the well-known optical properties of continuous thin films of the metallic gold (thinly beaten gold leaf), which in transmittance appear green. Since no chemical reaction was involved in the process, Faraday concluded that the gold must have always been present in the metallic state. With this discovery he became the founder of the science of metal colloids, a field that continued to develop steadily, but at times of revolutionary changes in the physical sciences, appeared to be moderate interest.

The surface plasmon absorption band can also provide information of the development of the band structure in metals[39,40] has led to a plethora of studies on the size dependent optical properties of metal particles, particularly those of silver and gold[41,42]. The optical response of these metal nanoparticles is both size and shape dependent and locally variable[43]. This sensitivity to morphology makes precise control over the growth of these nanoparticles and knowledge of their external and internal structures essentially.

A number of simple preparative methods for charge-stabilized gold hydrosols by reduction of gold salt with organic reducing agents such as formaldehyde or hydrazine were developed in the early twentieth century. The most popular method to date is Turkevich's modification of Hauser and Lynn's citrate reduction route, which was first described in 1940 and leads to very uniform gold particles in the size range of ca. 10 to 40 nm[44].

Plasmonic metal nanoparticles also show potential for biosensing[45] and cancer therapy[46]. Nanoscale shells of gold surrounding a silica core can be selectively tuned to convert near-IR photo energy into thermal energy—a nanofurnace which efficiently targets and destroys cells[47]. While some bulk metals have similar properties, only those with nanodimensions offer such tunable, and deliverable, possibilities.

During last years the electrochemical properties of gold nanoparticles have been of interest for the applications to biosensing systems. The direct or indirect detection of gold nanoparticles can be performed[48] and therefore they are used as an electrochemical label in DNA analysis[49,50] and immunoassays[51].

1.2.3 Synthesis of nanoparticles

The most important attribute for colloidal nanocrystals to be useful in biosensing systems is the obvious facility to be detected by any conventional analytical method and in the case of electrochemical biosensors (the case of this thesis) by an electroanalytical method. Their size distribution should be as narrow as possible to ensure enough reproducibility when used as a label for biological molecules. Colloidal nanocrystals, dispersed in a solvent, should allow stabilization in a way that prevents agglomeration.

Nanoparticles can be synthesized from various materials, being gold and semiconductor materials (QDs) the most important from electrochemical point of view.

The following sections describe the most important methodologies to synthesize nanoparticles.

1.2.3.1 Thermolitic method

Organometallic thermolysis is generally performed in organic solvent (trioctylphosphine oxide [TOPO] or trioctylphosphine [TOP]) at high temperature[52]. The precursors (i.e. Se; $Cd(CH)_3$; $InCl_3$ dissolved in tributylphosphine) are quickly injected into the rapidly stirred hot solvent. The QDs immediately start to nucleate. The desired size of the nanocrystals can be adjusted by changing the amount of injected precursors and the time that they are left to be grown in the hot surfactant solvent. The nanocrystals obtained are hydrophobic, since they are covered with a surfactant layer. The surfactant molecules also act as stabilizers preventing agglomeration of the QDs.

1.2.3.2 Reverse micelles

QDs can also be formed in the so-called reverse micelles mode. This technique is based on the natural structures created by water-in-oil mixtures upon adding an amphilic surfactant, such as sodium dioctyl sulfosuccinate (AOT) (see Fig. 1.3). By varying the water content of the mixture, the size of the water droplets suspended in the oil phase could be varied systematically. This led to the idea of using these self-enclosed water pools as micro-reactors for carrying out sustained nanoscale chemical reactions. A series of micelle protected PbS nanoparticles were synthesized using lead acetate and alkanethiols[53].

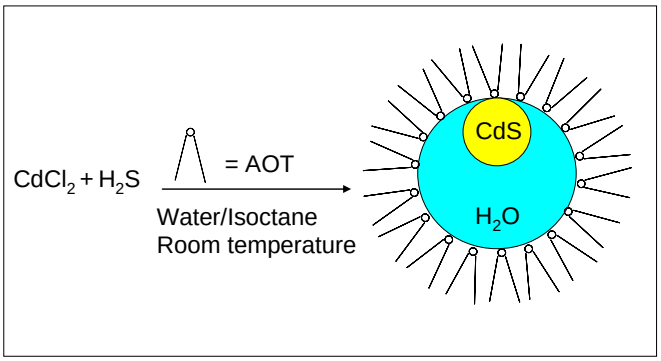

Figure 1.3 Growth of CdS QD nanoparticles in reverse micelles. This technique exploits natural geometrical structures created by water-in-oil mixtures upon adding an amphilic surfactant, such as sodium dioctyl sulfosuccinate (AOT). By varying the water content of the mixture, it was shown that the size of the water droplets suspended in the oil phase could be varied systematically.

1.2.3.3 Arrested precipitation

Arrested precipitation in solution or the controlled precipitation reactions can yield dilute suspensions of quasi monodispersed particles. This synthetic method sometimes involves the use of seeds of very small particles for the subsequent growth of larger ones. Brus et al.[54] described a synthetic process for the preparation of CdS nanoparticles which involves the controlled nucleation of CdS on mixing of dilute aqueous solutions of $CdSO_4$ and $(NH_4)_2S$. The stability of the initially small crystallites formed is influenced by the dynamic equilibrium:

$$(CdS)_{crystal} \leftrightarrow (Cd^{2+})_{solv} + (S^{2-})_{solv} \qquad (1.1)$$

Small crystallites are less stable than larger ones and tend to dissolve into their respective ions. Subsequently, the dissolved ions can recrystallize on larger crystallites, which are thermodynamically more stable. The use of acetonitrile, as a solvent, or the addition of styrene/maleic anhydride copolymer allowed the preparation of stable CdS nanoparticles, with an average size of 34 and 43 Å, respectively. Cubic ZnS and CdS nanocrystallites were synthesized in aqueous and methanolic solutions without organic surfactant (capping agent)[55].

1.2.4 Water solubilization of nanoparticles

Before the applications in bioanalytical assays, first the hydrophobic nanoparticles produced (prepared as explained in Section 1.2.3.1) must be modified again so as to be transformed to a water-soluble product. The resulting hydrophilic nanoparticles will then be attached to biological molecules through a bioconjugation step (see Section 1.2.6). Usually, these two steps are carried out independently. Alternatively, the water-solubilization and bioconjugation steps can be performed simultaneously. In any case it is important to maximize the stability of the linkages that connect the biomolecule to the nanocrystal.

As mentioned above, QDs are generally produced with an outer layer comprising one or more organic ligands, such as TOP or TOPO. These ligands are hydrophobic, so nanocrystals covered with these coatings are not compatible with aqueous assay conditions.

For this reason, hydrophilic layer agents must be introduced after synthesis of the QDs. The easiest way to obtain a hydrophilic surface is by exchanging the hydrophobic TOPO or TOP surfactant molecules with bifunctional molecules, such as mercaptocarboxylic, mercaptoacetic, mercaptopropionic or mercaptodecanoic acids that are hydrophilic on one end and bind to QDs (for example ZnS) on the other end (–SH). Carboxyl groups are negatively charged at neutral pH. QDs capped with carboxyl groups repel each other electrostatically, thus avoiding aggregation[56].

Another strategy to convert QDs into water-soluble particles was described by Alivisatos and co-workers[57]. The method consists of coating CdS/CdS (core/shell) QDs with a layer of silica.

1.2.5 Encapsulation of nanoparticles

Other strategies to maintain colloidal stability of QDs and decrease the non-specific adsorption are the encapsulations into micelles or other particles.

Phospholipid micelles. QDs can be encapsulated in the hydrophobic core of a micelle comprising n-poly(ethyleneglycol) phosphatidylethanolamine (PEG–PE) and phosphatidylcholine (PC) (see Fig. 1.4 A)[58]. The advantage of these micelles is that they are very regular in size, shape and structure. In addition, their outer surface of PEG acts as an excellent repellent for biomolecules.

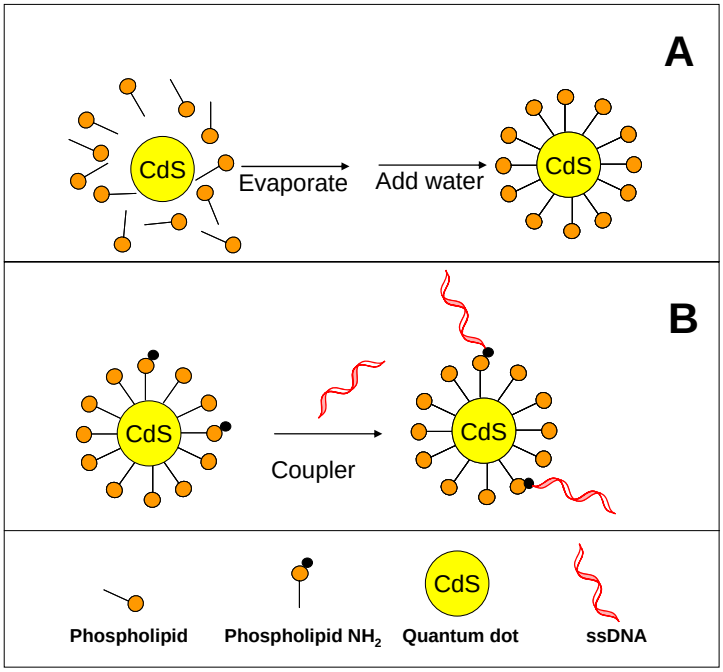

Figure 1.4 (A) Encapsulation of QDs in micelles; and, (B) QD–micelle conjugation with single-stranded DNA (ssDNA). CdS QDs can be encapsulated in the hydrophobic core of a micelle composed of a mixture of n-poly(ethyleneglycol) phosphatidylethanolamine (PEG–PE) and phosphatidylcholine (PC).

Polymeric beads. Encapsulation of QDs within polystyrene beads has been developed for electrochemical identification[59]. Cadmium sulfide, lead sulfide and zinc sulfide nanoparticles are deposited onto polystyrene beads to create a library of electrochemical codes.

*Carbon nanotubes***.** Single-wall carbon nanotubes (SWCNTs) carrying a large number of CdS QDs are used as labels for DNA detection[60]. The SWCNTs were first acetone activated and then the CdS nanoparticles were anchored onto the activated surface followed by attachment of streptavidin. The SWCNT–CdS streptavidin were used as labels for the biotinylated DNA probes.

1.2.6 Modification of nanoparticles with DNA

The chemistry of biomolecules attached to nanoparticles has a significant impact on their use in the analytical detection scheme. Nanoparticles functionalized in different ways have, for example in the case of their use in DNA detection, different oligonucleotide surface densities, different availability for hybridization to targets, and different tendencies to bind nonspecifically to surfaces[61].

*Gold nanoparticles modification with oligonucleotides***.** The attachment of oligonucleotides onto the surface of a gold nanoparticle can be performed by simple adsorption[62] or via biotin–avidin linkage, where the avidin is previously adsorbed onto the particle surface[63]. However, the most commonly method used to attach oligonucleotides onto gold nanoparticles is via thiol–gold bonds. Thiol-functionalized oligonucleotides stick strongly to gold surfaces. The attachment via thiol linkage to nanocrystals is much stronger and more efficient than non-specific adsorption. Unfortunately, the number of oligonucleotides attached per nanoparticle cannot be directly controlled. However, gold nanocrystals with a controlled number of attached oligonucleotides can be isolated using gel electrophoresis. In addition the gold nanoparticles can be connected selectively with one oligonucleotide. Nanogold maleimido was used in that case and connected with a thiolated DNA[64].

*QDs modification***.** Several strategies (e.g., adsorption[65], linkage via thiol groups[66], electrostatic interaction[67] and covalent linkage[68]) have been reported for the conjugation of water-soluble QDs.

Figure 1.5 represents schematics of QDs connected with DNA via streptavidin–biotin[69] (Fig. 1.5 a). The covalent linkage of proteins by mercaptoacetic acid[70] (Fig. 1.5 b) can also be extended for DNA.

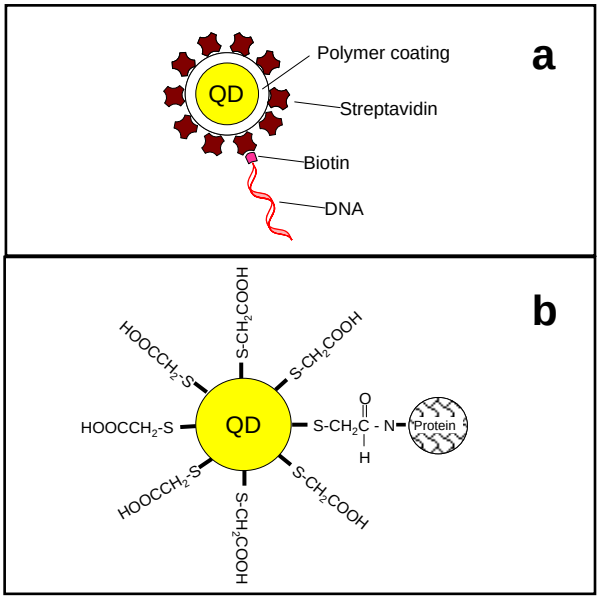

Figure 1.5 (a) A QD coated with a polymer modified with streptavidin. A biotin-functionalized DNA is attached onto the surface. (b) Schematic of a CdS QD that is covalently coupled to a protein through mercaptoacetic acid by using ethyl-3-(dimethyl-aminopropyl)carbodiimide) as a bifunctional reagent.

DNA immobilization onto QDs is one of the most studied. Mitchell et al.[71] immobilized the 50- or 30-thiolated oligonucleotides onto TOPO/mercaptoacetic acid-capped QDs. In this case, immobilization is formally non-covalent, since it arises as a result of displacement of some of the capping agents by the thiolated oligonucleotides. Willner et al.[72] also used cystaminecoated QDs to immobilize oligonucleotides.

QD micelles. QD micelles can be attached to DNA by replacing up to 50% of the PEG–PE phospholipids with an amino PEG–PE during micelle formation (Fig. 1.4 B), thus introducing a primary amine to the outer surface of the micelle. Thiol-modified DNA was then covalently coupled to the amines using a hetero-bifunctional coupler, with non-coupled DNA removed by ultracentrifugation.

1.2.7 Characterization of nanoparticles

Different kinds of techniques can be used to characterize the nanoparticles depending on the kind of the application. Table 1.1 shows several characterization techniques and the parameters that you can obtain from each.

Techniques	Characterization of NPs*
Transmission Electron Microscopy (TEM)	Size and shape (>10 nm) Structure crystalline (poorly)
High Resolution Transmission Electron Microscopy (HRTEM)	Size and shape (>0.1 nm) Structure crystalline (poorly) Crystalline lattice Microanalysis (poorly)
Atomic Force Microscopy (AFM)	Size and shape (>0.01 nm) Size distribution
Confocal Fluorescence Microscopy (CLSM)	Size and shape (>100 nm) Fluorescence properties
X ray diffraction (XRD)	Crystalline Structure (exactly)
Z potential	Electrical charge Size (poor)
Electrochemical	Concentration Redox potential

Table 1.1 Techniques used for nanoparticles characterization.

* The given values of sizes are only approximate

The following subsections show some more details on the techniques used in this work.

1.2.7.1 Transmission electron microscopy (TEM)

A sample shaped as a thin film is transilluminated by a beam of accelerated electrons with an energy of 50-200 keV in vacuum of ca. 10^{-6} mmHg. The electrons deflected at small angles by atoms in a sample pass through it and get into a system of magnetic lenses to form a bright-field image of the internal sample structure. A resolution of 0.1 nm can be achieved, which corresponds to magnification factor of 10^6. The resolution depends on the nature of the sample and its preparation method. Usually, films of 0.01-μm thickness are studied; the contrast range can be extended using carbon replicas. Diffraction

patterns, which provide information on the crystalline structure of the sample can be obtained by TEM.

1.2.7.2 Atomic force microscopy (AFM)

AFM is based on the use of a fine tip positioned at a characteristic short distance from the sample. The height of the tip above the sample is adjusted by piezoelectric elements. The images are taken by scanning the sample relative to probing tip and measuring the deflection of the cantilever as a function of lateral position[73].

In non contact mode (involving a distance higher than 1 nm between the tip and the sample surface), van der Waals, electrostatic, magnetic or capillary forces produce images, whereas in the contact mode, ionic repulsion forces take the leading role. In the non contact mode one can obtain a surface image with a true atomic resolution. However, in this case the sample has to be prepared under UHV conditions. Additionally, the non contact mode has the further advantage over the contact mode that the surface of very soft and rough materials is not influenced by frictional and adhesive forces as during scanning in the contact mode, i.e. the surface is not "scratched".

1.2.7.3 Confocal laser scanning microscopy (CLSM)

Confocal fluorescence microscopy has been widely used to obtain images of biological specimens[74]. Compared to the conventional fluorescence microscope, confocal configurations allow optical sectioning of the object and thereby three-dimensional imaging[75,76].

In a confocal laser scanning microscope, a laser beam passes through a light source aperture and then is focused by an objective lens into a small (ideally diffraction limited) focal volume within a fluorescent specimen. A mixture of emitted fluorescent light as well as reflected laser light from the illuminated spot is then recollected by the objective lens. A beam splitter separates the light mixture by allowing only the laser light to pass through and reflecting the fluorescent light into the detection apparatus. After passing a pinhole, the fluorescent light is detected by a photodetection device (a photomultiplier tube (PMT) or

avalanche photodiode), transforming the light signal into an electrical one that is recorded by a computer.

The detector aperture obstructs the light that is not coming from the focal point. The out-of-focus light is suppressed: most of their returning light is blocked by the pinhole, resulting in sharper images than those from conventional fluorescence microscopy techniques, and permits one to obtain images of various z axis planes (also known as z stacks) of the sample[77].

The detected light originating from an illuminated volume element within the specimen represents one pixel in the resulting image. As the laser scans over the plane of interest, a whole image is obtained pixel-by-pixel and line-by-line, whereas the brightness of a resulting image pixel corresponds to the relative intensity of detected fluorescent light. The beam is scanned across the sample in the horizontal plane by using one or more (servo controlled) oscillating mirrors. This scanning method usually has a low reaction latency and the scan speed can be varied. Slower scans provide a better signal-to-noise ratio, resulting in better contrast and higher resolution. Information can be collected from different focal planes by raising or lowering the microscope stage. The computer can generate a three-dimensional picture of a specimen by assembling a stack of these two-dimensional images from successive focal planes.

1.2.7.4 X ray diffraction (XRD)

X rays are electromagnetic radiations of wavelength of about 1 Å (10^{-10} m), which is about the same size as an atom. They occur in that portion of the electromagnetic spectrum between gamma-rays and the ultraviolet. The discovery of X rays in 1895 enabled scientists to probe crystalline structure at the atomic level. X ray diffraction has been in use in two main areas: for the fingerprint characterization of crystalline materials and the determination of their structure. Each crystalline solid has its unique characteristic X ray pattern which may be used as a "fingerprint" for its identification. Once the material has been identified, X ray crystallography may be used to determine its structure, i.e. how the atoms pack together in the crystalline state and what the interatomic distance and angle are etc.

X ray diffraction analysis is one of the most frequent and important tool in qualifying materials, both in research laboratories and industrial practice. In most cases,

materials are characterized not only by their chemical composition, but also by their crystal state and the amount of crystalline components[78]. In nanotechnology, XRD has special interest to be used for the determination of the crystalline structure of nanocrystals[79-81].

1.2.7.5 Z potential

Z potential is a physical property which is exhibited by any particle in suspension. It can be used to optimize the formulations of suspensions and emulsions. Knowledge of the zeta potential can reduce the time needed to produce trial formulations. It is also useful in predicting long-term stability.[82]

The development of a net charge at the particle surface affects the distribution of ions in the surrounding interfacial region, resulting in an increased concentration of counter ions (ions of opposite charge to that of the particle) close to the surface. Thus an electrical double layer exists around each particle. The liquid layer surrounding the particle has two parts; an inner region, called the Stern layer, where the ions are strongly bound and an outer, diffuse region where they are less firmly attached. Within the diffuse layer there is a notional boundary inside which the ions and particles form a stable entity. When a particle moves (e.g. due to gravity), ions within the boundary move with it, but any ions beyond the boundary do not move with the particle. This boundary is called the surface of hydrodynamic shear or slipping plane. The potential that exists at this boundary is known as the Z potential (see figure 1.6).

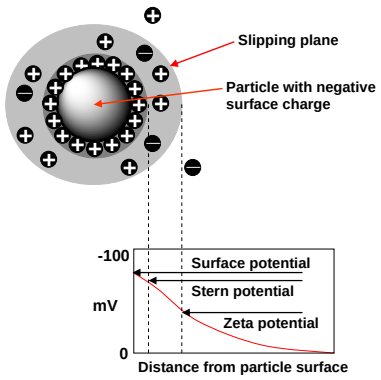

Figure 1.6 Schematic representation of Z potential

The magnitude of the Z potential gives an indication of the potential stability of the colloidal system. If all the particles in suspension have a large negative or positive Z

potential then they will tend to repel each other and there will be no tendency for the particles to come close to each other. However, if the particles have low Z potential values then there will be no force to prevent the particles coming together and flocculating.

The general dividing line between stable and unstable suspensions is generally taken at either +30 or -30 mV. Particles with Z potentials more positive than +30 mV or more negative than -30 mV are normally considered stable. However, if the particles have a density different form the dispersant, they will eventually aggregate.

1.2.7.6 Electrochemical detection

Most of the used nanoparticles contain a metal core that has redox properties. The electrochemical techniques used to detect nanoparticles take the advantages of their use for metals detection. Techniques such as cyclic voltammetry[83], differential pulse voltammetry[49,50], and square wave voltammetry can be used. In all these techniques, the electrochemical detection of metals is performed. Usually, the metal is concentrated onto the surface of the working electrode by electrodeposition and later the redissolution of the metal is carried out.

1.2.8 Applications of nanoparticles

Nanomaterials in general and particularly nanoparticles are being applied in different fields such as in energy cells, due to their optical properties, as catalytic compounds for their high surface activity and in the biomedicine field due to their bioconjugation possibilities and capability to be detected easily and rapidly.

1.2.8.1 Electronic and energy

Nanocrystals (NCs) in light-emitting devices (LEDs.). LEDs based on conducting polymers have received considerable attention in recent years. This interest is motivated by a wide range of possible applications, including flat-panel displays and large-area devices[84]. Luminiscent semiconductor NCs were successfully integrated into the thin film polymer-based LEDs as emitting materials[85-87]. Advantages of using polymer-nanocrystal composites

are the processing of both polymer and nanocrystal from solution and the superior luminescent properties of NCs. Additionally, there is a possibility to tune the emission color via control of the NCs size.

Nanocrystals for telecommunications amplifiers[88]. Another significant application for IR-emitting[89] NCs (HgTe, InAs/CdSe) is their use as optical amplifier media for telecommunication systems based on a silica fiber which has optimal transmission windows in the 1.3 and 1.5 micron regions of the IR spectrum.

NCs in solar cells. Photovoltaic cells based on low-cost poly- and nano-crystalline materials are of great interest for scientific and industrial purposes. Semiconductor nanoparticles have a number of potential advantages as light-absorbing materials in Grätzel-type cells. The photo- and thermo-stability of the NCs are similar to their bulk analogues and are superior to those of organic dyes. Efficient charge transfer from the NCs to the conduction band of wide-band gap semiconductor (TiO_2, ZnO, Ta_2O_5)[90,91] in combination with high extinction coefficients in the visible spectral range makes them attractive for Grätzel-type cells.

Another strategy for using nanoparticles in photovoltaic devices is the fabrication of blends of NCs and conducting polymers[92]. The combination of electron-conducting NCs and hole-conducting polymers in a single composite provides effective charge separation and transport. Power energy conversion efficiency has been achieved[93].

1.2.8.2 Materials science / industry

*Nanoparticles with catalytic effect***.** Because of their large surface-to-volume ratio, nanoparticles offer higher catalytic efficiency per gram than larger size materials. The field of nanocatalysis has been very active lately with numerous review articles published during the past decade in both heterogeneous catalysis in which the nanoparticles are supported on solid surfaces (e.g., silica or alumina)[94-96] and homogeneous catalysis with colloidal nanoparticles[97]. Being small in size is expected to increase the nanoparticle surface tension. This fact makes surface atoms very active[98].

1.2.8.3 Bioanalysis

Biosensor field is one of the most important focus of nanotechnology. The use of biomolecules labeled with nanoparticles is offering novel opportunities for (bio) detection systems[99]. The electrochemical detection of nanoparticles is offering high sensitive detection alternatives beside being the easiest and cheapest technique comparing to optical detections such as fluorescence spectroscopy between others. Biosensors applications using overall electrochemical techniques are described in the following sections.

1.3 Sensors and biosensors

A chemical sensor is defined as a device which responds to a particular analyte in a selective way through a chemical reaction and can be used for the qualitative or quantitative determination of this analyte[100].

According to International Union of Pure and Applied Chemistry (IUPAC) recommendations, a biosensor is a self-contained integrated receptor-transducer device, which is capable of providing selective quantitative or semi-quantitative analytical information using a biological recognition element[101].

Their two elements are essential: first, the powerful molecular recognition capability of bioreceptors (biorecognition element) such as antibodies, DNA, enzymes and cellular components of living systems, and secondly, the transducer element to translate the interactions of the biorecognition element into a detectable signal.

The amount of signal generated is proportional to the concentration of the analyte, allowing for both quantitative and qualitative measurements in time[102]. Biorecognition element imparts the selectivity that enables the sensor to respond selectively to a particular analyte or group of analytes, thus avoiding interferences from other substances[103].

Hence, a highly selective and sensitive biorecognition element is essential for the design of an efficient sensor.

1.3.1 Afinnity biosensors

Affinity electrochemical biosensors, based on enzyme labeling, solve the problems of radioactive detection (e.g., health hazards and short lifetimes) and open new possibilities in ultrasensitive and automated biological assays. Nevertheless, biological research and other scientific and technological fields need a broader range of more reliable and more robust labels to enable high throughput bioanalysis and simultaneous multi-analyte determination. The existing labeling techniques (e.g., enzymes or isotopes) have several drawbacks: the markers used have short life-times and they have a limited number of practical combinations (of more than two enzymes) for simultaneous analysis of various analytes.

1.3.1.1 Immunosensors

Immunosensors are affinity ligand-based biosensors in which the immunochemical reaction is coupled to a transducer[104]. These biosensors use antibodies as the biospecific sensing element, and are based on the ability of an antibody to form complexes with the corresponding antigen[105].

Immunoassays are among the most specific of the analytical techniques. They provide extremely low detection limits and can be used for a wide range of substances. As research moves into the era of proteomic, such assays become extremely useful for identifying and quantifying proteins.

Immunosensors are based on immunological reactions involving the shape recognition of the AG by the AB binding site to form the AB/AG stable complex:

$$AB + AG \leftrightarrow AB/AG \quad (1.2)$$

Immunoassays, based on the specific reaction of ABs with the target substances (AGs) to be detected, have been widely used for the measurement of targets of low concentration in clinical samples such as urine and blood and the detection of the trace amounts of drugs and chemicals such as pesticides in biological and environmental samples.

According to the nature of a label, immunoassays can be classified as label-free immunoassay[106-108], radio-immunoassay[109-111], enzyme immunoassay[112-114], fluorescent

immunoassay[115-117], chemiluminescent immunoassay[118-120], bioluminescent immunoassay[121-123], etc.

Metalloimmunoassay (immunoassay involving metals) has been developed and extended later on to the use of a variety of other metal-based labels such as colloidal metal particles[124,125].

1.3.1.2 Genosenors

DNA biosensors represent a very important type of affinity biosensors in which the biorecognition molecules are oligonucleotides of known sequence and the recognition event is the hybridization with the complementary sequences.

Among the various types of DNA sensors, the electrochemical sensor has some advantage such as the use of very simple equipment to perform measurements, low cost and possibility of miniaturization in order to obtain high density arrays.

DNA biosensors based on DNA hybridization are playing an increasing role in DNA analysis.

Some examples of DNA biosensors based in labeling with nanoparticles are described in the following sections.

Gold nanoparticles. Colloidal gold nanoparticles have been used as signal hybridization in various DNA detection assays. Three strategies for the detection of gold tracers have been reported (see Fig. 1.7 A).

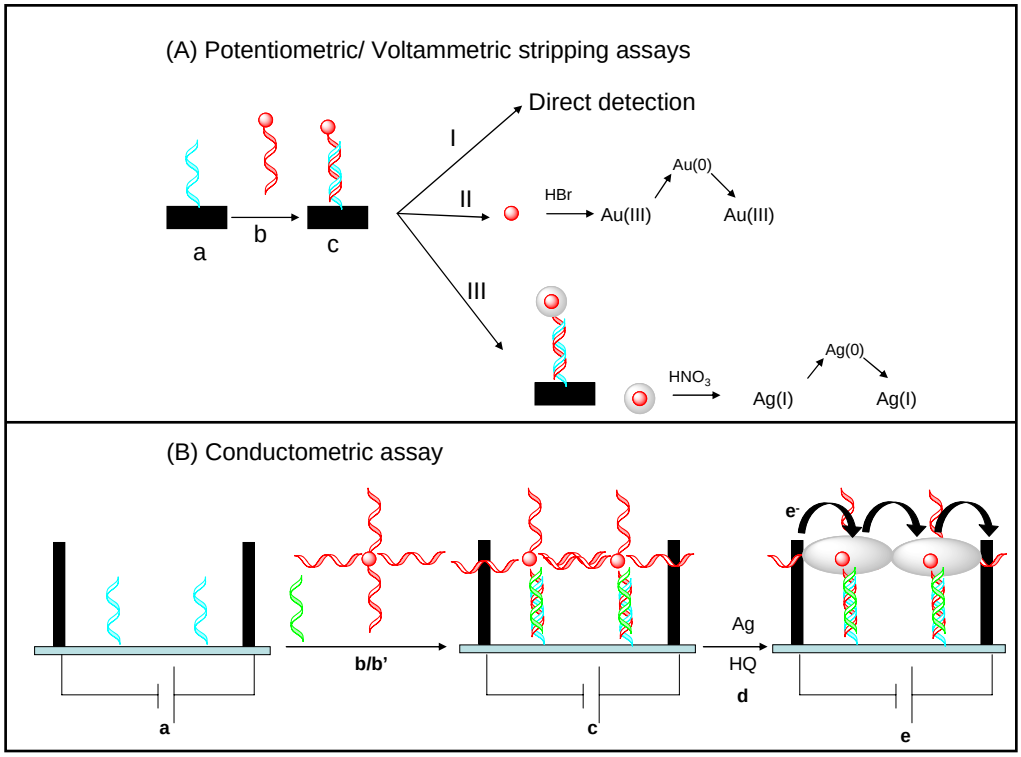

Figure 1.7 Detection strategies of gold nanoparticles. (A) Potentiometric/voltammetric stripping assay. The hybridization event occurs between DNA strand (a) and gold-tagged DNA (b). The gold-labeled duplex (c) formed is then detected according to each strategy: (I) direct detection of the nanoparticles onto the bare electrode without the need for tag dissolution; (II) the gold nanoparticles are dissolved with HBr/Br_2 treatment and then detected by stripping techniques; and, (III) the gold nanoparticles are first covered with Ag by a deposition treatment and then detected by stripping techniques via silver enhanced signal. (B). Conductivity assay. Probe DNA immobilized in a small gap between two electrodes (a) is hybridized with DNA target (b) and then with gold-modified DNA probes (b'). Gold is accumulated in the gap (c). Silver enhancement (d) is performed in the presence of hydroquinone (HQ). The silver precipitated onto the gold nanoparticles (e) improves the sensitivity of the assay by lowering the resistance across the electrode gap.

According to the first strategy, direct detection of the nanoparticle on the bare electrode without the need of nanoparticle dissolving is performed. A DNA biosensor based on a pencil-graphite electrode and modified with the DNA target was developed following this direct detection strategy[126]. To achieve their objective, the authors covalently bound PCR amplicons to a pencil-graphite electrode using carbodiimide/N-hydroxysuccinimide, and hybridized oligonucleotide–nanoparticle conjugates to these electrode-bound targets. Direct electrochemical oxidation of the particles was observed at a stripping potential of approximately +1.2 V.

According to the second strategy (Fig. 1.7 B), the intrinsic electrochemical signal of the nanoparticle can be observed after dissolving it with HBr/Br_2[127]. Gold(III) ions obtained were preconcentrated by electrochemical reduction onto an electrode and subsequently determined by anodic-stripping voltammetry.

As 'tracer amplification', silver deposition on the gold nanoparticles after hybridization is also used and an enhanced electrochemical signal attributable to silver is obtained[128 129]. This represents the third strategy. Stripping detection is used for gold nanoparticles/silver enhancement related strategy.

Nevertheless, other interesting methods have been reported. Mirkin and colleagues[130] have exploited the silver-deposition technique to construct a sensor based on conductivity measurements. In their approach, a small array of microelectrodes with gaps (20 μm) between the electrodes leads is constructed, and probe sequences are immobilized on the substrate between the gaps. Using a three-component sandwich approach, hybridized DNA target is used to recruit gold nanoparticle-tagged reporter probes between the electrode leads. The nanoparticle labels are then developed in the silver-enhancer solution leading to a sharp drop in the resistance of the circuit (see Fig. 1.7 B, adapted from reference 130)

QDs and other nanoparticles. A detection method of DNA hybridization based on labeling with CdS QD tracers followed by the electrochemical-stripping measurements of the cadmium have been developed[131]. Nanoparticle-promoted cadmium precipitation, using a fresh cadmium solution hydroquinone, is used to enlarge the nanoparticle tag and amplify the stripping DNA hybridization signal. In addition to measurements of the dissolved cadmium, it was demonstrated in direct ''solid-state'' measurements following a ''magnetic'' collection of a ''magnetic bead/DNA hybrid/CdS tracer'' assembly onto a thick-film electrode transducer. The low detection limit (100 fmol) is coupled to good reproducibility (RSD = 6%).

Besides QDs, gold-coated iron nanoparticles have also been used in DNA-detection assays[132]. After hybridization, the captured gold-iron nanoparticles are dissolved and the released iron is quantified by cathodic stripping voltammetry in the presence of the 1-nitroso- 2-naphthol ligand and a bromate catalyst. The DNA-labeling mode developed offers high sensitivity, well-defined dependence on concentration, and minimal contributions from non-complementary nucleic acids.

Electrochemical impedance spectroscopy (EIS) measurements based on CdS–oligonucleotides have been also possible, besides stripping techniques[133]. EIS was used to

detect the change of interfacial electron-transfer resistance (R_{et}) of a redox marker ($Fe(CN_6)^{4-/3-}$) from solution to transducer surface where the DNA hybridization occurs. It was observed that, when ssDNA-CdS nanoconjugates target hybridized with a DNA probe, the R_{et} value recorded increased markedly.

Nanoparticle carriers. Polymeric microbeads carrying numerous gold-nanoparticle tags have also been used as labels for DNA in electrochemical detection procedures. The gold-tagged beads were prepared by binding biotinylated nanoparticles to streptavidin-coated polystyrene spheres. Such carrier-sphere amplification platforms are combined with catalytic enlargement of the multiple gold tags and with the sensitive electrochemical-stripping detection of the dissolved gold tags (Fig. 1.8 A), allowing determination of DNA targets down to the 300-amol level[134].

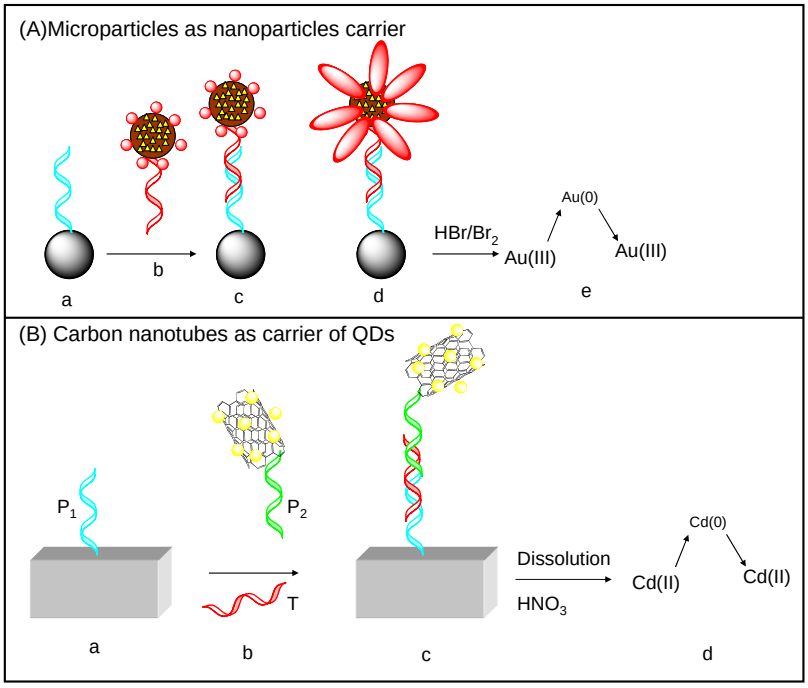

Figure 1.8 (A) Microparticles as nanoparticle carriers. The DNA target immobilized onto magnetic beads (a) hybridizes with the nucleic acid functionalized with Au-nanoparticle-carrier polystyrene beads (b) forming the Au-labeled hybrid (c) the tags of which are than enlarged (d) followed by magnetic separation and a dissolution process with HBr/Br_2 and then detected by stripping voltammetry (e). (B) Carbon nanotubes as carriers of QDs. The DNA probe P_1 is first immobilized onto the well of a streptavidin-assay plate (a). The DNA target (T) and the single wall carbon nanotube (SWCNT)–CdS–labeled probe (P_2) were then added, followed by a dual hybridization event (b) forming the final CdS-tagged sandwich (c). The QDs are dissolved with 1 M HNO_3 and then detected by stripping voltammetry using a mercury-coated glassy carbon electrode (d).

SWCNTs carrying a large number of CdS QDs are used as labels for DNA detection. A schematic view of the analytical protocol involving a dual hybridization event is shown in figure 1.8 B.

Nanoparticles as encoded electrochemical hosts. The potential of current DNA-microarray technology has some limitations. Both the fabrication and read-out of DNA arrays must be miniaturized to fit thousands of tests onto a single substrate. In addition, arrays must be selective enough to eliminate false-sequence calls and sensitive enough to detect few copies of a target.

Nanoparticles hold particular promise as the next generation of barcodes for multiplexing experiments. Genomic and proteomic research demands greater information from single experiments. Conventional experiments use multiple organic fluorophores to barcode different analytes in a single experiment, but positive identification is difficult because of the crosstalking signal between fluorophores.

The labeling of probes bearing different DNA sequences with different nanoparticles enables the simultaneous detection of more than one target in a sample, as shown in figure 1.9. The number of targets that can be readily detected simultaneously (without using high-level multiplexing) is controlled by the number of voltammetrically distinguishable nanoparticle markers. A multi-target sandwich hybridization assay involving a dual hybridization event, with probes linked to three tagged inorganic crystals and to magnetic beads has been reported. The DNA-connected QDs yielded well-defined and resolved stripping peaks at -1.12 V (Zn), -0.68 V (Cd) and -0.53 V (Pb) at the mercury coated glassy carbon electrode (vs. the Ag/AgCl reference electrode).

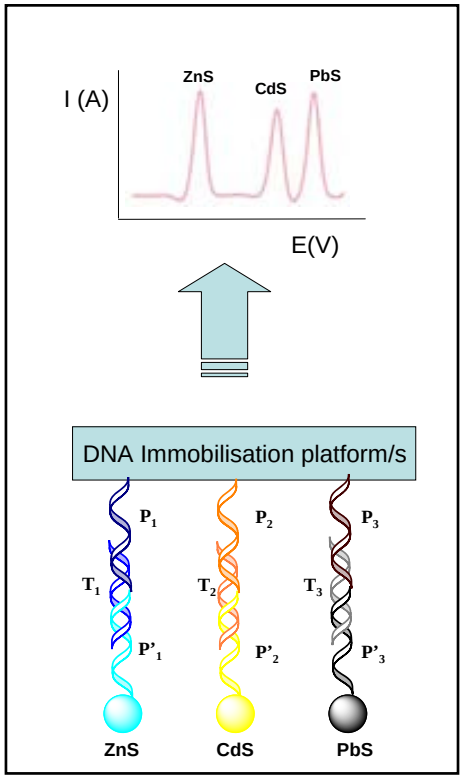

Figure 1.9 Schematic of multiple detection of DNA. DNA probes (P'_1, P'_2 and P'_3) bearing different DNA sequences with different nanoparticles (ZnS, CdS and PbS, respectively) that enable the simultaneous detection of three DNA targets (T_1, T_2 and T_3) hybridized with corresponding DNA-capturing probes (P_1, P_2 and P_3) immobilized onto a direct or an indirect (magnetic particles) transducing platform/s.

Other attractive nanocrystal tracers for creating a pool of non-overlapping electrical tags for such bioassays are ZnS, PbS, CdS, InAs, and GaAs semiconductor particles, in view of the attractive stripping behavior of their metal ions.

Some details of the genosensors based on nanoparticles are summarized in table 1.2

Nanoparticle label	Label connection with DNA	Detection Technique	Hybridization separate from detection	DNA detection limit	RSD	Reference
Au	Au-SH-DNA	DPV at pencil-graphite electrode	No	0.78 fmol/ml	≈ 8 %	126
Au	Au-SH-DNA	PSA and silver catalytic enhancement at screen-printed electrodes	Yes	150 pg/ml	7 %	128,129
Au	Au-SH-DNA	Conductivity at micro-electrodes	No	500 fM	-	130
Au carried into PVC beads	PVC(Au) strep-tavidin-biotin-DNA	PSA and silver catalytic enhancement at screen-printed electrodes	Yes	40 pg/ml	13 %	134
CdS QDs	CdS NH-DNA	EIS with gold electrode	No	$1.43 * 10^{-10}$ M	-	133
CNTs loaded with CdS QDs	CNT-CdS-strep-tavidin-biotin-DNA	DPV at Hg-film electrode	Yes	40 pg/ml	6.4 %	60
Au-Fe (core/shell)	Fe-Au-SH-DNA	DPV at Hg-film electrode	Yes	50 ng/ml	6.3 %	132
CdS QDs	CdS-SH-DNA	PSA and catalytic enhancement with Cd at screen-printed electrodes	Yes	20 ng/ml	6 %	131
CdS QDs PbS QDs ZnS QDs	CdS-SH-DNA PbS-SH-DNA ZnS-SH-DNA	Simultaneous detection with SWV at Hg-film electrode	Yes	5 ng/ml	9.4 %	35

Table 1.2 Details on some genosensors based on nanoparticles used as labels.
(PSA, Potentiometric stripping analysis; DPV, Differential pulse voltametry; SWV, Square wave voltammetry; EIS, Electrochemical impedance spectroscopy)

1.3.1.3 Cell sensors

Cell sensors are affinity ligand-based biosensors in which a component of the cell gives a specific response that can be detected.

Cells as analytes. Brown[135] et al. conjugated a QDs to 20-mer peptide-phage that only recognized a large cell lung carcinoma cell line, H1299 and use a fluorescence image of QDs to detect the specific cell.

Another example, is reported by Xie et al.[136] They monitored the aglutination process of human hepatic cells (L-02) at the quartz crystal microbalance (QCM) gold (Au) electrode in real time. The weight change is detected by the quartz crystal microbalance.

Cells as labels. Zare et al.[137] used an immune cell that expresses receptors for the constant region of immunoglobulin G (IgG) and is loaded with a Ca^{2+} indicating dye and with antibodies directed against the protein of interest. The addition of the analyte into the cells, cause a dramatic endocitosic response that can be detected by labelling cells with a dye and detect apoptosis cells using a fluorescence microscope[138].

1.4 References

[1] Ratner M., Ratner D. *"Nanotechnology: A Gentle Introduction to the Next Big Idea"* **2003** *Prentice Hall PTR* 1st edition.

[2] Dai H. *"Carbon nanotubes: opportunities and challenges"* **2002** *Surf. Sci.* 500, 218-241.

[3] Shimoda H., Oh S. J., Geng H. Z., Walker R. J., Zhang X. B., McNeil L. E., Zhou O. *"Self-Assembly of Carbon Nanotubes"* **2002** *Adv. Mater.* 14, 899-901.

[4] Merkoçi A., Pumera M., Llopis X., Pérez B., Valle M., Alegret S. *"New materials for electrochemical sensing VI: Carbon nanotubes"* **2005** *Trends in Analytical Chemistry* 24, 826-838.

[5] Pérez B., Merkoçi A. *"Improvement of the electrochemical detection of catechol by the use of a carbon nanotube based biosensor"* **2009** *Analyst* 134, 60-64.

[6] Pérez B., Sola J., Alegret S., Merkoçi A. *"A Carbon Nanotube PVC Based Matrix Modified with Glutaraldehyde Suitable for Biosensor Applications"* **2008** *Electroanalysis* 20, 603-610.

[7] Alarcón G., Pérez B., Palomar M., Ramírez M.T., Alegret S., Merkoçi A. *"Enhanced host–guest electrochemical recognition of dopamine using cyclodextrin in the presence of carbon nanotubes"* **2008** *Carbon* 46, 898-906.

[8] Alivisatos A. P. *"Nanocrystals: building blocks for modern materials design"* **1997** *Endeavour* 21, 56-60.

[9] Brust M., Fink J., Bethell D., Schiffrin D. J., Kiely C. *"Synthesis and Reactions of Functionalised Gold Nanoparticles"* **1995** *J. Chem. Soc., Chem. Commun*. 1655-1656.

[10] Brown L. O., Hutchison J. E. *"Controlled Growth of Gold Nanoparticles during Ligand Exchange"* **1999** *J. Am. Chem. Soc.* 121, 882-883.

[11] Quaroni L., Chumanov G. *"Preparation of Polymer-Coated Functionalized Silver Nanoparticles"* **1999** *J. Am. Chem. Soc.* 121, 10642-10643.

[12] Rivas L., Sanchez-Cortes S., García-Ramos J. V., Morcillo G. *"Growth of Silver Colloidal Particles Obtained by Citrate Reduction To Increase the Raman Enhancement Factor"* **2001** *Langmuir* 17, 574-577.

[13] Ershov B. G., Sukhov N. L., Janata E. *"Formation, Absorption Spectrum, and Chemical Reactions of Nanosized Colloidal Cobalt in Aqueous Solution"* **2000** *J. Phys. Chem. B* 104 6138-6142.

[14] Puntes V. F., Krishnan K. M., Alivisatos A. P. *"Colloidal Nanocrystal Shape and Size Control: The Case of Cobalt"* **2001** *Science* 291, 2115-2117.

[15] Murray C. B., Norris D. J., Bawendi M. G. *"Synthesis and characterization of nearly monodisperse CdE (E = sulfur, selenium, tellurium) semiconductor nanocrystallites"* **1993** *J. Am. Chem. Soc.* 115, 8706-8715.

[16] Merkoçi A, Marín S., Castañeda M. T., Pumera M., Ros J., Alegret S. *"Crystal and electrochemical properties of water dispersed CdS nanocrystals obtained via reverse micelles and arrested precipitation"* **2006** *Nanotechnology* 17, 2553-2559.

[17] Steigerwald M. L., Brus L. E. *"Semiconductor crystallites: a class of large molecules"* **1990** *Acc. Chem. Res.* 23, 183-188.

[18] Colvin V. L., Alivisatos A. P. *"CdSe nanocrystals with a dipole moment in the first excited state"* **1990** *J. Chem. Phys.* 97, 730-733.

[19] Eychmüller A., Rogach A. L. *"Chemistry and photophysics of thiol-stabilized II-VI semiconductor nanocrystals"* **2000** *Pure Appl. Chem.* 72, 1-331.

[20] Talapin D. V., Haubold S., Rogach A. L., Kornowski A., Haase M., Weller H. *"A Novel Organometallic Synthesis of Highly Luminescent CdTe Nanocrystals"* **2001** *J. Phys. Chem. B* 105, 2260-2263.

[21] Olshavsky M. A., Goldstein A. N., Alivisatos A. P. *"Organometallic synthesis of gallium-arsenide crystallites, exhibiting quantum confinement"* **1990** *J. Am. Chem. Soc.* 112, 9438-9439.

[22] Guzelian A. A, Katari J. E. B., Kadavanich A. V., Banin U., Hamad K., Juban E., Alivisatos A. P., Wolters R. H., Arnold C. C., Heath J. R. *"Synthesis of Size-Selected, Surface-Passivated InP Nanocrystals"* **1996** *J. Phys. Chem.* 100, 7212-7219.

[23] Micic O. I., H. Cheong M., Fu H., Zunger A., Sprague J. R., Mascarenhas A., Nozik A. J. *"Size-Dependent Spectroscopy of InP Quantum Dots"* **1997** *J. Phys. Chem. B* 101, 4904-4912.

[24] Rockenberger J., Scher E. C., Alivisatos A. P. *"A New Nonhydrolytic Single-Precursor Approach to Surfactant-Capped Nanocrystals of Transition Metal Oxides"* **1999** *J. Am. Chem. Soc.* 121, 11595-11596.

[25] Santra S., Tapec R., Theodoropoulou N., Dobson J., Hebard A., Weihong T. *"Synthesis and Characterization of Silica-Coated Iron Oxide Nanoparticles in Microemulsion: The Effect of Nonionic Surfactants"* **2001** *Langmuir* 17, 2900-2906.

[26] Trentler T. J., Denler T. E., Bertone J. F., Agrawal A., Colvin V. L. *"Synthesis of TiO_2 Nanocrystals by Nonhydrolytic Solution-Based Reactions"* **1999** *J. Am. Chem. Soc.* 121, 1613-1614.

[27] Peng X., Manna L., Yang W., Wickham J., Scher E., Kadavanich A., Alivisatos A. P. *"Shape control of CdSe nanocrystals"* **2000** *Nature* 404, 59-61.

[28] Jana N. R., Gearheart L., Murphy C. J. *"Wet chemical synthesis of silver nanorods and nanowires of controllable aspect Ratio"* **2001** *Chem. Commun.* 617-618.

[29] Jin R., Cao Y. W., Mirkin C. A., Kelly K. L., Schatz G. C., Zheng J. G. *"Photoinduced Conversion of Silver Nanospheres to Nanoprisms"* **2001** *Science* 294, 1901-1903.

[30] Manna L., Scher E. C., Alivisatos A. P. *"Synthesis of Soluble and Processable Rod-, Arrow-, Teardrop-, and Tetrapod-Shaped CdSe Nanocrystals"* **2000** *J. Am. Chem. Soc.* 122 , 12700-12706.

[31] Murphy C. J. *"Optical Sensing with Quantum Dots"* **2002** *Anal. Chem.* 520A-526 A.

[32] Empedocles S., Bawendi M. *"Spectroscopy of Single CdSe Nanocrystallites"* **1999** *Acc. Chem. Res.* 32, 389-396.

[33] Kuno M., Lee J. K., Dabbosi B. O., Mikulec F. V., Bawendi M. G. *"The band edge luminescence of surface modified CdSe nanocrystallites: Probing the luminescing state"* **1997** *J. Chem. Phys.* 106, 9869-9882.

[34] Norris D. J., Sacra A., Murray C. B., Bawendi M. G. *"Measurements of the Size Dependent Hole Spectrum in CDSe Quantum Dots"* **1994** *Physical Review Letters* 72, 2612-2615.

[35] Wang J., Liu G., Merkoçi A. *"Electrochemical Coding Technology for Simultaneous Detection of Multiple DNA Targets"* **2003** *J. Am. Chem. Soc.* 125, 3214-3215.

[36] Merkoçi A., Marcolino-Junior L. H., Marín S., Fatibello-Filho O., Alegret S. *"Detection of cadmium sulphide nanoparticles by using screen-printed electrodes and a handheld device"* **2007** *Nanotechnology* 18, 035502 (1-6).

[37] Liu G.,Wang J., Kim J., Jan M. R. *"Electrochemical Coding for Multiplexed Immunoassays of Proteins"* **2004** *Anal. Chem.* 76, 7126-7130.

[38] Faraday M. *"Experimental Relations of Gold (and other Metals) to Light"* **1857** *Philos. Trans. R. Soc. London* 147, 145-181.

[39] Scott A. B., Smith W. A., Thompson M. A. *"Alkali Halides Colored by Colloidal Metal"* **1953** *J. Phys. Chem.* 57, 757-761.

[40] Doyle W. T. *"Absorption of Light by Colloids in Alkali Halide Crystals"* **1958** *Phys. Rev.* 111, 1067-1072.

[41] Lee K. S., El-Sayed M. A. *"Gold and Silver Nanoparticles in Sensing and Imaging: Sensitivity of Plasmon Response to Size, Shape, and Metal Composition"* **2006** *J. Phys. Chem. B* 110, 19220-19225.

[42] Hanauer M., Pierrat S., Zins I., Lotz A., Snnichsen C. *"Separation of Nanoparticles by Gel Electrophoresis According to Size and Shape"* **2007** *Nano Lett.* 7, 2881-2885.

[43] Nelayah, J., Kociak M., Sthéphan O., García F. J., Tencé M., Henrard L., Taverna D., Pastoriza-Santos I., Liz-Marzán L. M., Colliex C. *"Mapping surface plasmons on a single metallic nanoparticle"* **2007** *Nature Phys.* 3, 348-353.

[44] Turkevich J., Stevenson P. C., Hillier J. *"A study of the nucleation and growth processes in the synthesis of colloidal gold"* **1951** *Discuss. Faraday Soc.* 11, 55-75.

[45] Willets K. A., Van Duyne R. P. *"Localized surface plasmon resonance spectroscopy and sensing"* **2007** *Annu. Rev. Phys. Chem.* 58, 267-297.

[46] Jain P. K., El-Sayed I. H., El-Sayed M. A. *"Au nanoparticles target cancer"* **2007** *Nano Today* 2, 18-29.

[47] Hirsch L.R., Stafford R. J., Bankson J. A., Sershen S. R., Rivera B,. Price R. E., Hazle J. D., Halas N. J., West J. L. *"Nanoshell-mediated near-infrared thermal therapy of tumors under magnetic resonance guidance"* **2003** *Proc Natl Acad Sci* 100, 13549-13554.

[48] Pumera M., Aldavert M., Mills C., Merkoçi A., Alegret S. *"Direct voltammetric determination of gold nanoparticles using graphite-epoxy composite electrode"* **2005** *Electrochim. Acta* 50, 3702-3707.

[49] Pumera M., Castañeda M. T., Pividori M. I., Eritja R., Merkoçi A., Alegret S. *"Magnetically Trigged Direct Electrochemical Detection of DNA Hybridization Using Au_{67} Quantum Dot as Electrical Tracer"* **2005** *Langmuir* 21, 9625-9629.

[50] Castañeda M. T., Merkoçi A., Pumera M., Alegret S. *"Electrochemical genosensors for biomedical applications based on gold nanoparticles"* **2007** *Biosensors and Bioelectronics* 22, 1961-1967.

[51] Ambrosi A., Castañeda M. T., Killard A. J., Smyth M. R., Alegret S., Merkoçi A. *"Double-codified gold nanolabels for enhanced immunoanalysis"* **2007** *Anal. Chem.* 79, 5232-5240.

[52] Peng X., Wickham J., Alivisatos A. P. *"Kinetics of II-VI and III-V Colloidal Semiconductor Nanocrystal Growth: "Focusing" of Size Distributions"* **1998** *J. Am. Chem. Soc*. 120, 5343-5344.

[53] Pileni M. P., Motte C., Petit C. *"Synthesis of Cadmium Sulfide in Situ in Reverse Micelles: Influence of the Preparation Modes on Size, Polydispersity, and Photochemical Reactions"* **1992** *Chem. Mater.* 4, 338-345.

[54] Rossetti R., Ellison J. L., Gibson J. M., Brus L. E. *"Size effects in the excited electronic states of small colloidal CdS crystallites"* **1984** *J. Chem. Phys.* 80, 4464-4469.

[55] Rossetti R., Hull R., Gibson J. M., Brus L. E. *"Excited electronic states and optical spectra of ZnS and CdS crystallites in the ≈ 15 to 50 Å size range: Evolution from molecular to bulk semiconducting properties"* **1985** *J. Chem. Phys.* 82, 552-559.

[56] Parak W. J., Gerion D., Pellegrino T., Zanchet D., Micheel C., Williams S. C., Boudreau R., Le Gros M. A., Larabell C. A., Alivisatos A. P. *"Biological applications of colloidal nanocrystals"* **2003** *Nanotechnology* 14, R15-R27.

[57] Bruchez M. P., Moronne M., Gin P., Weiss S., Alivisatos A. P. *"Semiconductor Nanocrystals as Fluorescent Biological Labels"* **1998** *Sciencie* 281, 2013-2016.

[58] Dubertret B., Skourides P., Norris D. J., Noireaux V., Brivanlou A. H., Libchaber A. *"In Vivo Imaging of Quantum Dots Encapsulated in Phospholipid Micelles"* **2002** *Science* 298, 1759-1762.

[59] Wang J., Liu G., Rivas G. *"Encoded Beads for Electrochemical Identification"* **2003** *Anal. Chem.* 75, 4667-4671.

[60] Wang J., Liu G., M. Jan R., Zhu Q. *"Electrochemical detection of DNA hybridization based on carbon-nanotubes loaded with CdS tags"* **2003** *Electrochemistry Communications* 5, 1000-1004.

[61] Niemeyer C. M.*"Nanoparticles, Proteins, and Nucleic Acids: Biotechnology Meets Materials Science"* **2001** *Angew. Chem. Int. Ed.* 40, 4128-4158.

[62] Gearheart L. A., Ploehn H. J., Murphy C. J. *"Oligonucleotide Adsorption to Gold Nanoparticles: A Surface-Enhanced Raman Spectroscopy Study of Intrinsically Bent DNA"* **2001** *J. Phys. Chem. B* 105, 12609-12615.

[63] Shaiu W. L., Larson D. D., Vesenka J., Henderson E *"Atomic force microscopy of oriented linear DNA molecules labeled with 5nm gold spheres"* **1993** *Nucleic Acids Res.* 21, 99-103.

[64] Torre B. G., Morales J. C., Aviño A., Iacopino D., Ongaro A., Fitzmaurice D., Murphy D., Doyle H., Redmond G., Eritja R. *"Synthesis of Oligonucleotides Carrying Anchoring Groups and Their Use in the Preparation of Oligonucleotide - Gold Conjugates"* **2002** *Helv. Chim. Acta* 85, 2594-2607.

[65] Mahtab R., Harden H. H., Murphy C. J. *"Temperature- and Salt-Dependent Binding of Long DNA to Protein-Sized Quantum Dots: Thermodynamics of "Inorganic Protein"−DNA Interactions"* **2000** *J. Am. Chem. Soc*. 122, 14-17.

[66] Willard D. M., Carillo L. L., Jung J., Orden A. V. "*CdSe−ZnS Quantum Dots as Resonance Energy Transfer Donors in a Model Protein−Protein Binding Assay"* **2001** *Nano Letters* 1, 469-474.

[67] Mattoussi H., Mauro J. M., Goldman E. R., Anderson G. P., Sundar V. C., Mikulec F. V., Bawendi M. G. *"Self-Assembly of CdSe−ZnS Quantum Dot Bioconjugates Using an Engineered Recombinant Protein"* **2000** *J. Am. Chem. Soc.* 122, 12142-12150.

[68] Parak W. J., Gerion D., Zanchet D., Woerz A. S., Pellegrino T., Micheel C., Williams S. C., Seitz M.,. Bruehl R. E, Bryant Z., Bustamante C., Bertozzi C. R., Alivisatos A. P. *"Conjugation of DNA to Silanized Colloidal Semiconductor Nanocrystalline Quantum Dots"* **2002** *Chem. Mater.* 14, 2113-2119.

[69] Bonanni A., Esplandiu M. J., Valle M. *"Signal amplification for impedimetric genosensing using gold-streptavidin nanoparticles"* **2008** *Electrochimica Acta* 53, 4022-4029.

[70] Chan W. C. W., Nie S. *"Quantum Dot Bioconjugates for Ultrasensitive Nonisotopic Detection"* **1998** *Science* 281, 2016-2018.

[71] Mitchell G. P., Mirkin C. A., Letsinger R. L. *"Programmed Assembly of DNA Functionalized Quantum Dots"* **1999** *J. Am. Chem. Soc.* 121, 8122-8123.

[72] Willner I., Patolsky F., Wasserman J. *"Photoelectrochemistry with Controlled DNA-Cross-Linked CdS Nanoparticle Arrays"* **2001** *Angew. Chem. Int. Ed.* 40, 1861-1864.

[73] Waser R. *"Nanoelectronics and Information Technology: Advaced Electronic Materials and Nobel Devices"* **2005** *Wiley-VCH* second edition.

[74] Shotton D. *"Electronic Light Microscopy: The Principles and Practice of Video-enhanced Contrast, Digital Intensifield Fluorescence, and Confocal Scanning Light Microscopy"* **1992** *Wiley-Liss*, chap 1, p.p. 17-20.

[75] Scivetti M., Pilolli G. P., Corsalini M., Lucchese A., Favia G. *"Confocal laser scanning microscopy of human cementocytes: Analysis of three-dimensional image Reconstruction"* **2007** *Ann. Anat.* 189, 169-174.

[76] Buwalda J., Colnot D. R., Bleys R. L. A. W., Groen G. J., Thrasivoulou C., Cowen T. *"Imaging and analysis of perivascular nerves in human mesenteric and coronary arteries: a comparison between epi-fluorescence and confocal microscopy"* **1997** *Journal of Neuroscience Methods* 73, 129-134.

[77] Pawley J. B. *"Handbook of Biological Confocal Microscopy"***1995** *Plenum Press* 2nd edn., chap. 10, pp.155-165.

[78] Hasek J. *"X-ray and Neutron Structure Analysis in Materials Science"* **1989** *Plenum Press*. chap. 1, pp 23-25.

[79] Mädler L., Stark W. J., Pratsinis S. *"E. Rapid synthesis of stable ZnO quantum dots"* **2002** *J. Appl. Phys.* 92, 6537-6540.

[80] Health J. R., Shiang J. J., Alivisatos A. P. *"Germanium quantum dots: Optical properties and synthesis"* **1994** *J. Chem. Phys.* 101, 1607-1615.

[81] Jose R., Biju V., Yamaoka Y., Nagase T., Makita Y., Shinohara Y., Baba Y., Ishikawa M. *"Synthesis of CdTe quantum dots using a heterogeneous process at low temperature and their optical and structural properties"* **2004** *Appl. Phys. A* 79, 1833-1838.

[82] Lyklema J. *"Fundamentals of Interface and Colloid Science: Volume 1"* **2000** *Academic Press*.

[83] Haram S. K., Quinn B. M., Bard A. J. *"Electrochemistry of CdS Nanoparticles: A Correlation between Optical and Electrochemical Band Gaps"* **2001** *J. Am. Chem. Soc.* 123, 8860-8861.

[84] Friend R. H., Gymer R. W., Holmes A. B, Burroughes J. H., Marks R. N., Taliani C., Bradley D. D. C., Dos Santos D. A., Brédas J. L., Lögdlung M., Salanek W. R. *"Electroluminescence in conjugated polymers"* **1999** *Nature* 397, 121-128.

[85] Schlamp M. C., Peng X., Alivisatos A. P. *"Improved efficiencies in light emitting diodes made with CdSe(CdS) core/shell type nanocrystals and a semiconducting polymer"* **1997** *J. Appl. Phys.* 82, 5837-5842.

[86] Mattoussi H., Radzilowski L. H., Dabbousi B. O., Thomas E. L., Bawendi M. G., Rubner M. F. *"Electroluminescence from heterostructures of poly(phenylene vinylene) and inorganic CdSe nanocrystals"* **1998** *J. Appl. Phys.* 83, 7965-7974.

[87] Colvin V. L., Schlamp M. C., Alivisatos A. P. *"Light-emitting diodes made from cadmium selenide nanocrystal"* **1994** *Nature* 370, 354-357.

[88] Cheng C. "*A Multiquantum-Dot-Doped Fiber Amplifier With Characteristics of Broadband, Flat Gain, and Low Noise"* **2008** *Journal of Lightwave Technology* 26, 1404-1410.

[89] Kershaw S. V., Harrison M., Rogach A. L., Kornowski A. *"Development of IR-Emitting Colloidal II–VI Quantum-Dot Materials"* **2000** *IEEE Journal of Selected Topics in Quantum Electronics* 6, 534-543.

[90] Hotchandani S., Kamat P.V. *"Charge-transfer processes in coupled semiconductor systems. Photochemistry and photoelectrochemistry of the colloidal cadmium sulfide-zinc oxide system"* **1992** *J Phys. Chem*. 96, 6834-6839.

[91] Vogel R., Hoyer P., Weller H. *"Quantum-Sized PbS, CdS, Ag_2S, Sb_2S_3, and Bi_2S_3 Particles as Sensitizers for Various Nanoporous Wide-Bandgap Semiconductors"* **1994** *J. Phys. Chem.* 98, 3183-3188.

[92] Greenham N. C., Peng X., Alivisatos A. P. *"Charge separation and transport in conjugated-polymer/semiconductor-nanocrystal composites studied by photoluminescence quenching and photoconductivity"* **1996** *Phys. Rev. B* 54, 17628-17637.

[93] Huynh W. U., Dittmer J. J., Alivisatos A. P. *"Hybrid Nanorod-Polymer Solar Cells"* **2002** *Science* 295, 2425-2427.

[94] Chusuei C.C., Lai X., Luo K., Goodman D.W. *"Modeling heterogeneous catalysts: metal clusters on planar oxide Supports"* **2001** *Top. Catal.* 14, 71-83.

[95] Thomas J. M., Raja R. *"Nanopore and Nanoparticle Catalysts"* **2001** *Chem. Rec.* 1, 448-466.

[96] Thomas J. M., Johnson B. F. G., Raja R., Sankar G., Midgley P. A. *"High-Performance Nanocatalysts for Single-Step Hydrogenations"* **2003** *Acc. Chem. Res.* 36, 20-30.

[97] Moiseev I. I., Vargaftik M. N. *"Clusters and Colloidal Metals in Catalysis"* **2002** *Russ. J. Chem.* 72, 512-522.

[98] Narayanan R., El-Sayed M. A. *"Effect of Catalysis on the Stability of Metallic Nanoparticles: Suzuki Reaction Catalyzed by PVP-Palladium Nanoparticles"* **2003** *J. Am. Chem. Soc.* 125, 8340-8347.

[99] Murphy L. *"Biosensors and bioelectrochemistry"* **2006** *Current Opinion in Chemical Biology* 10, 177-184.

[100] Catterall R.W. *"Chemical Sensors"* **1997,** Oxford, UK: Oxford University Press.

[101] Thevenot D. R., Toth K., Durst R. A., Wilson G. S. *"Electrochemical Biosensors: Recommended Definitions and Classification (Technical Report)"* **1999** *Pure Appl. Chem.* 71, 2333-2348.

[102] Mairal T., Özalp V. C., Sánchez P. L., Mir M., Katakis I., O'Sullivan C. K. *"Aptamers: molecular tools for analytical applications"* **2008** *Anal. Bioanal. Chem.* 390, 989-1007.

[103] Eggins B. R. *"Chemical Sensors and Biosensors. Analytical Techniques in the Sciences*" **2002** ed. D. J. Ando., Northern Ireland, UK: *John Wiley & Sons*.

[104] Luppa P. B., Sokoll L. J., Chan D. W. *"Immunosensors—principles and applications to clinical chemistry"* **2001** *Clin. Chim. Acta* 314, 1-26.

[105] Shankaran D. R., Gobi K. V., Miura N. *"Recent advancements in surface plasmon resonance immunosensors for detection of small molecules of biomedical, food and environmental interest"* **2007** *Sensors and Actuators B* 121, 158-177.

[106] Jung J. W., Jung S. H., Yoo J. O., Suh I. B., Kim Y. M., Ha K. S. *"Label-free and quantitative analysis of C-reactive protein in human sera by tagged-internal standard assay on antibody arrays"* **2009** *Biosensors and Bioelectronics* 24, 1469-1473.

[107] Wang Z. H., Meng Y. H., Ying P. Q., Qi C., Jin G. *"A label-free protein microfluidic array for parallel immunoassays"* **2006** *Electrophoresis* 27, 4078-4085.

[108] Okuno J., Maehashi K., Kerman K., Takamura Y., Matsumoto K., Tamiya E. *"Label-free immunosensor for prostate-specific antigen based on single-walled carbon nanotube array-modified microelectrodes"* **2007** *Biosensors and Bioelectronics* 22, 2377-2381.

[109] Higashi Y., Ikeda Y., Yamamoto R., Yamashiro M., Fujii Y. *"Pharmacokinetic interaction with digoxin and glucocorticoids in rats detected by radio-immunoassay using a novel specific antiserum"* **2005** *Life Sciences* 77, 1055-1067.

[110] Grulke S., Deby-Dupont G., Gangl M., Franck T., Deby C., Serteyn D. *"Equine trypsin: purification and development of a radio-immunoassay"* **2003** *Vet. Res.* 34, 317-330.

[111] Rasmussen P. H., Nielsen M. D., Giese J. *"Solid-phase double-antibody radio-immunoassay for atrial natriuretic factor"* **1990** *Scan. J. Clin. Lab. Invest.* 50, 319-324.

[112] Ishikawa S., Hashida S., Hashinaka K., Ishikawa E. *"Rapid and Ultrasensitive Enzyme Immunoassay (Thin Aqueous Layer Immune Complex Transfer Enzyme Immunoassay) for HIV-1 p24 Antigen"* **1998** *J. Clin. Lab. Anal.* 12, 205-212.

[113] Yang X., Janatova J., Andrade J. D. *"Homogeneous enzyme immunoassay modified for application to luminescence-based biosensors"* **2005** *Anal. Biochem.* 336, 102-107.

[114] Kamahori M., Ishige Y., Shimoda M. *"A novel enzyme immunoassay based on potentiometric measurement of molecular adsorption events by an extended-gate field-effect transistor sensor"* **2007** *Biosensors and Bioelectronics* 22, 3080-3085.

[115] Choi S., Choi E. Y., Kim D. J., Kim J. H., Kim T. S., Oh S. W. *"A rapid, simple measurement of human albumin in whole blood using a fluorescence immunoassay (I)"* **2004** *Clin. Chim. Acta* 339, 147-156.

[116] Yang H. H., Zhu Q. Z., Qu H. Y., Chen X. L., Ding M. T., Xu J. G. *"Flow injection fluorescence immunoassay for gentamicin using sol-gel-derived mesoporous biomaterial"* **2002** *Anal. Biochem.* 308, 71-76.

[117] Zhu S., Zhang Q., Guo L. H. *"Part-per-trillion level detection of estradiol by competitive fluorescence immunoassay using DNA/dye conjugate as antibody multiple labels"* **2008** *Anal. Chim. Acta* 624, 141-146.

[118] Cadieux B., Blanchfield B., Smith J. P., Austin J. W. *"A rapid chemiluminescent slot blot immunoassay for the detection and quantification of Clostridium botulinum neurotoxin type E, in cultures"* **2005** *International Journal of Food Microbiology* 101, 9-16.

[119] Lin Zhen, Wanga X., Li Z. J., Rena S. Q., Chen G. N., Ying X. T., Lin J. M. *"Development of a sensitive, rapid, biotin–streptavidin based chemiluminescent enzyme immunoassay for human thyroid stimulating hormone"* **2008** *Talanta* 75, 965-972.

[120] Yang Z., Fu Z., Yan F., Liu H., Ju H. *"A chemiluminescent immunosensor based on antibody immobilized carboxylic resin beads coupled with micro-bubble accelerated immunoreaction for fast flow-injection immunoassay"* **2008** *Biosensors and Bioelectronics* 24, 35-40.

[121] Ohkuma H., Abe K., Kosaka Y., Maeda M. *"Simultaneous assay of pepsinogen I and pepsinogen II in serum by bioluminescent enzyme immunoassay using two kinds of Luciola lateralis luciferase"* **1999** *Anal. Chim. Acta* 395, 265-272.

[122] Jackson R. J., Fujihashi K., Kiyono H., McGhee J. R. *"Luminometry: a novel bioluminescent immunoassay enhances the quantitation of mucosal and systemic antibody responses"* **1996** *Journal of Immunological Methods* 190, 189-197.

[123] Frank L., Markova S., Remmel N., Vysotski E., Gitelson I. *"Bioluminescent signal system: bioluminescence immunoassay of pathogenic organisms"* **2007** *Luminescence* 22, 215-220.

[124] Dequaire M., Degrand C., Limoges B. *"An Electrochemical Metalloimmunoassay Based on a Colloidal Gold Label"* **2000** *Anal. Chem.* 72, 5521-5528.

[125] Chu X., Fu X., Chen K., Shen G.-L., Yu R.-Q. *"An electrochemical stripping metalloimmunoassay based on silver-enhanced gold nanoparticle label"* **2005** *Biosens. Bioelectron*. 20, 1805-1812.

[126] Ozsoz M., Erdem A., Kerman K., Ozkan D., Tugrul B., Topcuoglu N., Ekren H., Taylan M. *"Electrochemical Genosensor Based on Colloidal Gold Nanoparticles for the Detection of Factor V Leiden Mutation Using Disposable Pencil Graphite Electrodes"* **2003** *Anal. Chem.* 75, 2181-2187.

[127] Wang J., Xu D. A., Kawde N., Polsky R. *"Metal Nanoparticle-Based Electrochemical Stripping Potentiometric Detection of DNA Hybridization"* **2001** *Anal. Chem.* 73, 5576-5581.

[128] Wang J., Polsky R., Xu D. *"Silver-Enhanced Colloidal Gold Electrochemical Stripping Detection of DNA Hybridization"* **2001** *Langmuir* 17, 5739-5741.

[129] Wang J., Xu D., Polsky R. *"Magnetically-Induced Solid-State Electrochemical Detection of DNA Hybridization"* **2002** *J. Am. Chem. Soc.* 124 , 4208-4209.

[130] Park S. J., Taton T. A., Mirkin C. A. *"Array-Based Electrical Detection of DNA with Nanoparticle Probes"* **2002** *Science* 295, 1503-1506.

[131] Wang J., Liu G., Polsky R., Merkoçi A. *"Electrochemical stripping detection of DNA hybridization based on cadmium sulfide nanoparticle tags"* **2002** *Electrochem. Commun.* 4, 722-726.

[132] Wang J., Liu G., Merkoçi A. *"Particle-based detection of DNA hybridization using electrochemical stripping measurements of an iron tracer"* **2003** *Analytica Chimica Acta* 482, 149-155.

[133] Xu Y., Cai H., He P. G., Fang Y. Z. *"Probing DNA Hybridization by Impedance Measurement Based on CdS-Oligonucleotide Nanoconjugates"* **2004** *Electroanalysis* 16, 150-155.

[134] Kawde A. N., Wang J. *"Amplified Electrical Transduction of DNA Hybridization Based on Polymeric Beads Loaded with Multiple Gold Nanoparticle Tags"* **2004** *Electroanalysis* 16, 101-107.

[135] Oyama T., Rombel I. T., Samli K. N., Zhou X., Brown K. C. *"Isolation of multiple cell-binding ligands from different phage displayed-peptide libraries"* **2006** *Biosensors and Bioelectronics* 21, 1867-1875.

[136] Tan L., Jia X., Jiang X., Zhang Y., Tang H., Yao S., Xie Q. *"Real-time monitoring of the cell agglutination process with a quartz crystal microbalance"* **2008** *Analytical Biochemistry* 383, 130-136.

[137] Whelan R. J., Zare R. N. *"Single-cell immunosensors for protein detection"* **2003** *Biosensors and Bioelectronics* 19, 331-336.

[138] Curtis T., Naal R. M. Z. G., Batt C., l Tabb J., Holowka D. *"Development of a mast cell-based biosensor"* **2008** *Biosensors and Bioelectronics* 23, 1024-1031.

Chapter 2

Objectives

Chapter 2 Objectives

The general objective of this thesis is to synthesize and characterize nanoparticles for their use as labels in affinity biosensors based on electrochemical detection with interest for application in DNA hybridization detection and cells studies.

In order to fulfill this general objective, the following particular ones were established:

1. To synthesize and characterize nanoparticles those are soluble in aqueous media and have electrochemical activity that would make them useful to be applied as labels in affinity electrochemical biosensors.

1.1 To evaluate different synthesis alternatives for nanoparticles. Use of arrested precipitation and reverse micelles methods.

1.2 To characterize the obtained nanoparticles through the use of various techniques such as a TEM, XRD, AFM, Zpotential and electrochemical analysis.

1.3 To evaluate and select the best nanoparticles to be used in electrochemical biosensing systems

2. To develop a new electrochemical detection strategy for QDs, without previous chemical dissolving step, using square wave voltammetry and screen printed electrodes (SPEs) in connection to a portable potentiostatic measuring system.

2.1 To optimize the volume and the pH of the QDs suspension as well as the electrochemical parameters such as the frequency of the pulse, the modulation amplitude, deposition potential etc.

2.2 To evaluate the analytical performance of the QDs detection by using the developed technique.

3. To design and develop a genosensor based on SPEs (integrating a magnet under the surface of the working electrode) able to collect paramagnetic microparticles modified with DNA molecules labeled with QDs and use of the electrochemical stripping analysis without previous dissolving as a measuring technique.

3.1 To evaluate the specificity of the DNA assay and solve the nonspecific adsorption problems by using blocking agents.

3.2 To evaluate the performance of the designed genosensor (operational range, detection limit, etc.)

4. To apply the developed QDs and the direct electrochemical detection technique with SPE for cell detection.

4.1 To conjugate QDs with a peptide and evaluate its possibility to be used in the future as model vehicle that can cross the cell membrane.

4.2 To evaluate the electrochemical detection of HeLa cells interaction with QDs modified with peptide and compare the results obtained with confocal light scanning microscopy.

Chapter 3

Synthesis of nanoparticles

Chapter 3 Synthesis of nanoparticles

3.1 Synthesis of quantum dots (QDs)

3.1.1 Introduction

The previous reported synthesis of semiconductor nanoparticles are based organometallic thermolysis[1], but the quantum dots obtained are not water-dispersed and the bioanalysis applications want to be in aqueous media. For this reason organometallic thermolysis methods need a solubilization step[2]. Nowadays, QDs are synthesized by aqueous methods by reverse micelles methods[3].

The potential benefits and use of conjugated QDs probes for various applications in biomedicine in general, and in the field of biosensors in particular, has prompted extensive efforts to develop methods to synthesize water-dispersed and biocompatible QDs.

The aim of this chapter is to present and highlight various synthetic strategies for obtaining water dispersed CdS QDs, optically characterize them and then develop a simple and direct mode for electrochemical detection.

Herein we describe and discuss the current use of chemical methods such as those based on either reverse micelles or arrested precipitation to prepare water dispersed CdS QDs. Aspects related to crystal characterization as well as the possibility for the direct electrochemical detection of the obtained QDs will be shown. While the electrochemistry of QDs is usually focused on organic solvents such as N,Ndimethylformamide (DMF)[4], we present here for the first time a simple and efficient method for their direct detection in an aqueous medium.

The obtained material, as well as the novel electrochemical detection strategy, holds great promise for future application in genosensors and immunosensors. The CdS QDs produced as described are just an example. Other heavy metal based NCs such as PbS, ZnS or CuS can be obtained by using similar procedures. Their application in electrochemical coding technology[5] is of great importance for the development of DNA biosensors for the simultaneous detection of several DNA strands.

3.1.2 Reagents and materials

Syntheses were carried out using Schlenk techniques under nitrogen. Chemicals and solvents were used as-received from Sigma-Aldrich: cadmium perchlorate, cadmium chloride, 100% sodium dioctyl sulfosuccinate (AOT), 98% heptane, 99.9% sodium sulfide hydrate, 98% cystamine, 100% mercaptoethanosulfonate, methanol, hexamethyldisilathiane (HMSDT), 97% thioglycerol, 99% glutathione, tetramethylammoniumhydroxide (TMAH) and ethanol. Pyridine, tetrahydrofuran, hydrochloric acid, nitric acid and acetone were from Panreac (Spain).

Electrochemical measurements solution was composed by 10 ml HCl 0.1 M and 250 µl of HNO_3 1 M.

3.1.3 Equipment

Transmission electron microscopy (TEM) was performed on a JEOL JEM-2010.

The X ray diffraction (XRD) was performed on a Bruker D8 Discover Siemens EM-10110BU model D5000.

Differential pulse voltammetry (DPV) was performed with an electrochemical analyzer Autolab PGSTAT 20 (Eco Chemie, The Netherlands) connected to a personal computer. Electrochemical measurements were carried out in a 10 ml voltammetric cell at room temperature (25 ◦C). The electrode system consisted of a platinum wire that served as an auxiliary electrode, an Ag/AgCl as reference (obtained in CH Instrument) electrode and working electrode ($Bi(NO_3)_3$-GECE) used for the stripping analysis. The working electrode was based on a graphite–epoxy composite electrode (GECE) mixed with the bismuth nitrate salt. It was prepared as reported previously[6]. The percentage of $Bi(NO_3)_3$ in the prepared composite was 2.0% (w/w).

Atomic force microscopy (AFM) images were obtained by a PicoSPM, Molecular Imaging (from Canada).

3.1.4 Synthesis of QDs by reverse micelles methods

3.1.4.1 Method 1

This method is based on the interaction of two reverse micelle solutions. According to this method an AOT/n-heptane water-in-oil microemulsion was prepared by the solubilization of 4 ml of double distilled water in 200 ml n-heptane in the presence of 14 g of AOT surfactant. The resulting mixture was separated into 120 and 80 ml sub-volumes of reverse micelles where 0.48 ml of 1.0 M $Cd(ClO_4)_2$ and 0.32 ml of 1.0M Na_2S solutions, respectively, were added into the 120 and 80 ml sub-volumes of reverse micelles. The two sub-volumes were then mixed under nitrogen for 1 h. The appearance of a fluorescent yellow indicates the formation of the CdS QDs . After that, the formed QDs underwent two modifications: (a) modification by adding 0.12 ml of thioglycerol; (b) modification by adding 0.66 ml of 0.32 M mercaptoethanosulfonate and 0.34 ml of 0.32 M cystamine solutions. In both cases the resulting mixture was then stirred for 24 h under nitrogen. It was subsequently evaporated under vacuum and the residue successively washed with pyridine, n-heptane, acetone and methanol by means of ultracentrifugation. Methanol instead of tetrahydrofuran was used in the case of modification by thioglycerol.

Two kind of water-dispersed CdS nanoparticles covered either by cystamine and mercaptoethanosulfonate or by thioglycerol (figure 3.1 A&B) were obtained.

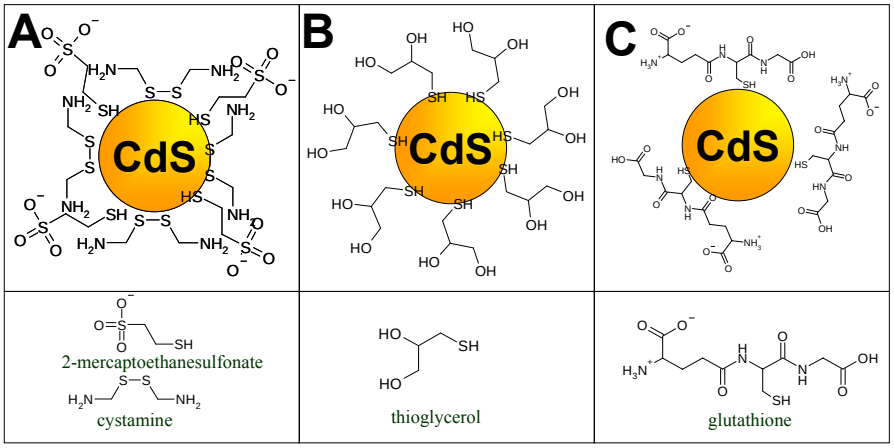

Figure 3.1 Schematic of CdS QDs coated with : A) mercaptoethanosulfonate and cystamine. B) thioglycerol and C) glutathione. The shown sizes are not in scale.

3.1.4.2 Method 2

In this method HMSDT was used as an organometallic reagent to generate sulfide ions[7] instead of sodium sulfide micelles (method 1). HMSDT was added directly to the $Cd(ClO_4)_2$ micelle solution (prepared as in method 1), avoiding the reaction between two micelle solutions as in method 1.

The $Cd(ClO_4)_2$ reverse micelle solution was prepared in the following way: 13 g AOT, 500 ml n-heptane, 1.7 ml of double distilled water and 0.44 ml of 1 M $Cd(ClO_4)_2$ solution were mixed well. A solution of 50 ml n-heptane containing 0.05 ml of HMSDT was then quickly added. The resulting mixture was stirred for 1 h under nitrogen. The appearance of a fluorescent yellow indicates the formation of CdS QDs as in method 1. The water dispersed thiol-capped CdS QDs were then prepared as described in method 1.

3.1.5 Synthesis of QDs by arrested precipitation (method 3)

This method is based on arrested precipitation of water dispersed cadmium with sulfide precursors[8]. According to this method 3.228 g glutathione as modifier and 0.799 g $CdCl_2$ were first dissolved in 176 ml water and stirred for 5 min. Subsequently, 8.5 ml TMAH and 315 ml ethanol were added and after 10 min the precursor solution was thoroughly degassed. HMDST (0.738 ml) was added quickly to the degassed precursor solution giving a clear (slightly yellow) colloidal solution of glutathione-coated CdS nanoparticles (see figure 3.1 C). The mixture was magnetically stirred for 1 h and the prepared particles were precipitated by adding tetrahydrofuran (THF). One day later the supernatant was decanted and the precipitate was dissolved in a water/THF mixture and precipitated again with THF to remove excessive reagents and reaction by products. Finally, the supernatant liquid was decanted and the precipitate was dried under vacuum (<1 mbar). The powdery CdS nanoparticles were dissolved again in water, giving a clear colloidal solution.

3.1.6 Characterization

3.1.6.1 Optical

To obtain the TEM images a drop of the nanoparticle solution on a 3 mm copper grid covered with carbon film was firstly introduced. The excess film was removed with an absorbent paper. The following parameters were applied: Operating at 200 kV. The objective lens parameters of JEM-2010 (Cs D 0.5 mm and Cc D 1.0 mm) and an interpretable point resolution of <0.2 nm.

X-ray powder diffraction patterns were recorded using Cu Kα radiation. Solid nanocrystals were placed on quartz plates for measurement. The measurements were performed the 0 to 60 2θ.

For AFM the samples were prepared by adding a drop of nanoparticle supension onto the silica wafer while spinning at 4000 rpm in the clean room. The following parameters were applied: Using a tapping mode and a silicon tip (NCH, fo= 280-365 kHz) (Nanosensors). Amplitude set point 1.8-2.0 V. The height is the reliable parameter for measuring the particle size. The width is a convolution between tip and sample and size distribution was calculated.

3.1.6.2 Electrochemical detection

The proposed protocol for detection of CdS QDs is similar to the detection protocol for Au nanoparticles described previously by our group[9]. It involves adsorption of CdS QDs (glutathione modified CdS obtained according to method 3) onto the surface of the $Bi(NO_3)_3$-GECE and the subsequent electrochemical stripping detection of the adsorbed QDs in a mixture of HCl and HNO_3. The final measurements employed a background subtraction protocol involving storing the response for the blank solution and subtracting it from the analytical signal.

The $Bi(NO_3)_3$-GECE in an open circuit (figure 3.2 A) was immersed in a solution containing an appropriate concentration of CdS QDs for 10 min. After the accumulation step, the electrode was carefully washed with distilled water before being immersed into a voltammetric cell containing 10 ml of 0.1 M HCl and 250 µl of 1 M nitric acid. The

electrochemical reduction of CdS QDs to Cd(0) was performed at −1.4 V (versus Ag/AgCl) for 120 s in an unstirred solution (figure 3.2 B). Immediately after the electrochemical reduction step, differential pulse voltammetry (DPV) was performed. During this step (figure 3.2 C) the potential was scanned from −0.83 to −0.43 V (step potential 10 mV, modulation amplitude 50 mV, scan rate 33 mV s^{-1}; unstirred solution), resulting in an analytical signal due to reoxidation of Cd(0) to Cd^{2+}.

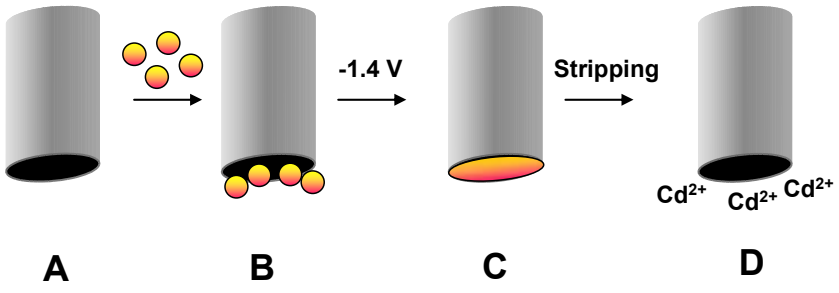

Figure 3.2 Schematic of the electrochemical detection scheme used for CdS QDs. The graphite–epoxy composite electrode ($Bi(NO_3)_3$-GECE) is incubated for 10 min in a solution containing CdS QDs (A). The $Bi(NO_3)_3$-GECE that contains CdS QDs is then polarized at −1.4 V which leads to the formation of a reduced Cd^0 layer (B) which is then reoxidized to Cd^{2+}(C).

3.1.7 Results and discussion

A detailed description of the obtained results is given in the published article[10]. In brief, the results are described and discussed in the following sections:

Generation of CdS QDs The methods based on reverse micelles exploit natural geometrical structures created by water-in-oil mixtures upon adding an amphiphilic surfactant such as AOT. By varying the water content of the mixture, it was shown that the size of the water droplets suspended in the oil phase could be varied systematically. The water-in-oil reverse micelles are characterized by ω_0, the molar ratio of water/surfactant (S): $\omega_0 = [H_2O]/[S]$. The size of the water pool at the reverse micelle core can be carefully controlled by adjusting the $[H_2O]/[S]$ ratio[11].

The shown schematics of Figure 3.3 A & B correspond to CdS QD formation until the state when the AOT surfactant is still covering the surfaces. The substitution of AOT with thiol protector groups is not shown.

The generation of CdS QDs according to method 1 (see figure 3.3 A) happens after the collision between two AOT reverse micelles: the Cd^{2+} one with thus of S^{2-}. The collisions between the two micelles result in the formation of a short lived dimer formed by expulsion of some AOT molecules into the bulk heptane phase (figure 3.3 A). During the lifetime of the dimer, the two reverse micelles exchange the contents (S^{2-} and Cd^{2+}) of their aqueous cores before decoalescing, resulting in the eventual equilibrium and distribution of all contents. Since the size of the water pools in reverse micelles can be controlled by adjusting the ω_0, the above micelle interaction model corresponds to that of a nanoreactor reported earlier . Nevertheless, the reaction dynamics of the microemulsions are still not fully understood. The formed CdS QDs coming from the intermediate (dimer) nanocrystal covered with AOT were subject of further surface modification as described in the experimental part (not shown in the schematic of figure 3.3 A).

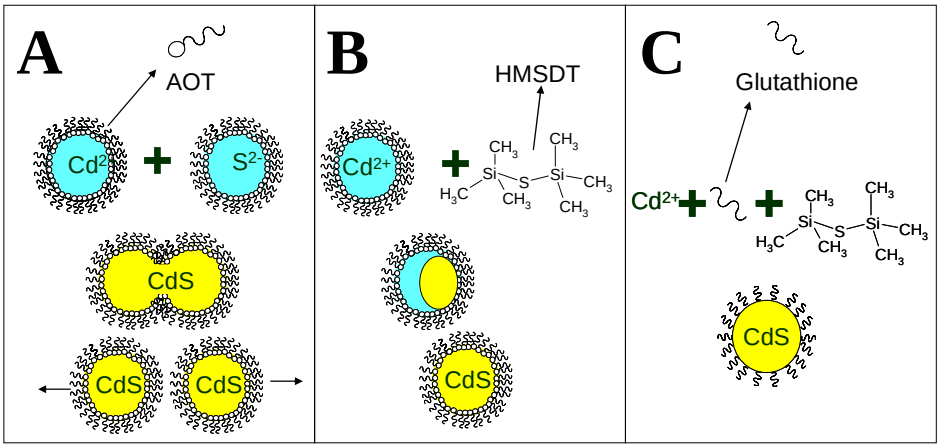

Figure 3.3 Schematic representation of generation's mechanism for CdS QDs according to method 1 (A), 2 (B) and 3 (C). Shown are the schematic of the AOT molecules used in the micelles of method 1 & 2 along with the molecular formula of the hexamethildisilathiane (HMSDT) used in the method (2) and the thiol glutathione modifiers used for CdS QDs obtained according to the method 3.

In method 2, the addition of the sulfide generator, in that case HMSDT, is substituting the use of a second micelle. This sulfide generator reacts directly with the Cd (II) AOT micelle which serves at the same time as a nanoreactor moulding the formed CdS QDs (figure 3.3 B).

Controlled or arrested precipitation reactions can yield dilute suspensions of quasi monodispersed particles. This precipitation strategy is followed in method 3. The sulfide generator HMSDT, as in method 2, acts as a precipitant of the Cd (II) from its chloride solution in the presence of glutathione thiol. The stability of the initially formed small crystallites is influenced by the dynamic equilibrium illustrated by

$$(CdS)_{crystal} \leftrightarrow (Cd^{2+})_{solv} + (S^{2-})_{solv.} \qquad (3.1)$$

Small crystallites are less stable than larger ones and tend to dissolve into their respective ions. Subsequently, the dissolved ions can recrystallize on larger crystallites which are thermodynamically more stable. The generated CdS QDs are passivated by being covered immediately with them glutathione thiol protective groups, preventing their further growth (figure 3.3 C).

Optical characterization. CdS QDs obtained by method 1 show an average size in the range of 3-4 nm (figure 3.4 A) Each CdS particle shows well-defined lattice fringes which indicate that the particles are highly crystallized even at such small size.

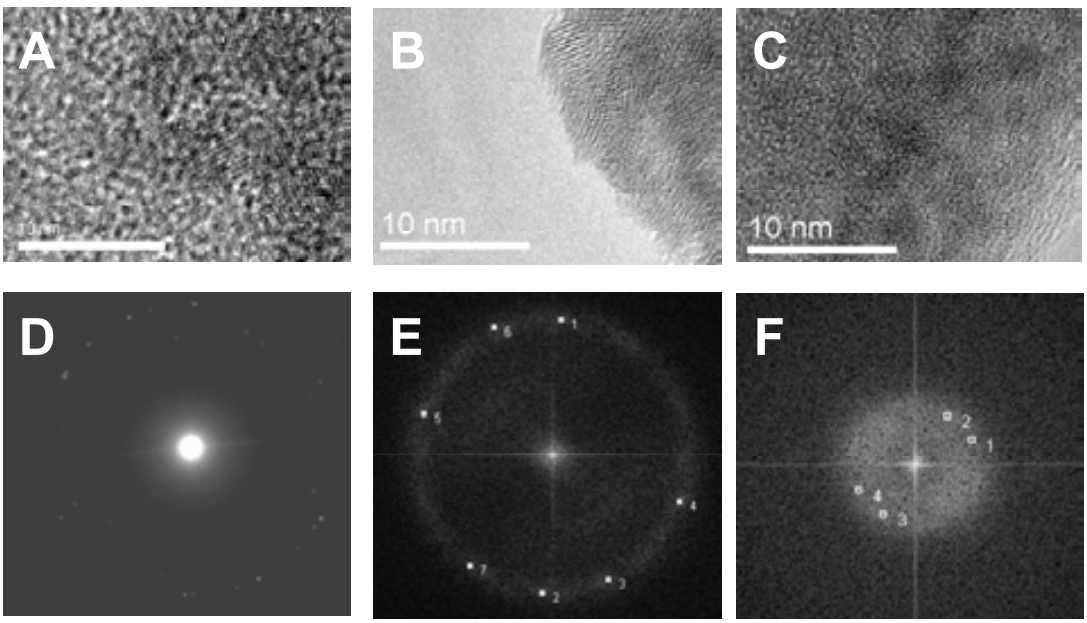

Figure 3.4 HRTEM (A,B,C), and Fourier transform images (D,E,F) of CdS QDs prepared by the method 1 (A,D), 2 (B,E) and 3 (C,F). CdS QDs prepared as described in the text.

The HRTEM image (figure 3.4 B) of CdS nanoparticles recovered with thioglycerol shows spherical particles of 2–3 nm in size; these are smaller than the CdS produced by method 1 (3–4 nm). The crystallinity of the produced material is also shown by clear lattice fringes of single CdS dots like those produced by method 1 (figure 3.4 A).

In method 3 the average of CdS QDs obtained was in the range of 3-4 nm (figure 3.4 C). This was confirmed also by AFM image (figure 3.5) giving an average range of 4 nm. The lattice fringes are less defined than the others CdS QDs obtained by reverse micelles methods (figure 3.4 A&B). This suggests that the QDs obtained according to method 3 were more amorphous than those obtained with the other methods. The same amorphous aspects were observed for the CdSe synthesized using the thermolytic method[12] with a 10 min particle formation time instead of 90 min that gave a well crystallized and fringed lattice structure.

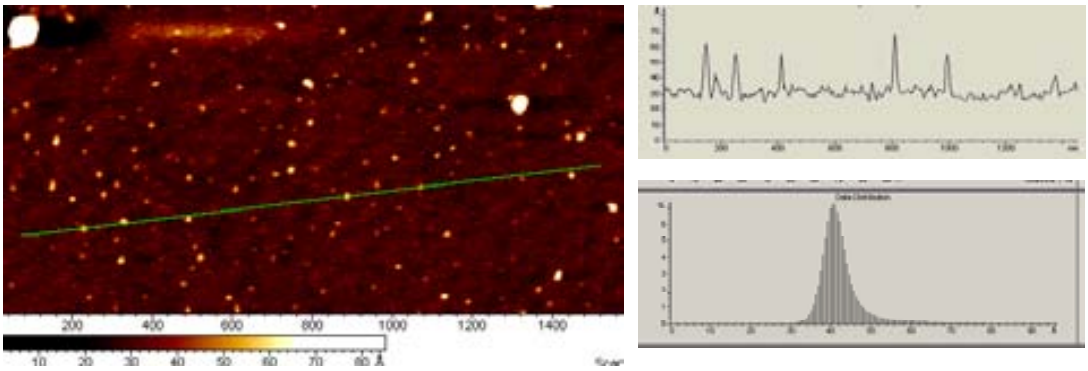

Figure 3.5 AFM image (Tapping mode) of CdS QDs obtained by the method 3 using a silicon tip (NCH, fo= 280-365 kHz) (Nanosensors). Amplitude set point 1.8-2 V. The height is the reliable parameter for measuring the particle size. The width is a convolution between tip and sample and size distribution was calculated.

The Fourier transform (FT) of the experimental images (figures 3.4 (D), (E) and (F)) of the CdS QDs obtained with methods 1, 2 and 3, respectively, are also presented. The white dots correspond to the crystalline planes of the CdS QDs obtained by methods 1, 2 and 3, respectively. FT data for each dot were calculated. The d-spacings (0.33 nm) of similar order to those obtained by Kadirgan et al[13] demonstrate the presence of hexagonal phase cadmium sulfide obtained by methods 1, 2 and 3. (See more details at supporting information of article)

Characterization by XRD. As already demonstrated, the obtained CdS QDs seem to be closed packed. Assuming this fact, the reflection in the small angle regime can be correlated with lattice planes through the mass particles' centers[14].

The diffraction patterns (figure 3.6) of CdS QDs show typical features of nanodimensional particles. Nevertheless, comparing the three patterns of CdS QDs we can conclude that in the three cases the peaks (in the region $d\theta \approx 25\text{-}30^{o}$) related to the crystalline planes of the cadmium sulfide structure are not observed. The (110), (103) and (112) planes of wurzite CdS[15] are not well defined (see figure 3.6, appearing as broad peaks. There might be two reasons for the absence of sharp peaks[16]: firstly, due to the very small size of the particles (4 nm) obtained in each of the three methods, the intensity of reflections (figures 3.6) in the wide angle region of the diffraction patterns is broadened and secondly, due to impurities such as silicon byproducts from HMSDT used in the in situ generation of the sulfide ions. Similar results were also obtained by Weller et al[17]. According to Weller et al, a clear identification of the crystalline structure was not possible, maybe due to the small particle size; the identification was easier for bigger QDs.

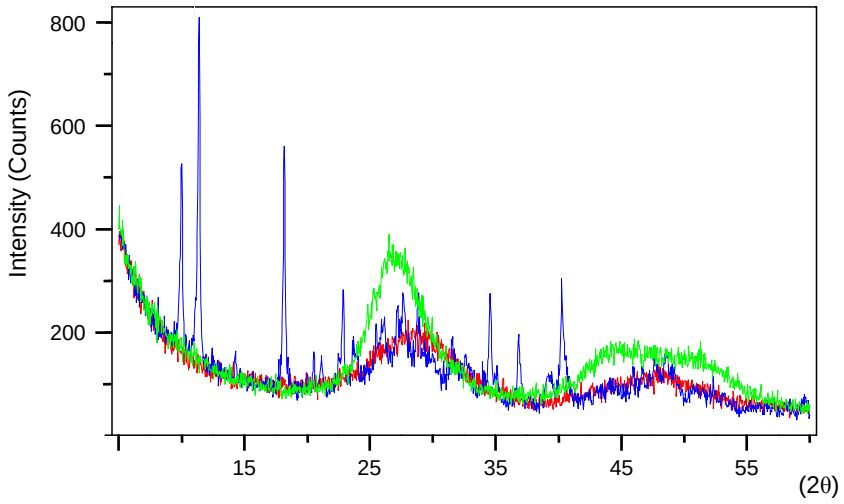

Figure 3.6 Powder X-ray diffraction patterns of CdS QDs prepared using methods 1 (green), 2 (blue) and 3 (red).

Electrochemical detection of CdS QDs . Figure 3.7 shows the proposed mechanism for the direct detection of CdS QDs using the $Bi(NO_3)_3$-GECE. The built-in bismuth property is the distinctive feature of this $Bi(NO_3)_3$ modified GECE which is used for the generation of bismuth adjacent to the electrode surface. The $Bi(NO_3)_3$-GECE ensures in situ generation of bismuth ions and film formation without the need for external addition of

bismuth in the measuring solution. The rich microstructure of $Bi(NO_3)_3$-GECE, composed of a mixture of carbon microparticles within the epoxy-resin forming internal microarrays, might have a profound effect not only on the NC adsorption (as in the case of gold nanoparticles) but also upon the formation of Cd film and consequently its stripping, producing a high sensitivity analytical signal.

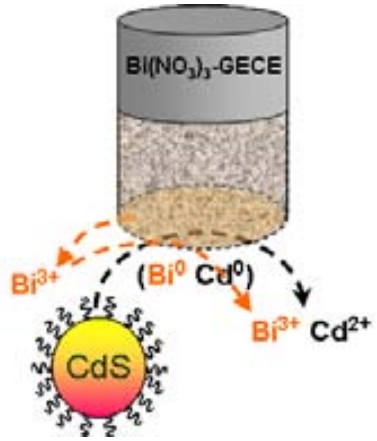

Figure 3.7 Proposed schematic of the electrochemical detection of CdS QDs. Bi^{3+} is released from the surface of the electrode and reduced back to Bi^0 together with the Cd^{3+} (defects) to Cd^0. During the stripping process both Bi^{3+} and Cd^{2+} are released.

In analogy with the electrochemistry of PbS nanocrystals in aqueous solution[18], a cathodic reduction that depends on the pH of the solution occurs:

$$CdS + 2H^+ + 2e \rightarrow Cd^0 + H_2S \quad (3.2)$$

The CdS QDs are reduced in this way to Cd^0 while a potential of -1.4 V is applied for 120 s. After this 'preconcentration' redissolution of the formed Cd^0 occurs, giving a DPV response that depends on the quantity of CdS QDs .

Various relevant parameters influencing the analytical DPV response of the CdS QDs were investigated and the optimal parameters obtained were: 10 min of CdS QDs incubation; -1.4 V of deposition potential and 120 s of deposition potential (see more details at section 3.4 in the published article).

The $Bi(NO_3)_3$-GECE based protocol for detection of CdS QDs shows a defined concentration dependence. Typical DPASV curves for increasing concentrations of CdS QDs are shown in figure 3.8. The corresponding calibration plot for CdS QDs is also shown,

and is linear over the range from 0.5 * 10^{16} to 2.0 * 10^{17} CdS QDs cm^{-3} with a sensitivity of 10^{-16} (μA cm^3/nanoparticle) and an intercept of 18.9 μA (correlation coefficient 0.997). The detection limit, based on a S/N ratio of 3, was around 10^{15} CdS QDs cm^{-3}. Favorable signal-to-noise characteristics were observed for the whole range of CdS NC concentrations. The obtained sensitivity is coupled to a good CdS QD detection reproducibility using the $Bi(NO_3)_3$-GECE. Reproducible DPV signals for CdS QDs over the entire $Bi(NO_3)_3$-GECE operation protocol were observed (RSD = 10%).

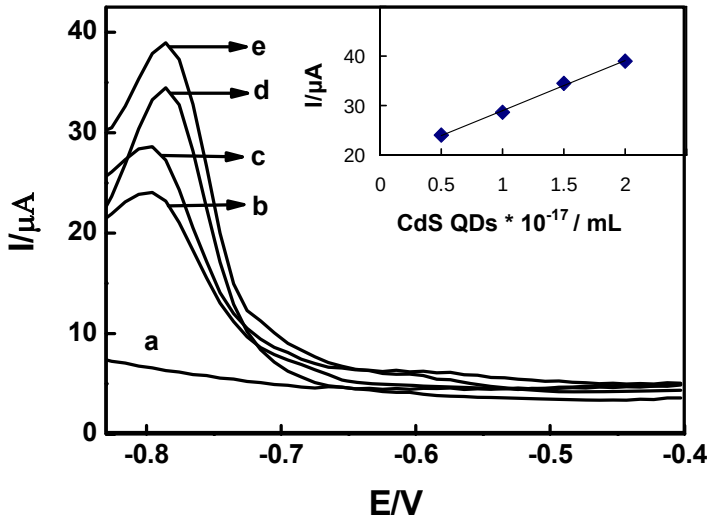

Figure 3.8 Typical DPASV curves along with the calibration curve (inset) of CdS QDs at the range concentrations 0.5 (b); 1.0 (c); 1.5 (d); 2.0 (e) *10^{17} CdS QDs / mL colloidal solution. Shown is also the blank (a). Experimental conditions as described in the text.

CdS QDs obtained according to methods 1 and 2 were also characterized using the same methods (results not shown) and similar results as those for method 3 were obtained.

3.1.8 Conclusions

CdS QDs were synthesized using templates such as reverse micelles or directly by arrested precipitation. Two kinds of water-dispersed CdS QDs covered either by cystamine and mercaptoethanosulfonate or by thioglycerol have been obtained using the reverse micelle method, while glutathione modified ones were obtained using the arrested precipitation method.

Reverse micelles method allows an easily changing of the size of nanoparticles by changing the size of micelles. However in arrested precipitation method the conditions are more restrictive. One of the drawbacks of the reverse micelles method is the difficulty to eliminate the surfactant. The XRD images show some impurities like the silica in method 2 (see figure 3.6) (due to silicon residues generated by decomposition of HMSTD). In the case of method 3 the silicon impurities were eliminated during the cleaning step. The reverse micelles method requires the use of a centrifugation process during the cleaning steps. This centrifugation can cause QDs agglomeration so decrease their solubility compared to QDs obtained by using the arrested precipitation method which requires only decanting the supernatant.

The direct electrochemical detection of the obtained CdS QDs was achieved due to the physical absorption of metal nanoparticles onto the surface of a graphite epoxy composite electrode modified with bismuth nitrate salt. The electrochemical study revealed a linear dependency of the stripping current on the CdS NC concentration. The well defined peak at around -0.78 V is attributed to the oxidation of the cadmium layer arising from the previous cathodic reduction of CdS QDs. These observations indicate that there is the possibility of directly detection of CdS QDs by using the built in bismuth precursor electrode which combines the QD adsorption properties of graphite–epoxy electrode with the stripping ability of bismuth film.

The small label size, established bioconjugation chemistry and the unusual optical and electrical properties of CdS QDs make them unique tools for DNA detection. Other QDs such as ZnS, PbS, etc. can be obtained and detected in a similar way.

The developed protocol will be of interest for DNA hybridization studies in connection with paramagnetic particles as DNA immobilization platforms[19].

3.2 Synthesis gold and silver nanoparticles including core-shell ones

3.2.1 Introduction

There is currently immense interest surrounding the synthesis and characterization of mono- and bimetallic NPs. This field presents a broad scope of research, as NPs can exhibit unusual chemical, physical and electrical properties that are not apparent in bulk

materials[20,21], as well as possessing size dependent properties and the potential for constructing nano- and micro assemblies[22]. The field of bimetallic NPs synthesis is currently an area of considerable interest, especially in the area of catalysis, where the bimetallic NPs often posses greater catalytic activity than that of their monometallic counterparts. Much work has been carried out in creating Au–Pd and Au–Pt alloys, given the relatively low reactivity of gold and the high selectivity that these catalysts posses in a wide variety of reactions, for example the hydrogenation[23]. In the last years, the most important application of colloidal gold particles have been their use as labeling biomolecules such as DNA[24,25,26], an area of much interest as NP labels present none of the associated health or waste disposal issues as their radioactive counterparts. Several applications of gold nanoparticles for DNA[19,27] and protein[28] sensing have been reported by our group. For the case of silver, a number of interesting optical properties arise from the size and shape dependence of the position and shape of the Plasmon absorption band[29]. The well known anti-bacterial properties of silver have directed research towards the development of new processes to make new antibacterial fabrics[30] and engineering new methods to inhibit microbial activity[31].

There are many known methods of NP preparation. Most reported methods detail the reduction of a metal salt by a suitable reducing agent, and by carefully controlling the reagents and reaction conditions, it is possible to direct NP formation to give a specific final size and/or shape.

In this chapter, we aim to examine a simple synthetic strategy for producing Ag and AuNPs by reduction of the metal salts $AgBF_4$ and $HAuCl_4$ by $NaBH_4$ in water. Methods for producing Au–Ag and Ag–Au alloy clusters are also examined, where the morphology is determined by the order of reactant addition.

The obtained NPs are characterized by transmission electronic microscopy (TEM) and UV–Vis absorption spectroscopy, so as to evaluate their qualities. Moreover, a direct electrochemical detection protocol that involves the use of glassy carbon electrode is also applied to characterize the prepared NPs. Cyclic voltamperometry that allows a simple and fast detection and quantification of either silver or gold NPs is used. The developed NPs and the related electroanalytical method seem to be with interest for future sensing and biosensing applications including DNA sensors and immunosensors.

3.2.2 Reagents and materials

Silver tetrafluoroborate 98%, was purchased from Aldrich. Hydrogen tetrachloroaurate (III) hydrate 99.9% was purchased from Strem Chemicals and sodium borohydride powder 98.5% was purchased from Sigma-Aldrich. Milli-Q water from ELGA Labwater system was used. Analytical grade (Merck) HCl and NH_3 and ultra-pure water have been used for the electrochemical measurements.

All reagents were used as received without any further purification. All glassware and magnetic stirrers were cleaned with aqua regia followed by copious rinsing with de-ionized water.

3.2.3 Equipment

UV-VIS Spectroscopy measurements were performed using a UV-Unicam 5625 UV-VIS spectrometer and 10 mm quartz cuvettes.

Transmission electron microscopy (TEM) was performed on a JEOL JEM-2011.

A centrifugal from Fisher Bioblock Scientific-Sigma (Germany) was used for the nanoparticles purification.

Electrochemical measurements were performed with a Compactstat potentiostat (Ivium Technologies-The Netherlands) interfaced to a personal computer. Electrochemical measurements were carried out in a 1 ml voltammetric cell at room temperature (25 º C). The electrode system consisted of a platinum wire that served as an auxiliary electrode, an Ag/AgCl as reference (obtained in CH Instrument) electrode and glassy carbon electrode as working electrode (obtained in CH Instrument).

3.2.4 Synthesis of silver nanoparticles

Water-dispersible unprotected silver nanoparticles have been prepared based on a method reported earlier by Dirk et al. (1998)[32], which involved the reduction of silver perchlorate by sodium borohydride. The procedure outlined below is adapted from the above

but using the metal salt $AgBF_4$ in place of $AgClO_4$, to see what effect (if any) changing of the anion has on NP characteristics such as size and shape.

Briefly, a typical experiment involved the required amount (usually from 1 µl to 5.08 ml, 0.295 M) of freshly prepared ice-cold aqueous $NaBH_4$ being added, under vigorous stirring, to 100 ml of Milli-Q water in an ice bath. To this, the required amount of $AgBF_4$ solution (from 1 µl to 5 ml, 0.1 M) was then added as quickly as possible via a syringe. The reaction was left under vigorous stirring for 40 min, to ensure that it continued to completion. The AgNPs were then stored in darkness to prevent precipitation.

3.2.5 Synthesis of gold nanoparticles

The gold nanoparticle solution was prepared by adapting the previous report for the synthesis of AgNPs (sect. 3.2.4 Synthesis of AgNP). Briefly, a red solution of AuNPs (representing a $HAuCl_4$ concentration of $1 * 10^{-9}$ M) was prepared first by rapid injection of 1 ml 0.01 M $HAuCl_4$ solution into 100 ml of ice-cold milli-Q water containing $3 * 10^{-4}$ l of 0.295 M $NaBH_4$ solution, then allowed to stir for 40 minutes to ensure the reaction had continued to completion. The AuNPs were then stored in darkness to prevent precipitation.

3.2.6 Synthesis of Ag-AuNPs

The Ag–AuNP suspension was prepared by reaction of a previously prepared AgNP solution (a 50 ml aliquot) with a 0.01 M $HAuCl_4$ stock solution, so as to ensure concentration ratios (Ag/Au ions): 2:1; 1:1 and 1:2.

The required volumes of $HAuCl_4$ solution (0.25, 0.5 and 1 ml from 0.01 M) were added drop wise to the 50 ml AgNP aliquots in an ice bath. The solutions were allowed to stir for 30 min to ensure complete reaction. The Ag–AuNPs were then stored in darkness to prevent precipitation.

3.2.7 Synthesis of Au-AgNPs

To a 100 mL AuNP suspension as prepared above (sect. 3.2.5 Synthesis of gold nanoparticles), 50 μL of 0.1 M $AgBF_4$ solution was added rapidly and the solution was left to stir in an ice bath for 30 min. The Au–AgNPs were then stored in darkness to prevent precipitation.

3.2.8 Characterization

3.2.8.1 Optical

To obtain the TEM images a drop of the nanoparticle solution on a 3 mm copper grid covered with carbon film was firstly introduced. The excess film was removed with an absorbent paper. The following parameters were applied: Operating at 200 kV. The objective lens parameters of JEM-2010 (Cs D 0.5 mm and Cc D 1.0 mm) and an interpretable point resolution of <0.2 nm.

UV-visible samples were diluted with milli-Q water in appropriate concentration before the measuring. Sample was added a 10 mm quartz cell (Before the measures the quartz cell was cleaned with aqua regia to eliminate the nanoparticles adsorbs in their surface). The following parameters were applied: The λ was scanning 195 to 695 nm.

3.2.8.2 Electrochemical detection

Cyclic voltammetry (CV) was the electrochemical technique used for the electrochemical detection of NPs. Before the electrochemical measurements, NPs solutions in appropriate electrolytes media were prepared. The electrolytes used were NH_3 1 M in the case of the AgNPs and HCl 0.1 M for the AuNPs detection.

AgNPs electrochemical detection was performed by immersing the three electrodes system in a stirred solution of AgNPs in NH_3 1 M, and applying a potential of -0.80 V for 60

s. After that, cyclic voltammograms were scanned from -0.80 V to 0.30 V at a scan rate of 50 mV s^{-1}.

In the case of AuNPs, the electrodes (the same as for AgNPs) were immersed in a stirred solution of AuNPs in HCl 0.1 M and held at a potential of - 0.80 V for 240 s. Then, an anodic scan was performed from -0.80 V to 1.30 V, at a scan rate of 50 mV s^{-1}. The silver and gold oxidations are observed at 0.10 and 0.95 V, respectively and constitute the analytical signals.

The negative conditioning potential is necessary in both cases to reduce the possible metal oxides on the surface of the nanoparticles and assure the maximum re-oxidation signal—the measuring signal—during the stripping step.

To prove that in all cases the analytical signal corresponds to nanoparticles and not to possible excess of metallic ions from the synthesis solutions, aliquots of 2 ml of these solutions were centrifuged at 14000 rpm for 30 min and then the supernatant was separated from the precipitated nanoparticles. The supernatant solutions were mixed with the appropriate electrolyte and measured in the same way as the NPs solutions.

3.2.9 Results and discussion

A detailed description of the obtained results is given in the published article[33]. In brief, the results are described and discussed in the following sections:

Nanoparticle generation. Four kinds of nanoparticles: AgNP, AuNP, Ag–AuNP and Au–AgNP have been synthesized and characterized using different techniques. Figure 3.9 is a schematic of the synthesis principles applied for each NP.

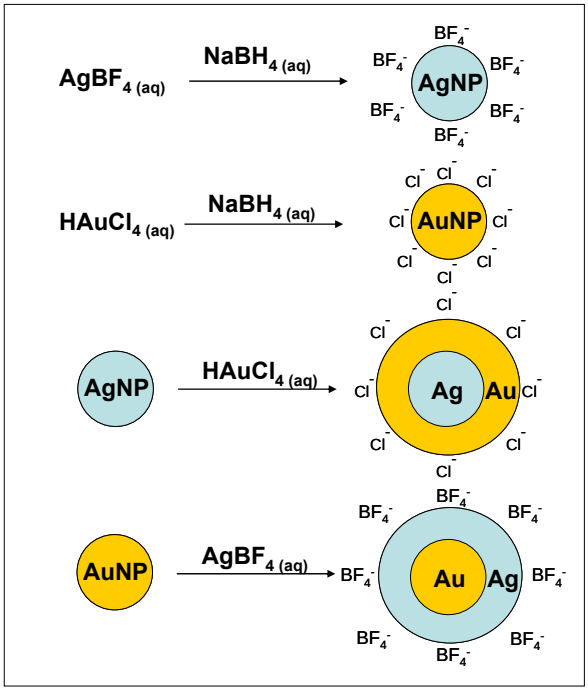

Figure 3.9 Schematic (not in scale) detailing the synthesis of the different nanoparticles.

AgNP generation. The AgNP generation method proposed avoid the use of $AgNO_3$ as silver precursor, since the presence of the NO_3^- oxidant anion on the surface of the AgNP formed could harm their future applications as labels for affinity biosensors.

Upon injection of the silver ions (as $AgBF_4$) into the ice-cold $NaBH_4$ solution, an initial aggregation stage was visible, represented by a darkening in the solution. This darkening lasted only a fraction of a second before the solution became clear again. As argued by Dirk et al. this initial aggregation could be due to the presence of small (1-3 nm), borohydride bound particles of silver. These clusters grow by an aggregative mechanism to their final sizes, giving rise to the colour changes observed.

The effect of silver ions concentration on the AgNP size was studied first (figure 3.10). It can be seen that an increase in $AgBF_4$ concentration increases both the maximum size and the range of sizes adopted by the nanoparticles formed. AgNPs were aggregated in concentrate solutions of $AgBF_4$ ($5 * 10^{-3}$ M) and the solution was precipitated. The more dilute AgNP solutions samples (representing concentrations $1 * 10^{-6}$–$1 * 10^{-5}$ M $AgBF_4$) were colorless, because the AgNPs are too diluted.

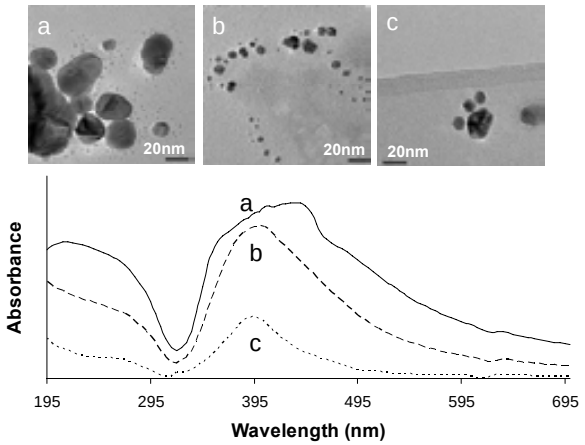

Figure 3.10 (Upper part) TEM images of AgNPs obtained from (a) 1 * 10^{-3} (b) 1 * 10^{-4} and (c) 1 * 10^{-5} M $AgBF_4$. Other experimental conditions of NP preparation as described in the text. (Lower part) UV-VIS spectra for: AgNPs corresponding to (a) 1 * 10^{-3} (b) 1 * 10^{-4} and (c) 1 * 10^{-5} M $AgBF_4$. used during the AgNP synthesis.

Figure 3.10 upper part a (corresponding to $AgBF_4$ concentration 1 * 10^{-3} M) shows the range of particle size visible in the concentrated sample. Nanoparticles with diameters ranging from 5 to 40 nm are present. These larger particles, with diameters >20 nm, were found to be surrounded by a large number of ≈5 nm particles. This finding is supported by the UV-VIS spectra (figure 3.10 lower part a) showing a very broad 400 nm peak, which is indicative of a wide range of nanoparticle size[34]. It can be seen that the larger nanoparticles generally do not adopt a spherical shape; instead an elongated form is preferred. This longer shape could be due to the aggregation of two or more particles together. The smaller 5 nm particles are generally more rounded, adopting a spherical shape like that of the NPs found in the lesser concentrated samples.

Figure 3.10 b (corresponding to $AgBF_4$ concentration 1 × 10^{-4} M) shows a number of NPs with diameters of approximately up to 20 nm. Figure 3.10 c (corresponding to $AgBF_4$ concentration 1 × 10^{-5} M) shows a typical NP: spherical and with a diameter between 15 and 20 nm. (See more images of supporting information of article)

Ag–AuNPs generation. Addition of the yellow $HAuCl_4$ solution to the yellow AgNP aliquots caused an instantaneous colour change from yellow to lilac. After 30 min of stirring, no further colour change occurred to the Ag–AuNPs. An identical lilac colour was obtained for each of the Ag:Au ratios tested (2:1, 1:1 and 1:2). No precipitation of the particles occurred after 3 months, although after two weeks a darkening from lilac to purple occurred

in each of the samples. This darkening could presumably be attributed to NP aggregation, though not to such an extent to cause a complete Ag–AuNP precipitation.

It can be seen (see figure 3.11 upper part) that an increase in Au concentration causes an increase the agglomeration of nanoparticles.

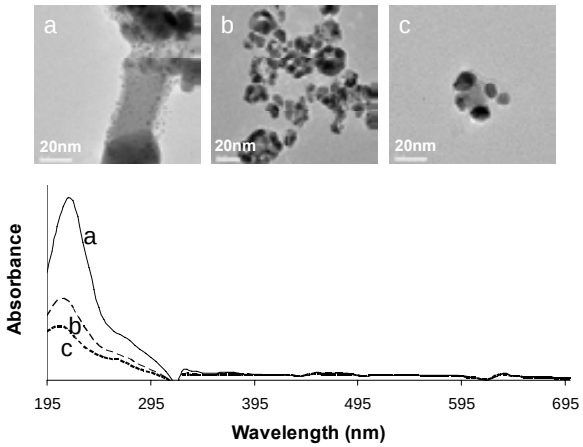

Figure 3.11 (Upper part) TEM images of Ag–Au NPs with Ag: Au ratios of (a) 1:2 (b) 1:1 (c) 2:1.Other experimental conditions of NP preparation as described in the text. (Lower part) UV-VIS spectra for: Ag–Au NP solutions corresponding to Ag: Au molar ratios (of the 1 * 10^{-4} M salt solutions) of (a) 1:2, (b) 1:1, (c) 2:1.

First image, figure 3.11 upper part a, (corresponding to Ag:Au ratio 1:2) shows the presence of a number of different sizes of AgNP, with the larger particles apparently surrounded by the same light grey coloured material that could be seen in figure 3.11 upper part c. In addition to this, a number of much smaller (<5 nm) particles can also be seen, surrounding the dark Ag particle. It is not clear whether these smaller particles are of gold or silver, the presence of gold nanoparticles requiring that the $HAuCl_4$ ions are reduced, although no further $NaBH_4$ was added after the injection of $HAuCl_4$. This reduction could only be possible by those BH_4^- ions remaining in solution or by those bound to the surface of the AgNP. To test this, an Ag–Au mixture was prepared again, but this time the AgNPs were left for 24 h before $HAuCl_4$ was added, as several studies[35,36] have shown that BH_4^- ions in water will decompose into non reductive species, as indicated in the equation below:

$$BH_4^- + H^+ + 2H_2O \rightarrow \text{intermediate} \rightarrow HBO_2 + 4H_2 \qquad (3.3)$$

Upon $HAuCl_4$ injection, the same colour change as before occurred, indicating the formation of a similar chemical species as before. These results imply that $HAuCl_4$ is reduced by the BH_4^- ions found on the AgNP surface, rather than those free in solution as we expect these free ions to have decomposed in the time between $NaBH_4$ addition and the addition of $HAuCl_4$. A galvanic replacement reaction similar to the described one by Lu et al.[37] between the added Au(III) and Ag(0) of the NPs surface is also possible:

$$Au(III) + 3Ag(0) \rightarrow 3Ag^+ + Au(0) \qquad (3.4)$$

In a similar mode, nearly monodisperse hollow gold nanospheres have been reported to be synthesized by sacrificial galvanic replacement of cobalt nanoparticles[38].

Figure 3.11 upper part b (corresponding to Ag:Au ratio 1:1) shows aggregation of Ag nanoparticles to a smaller degree; a number of large ‘‘wheel’’ like structures can be seen, each consisting of separate AgNPs joined together. The formation mechanism of such circular formations is still unclear. One proposed mechanism could be similar to that proposed by Kim et al[39]. For the formation of hollow nanoframes, whereby the AgNP is disrupted by the presence of Au, causing the Ag cluster to fall apart and Au to fill the spaces thus created. This fact would explain that the size of AgNPs in these ‘‘wheels’’ is smaller than in Ag–AuNPs with lower Ag:Au ratio (figure 3.10 upper part b). Figure 3.11 upper part c (corresponding to Ag:Au ratio 2:1) shows agglomeration of 4 AgNPs held together by an apparently lighter grey coloured substance between them, which is presumably a form of gold formed by reduction of $HAuCl_4$.

Figure 3.12 A shows the microanalysis result of the Ag–AuNP (1:1) mixture, with traces of both silver and gold present, taken from the middle of one of the ‘‘wheel’’ structures. By the above mentioned method of Kim et al.. This would imply that the AgNPs form the ‘rim’ of the wheel and the addition of $HAuCl_4$ forms the ‘spokes’.

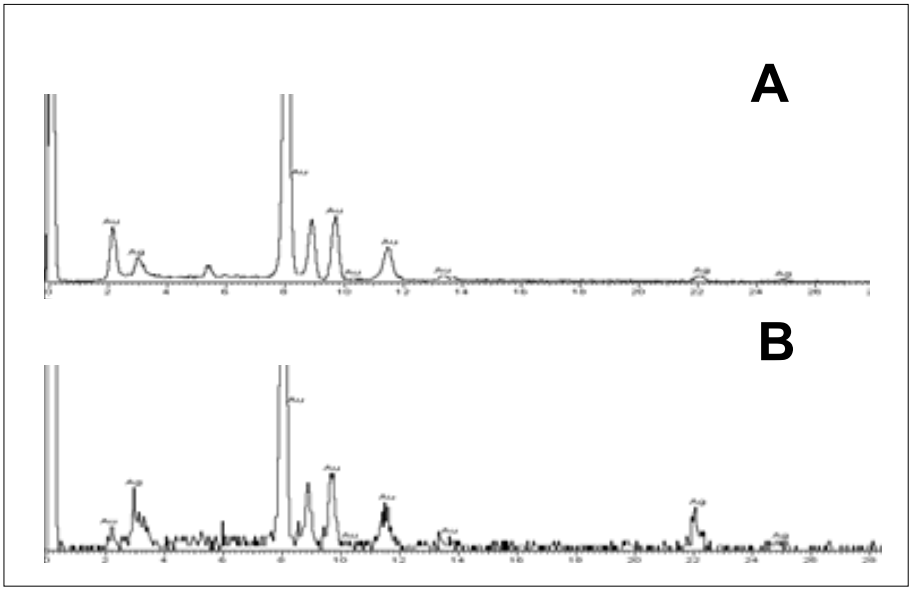

Figure 3.12 Microanalysis results of (A) Ag–Au NPs corresponding to 1:1 Ag: Au ratio and (B) Au–Ag NPs corresponding to 1:1 Au: Ag ratio showing presence of both gold and silver in the NP formed. (See corresponding table at Supporting Information).

The spectra obtained for the different Ag:Au ratios (figure 3.11 lower part) show an increase in the intensity of absorbance at 215 nm with an increase in the gold content of the mixture (due to the increasing concentration of $HAuCl_4$). It is apparent that the defined peaks associated with AgNPs at around 400 nm have dramatically decreased in intensity, indicating the possible loss of Ag nanoparticle character (concerning to the Ag surface plasmon).

AuNPs and Au–AgNPs generation. Upon injection of the Au metal ions (as $HAuCl_4$ solution), no initial aggregation was visible as happened in the AgNP preparation. Instead, the solution became an intense orange colour, which finally darkened gradually to a pale red colour after 40 minutes agitation, indicating the formation of AuNPs. Injection of a clear $AgBF_4$ solution to the AuNPs solution caused an instantaneous colour change from pale red to a deeper red/purple due to the formation of Au–AgNPs. No change in colour was apparent after 3 months of storage, indicating that no nanoparticle aggregation occurred.

As seen from figure 3.13 upper part a, the AuNPs prepared by the above method were found to be spherical and typically 3–5 nm in size. The AuNPs were found to exist in large and often circular clusters varying in size from several tens to several hundreds of

particles. Individual AuNPs could not be found separate from these large clusters, implying that some electrostatic force could be responsible for keeping them held together.

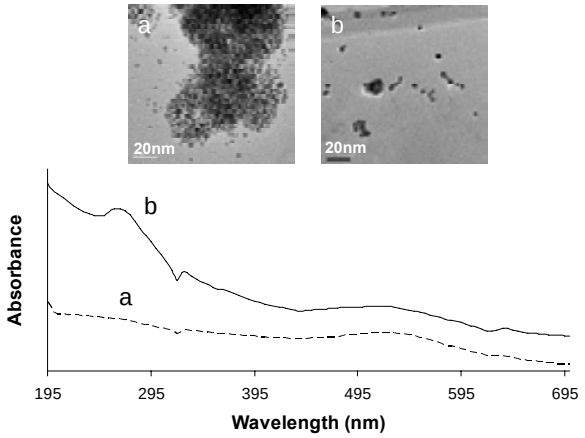

Figure 3.13 (Upper part) TEM images of (a) Au NPs and (b) Au-Ag NPs of 1:1 Au:Ag. Other experimental conditions of NP preparation as described in the text. (Lower part) UV-VIS spectra for solutions of (a) Au NPs corresponding to 1 * 10^{-4} M $HAuCl_4$ used during the synthesis of AuNPs and (b) Au–Ag NPs of 1:1 Au: Ag molar ratios (of the salt solutions used).

Figure 3.13 upper part b shows the NPs resulting from addition of $AgBF_4$ to a solution of AuNPs. The large AuNP clusters were found to be completely disrupted and a number of the smaller AuNPs can be seen to have agglomerated together, though not to the extent seen in some of the Ag–Au mixtures. There is no evidence to support the formation of AgNPs. The microanalysis results (figure 3.12 B) show only a slight amount of silver is present. It appears that, the only effect silver addition has had was to disrupt the AuNP clusters, with the overall shapes and sizes of the Au– AgNPs not vastly different from that of the AuNPs.

In Au-Ag spectra (see figure 3.13 lower part b) shows strong absorbance at 275 nm. This absorbance range is commonly associated with a silver-borohydride nano-species (see Figure 3.10 lower part), although the peaks at 400 nm that we would expect from silver are not apparent. The broad peak visible at 530 nm is a peculiar characteristic of the gold surface plasmon[40] and is present in both the Au and Au–Ag cases (see figure 3.13 lower part), implying that AuNPs have retained their nanoparticle character after the addition of $AgBF_4$.

The disappearance of the primary bands of AuNPs and AgNPs and the appearance of new bands located at i.e. 215 nm for the Ag–Au NPs indicates the formation of core-shell composites. The absorption edges show a strong blue shift with respect to bulk Ag or Au

materials. This blue shift is an obvious quantum size effect and has been observed in many nanometer-sized semiconductor materials[41]. (See more details in the article)

Electrochemical characterizations. To confirm the possibility for future applications of the developed nanoparticles for sensors, their electrochemical characterization was performed. Figure 3.14 left shows cyclic voltammograms in 1 M NH_3 obtained for a 25 µM AgNPs solution (black curve), the supernatant solution after centrifugation (grey curve) and for the electrolyte (blank-dot line). It can be observed that the current peak corresponds to the oxidation of the silver at approximately +0.10 V for the AgNPs solution (see figure 3.15 right), the oxidation mechanism implicates the complex formation:

$$AgNP + 2NH_3 \rightarrow [Ag(NH_3)_2]^+ + e \qquad (3.5)$$

The supernatant solution does not exhibit any peak, so can be assured that the entire signal observed corresponds to NPs and not to possible excess of silver ions from the synthesis solution.

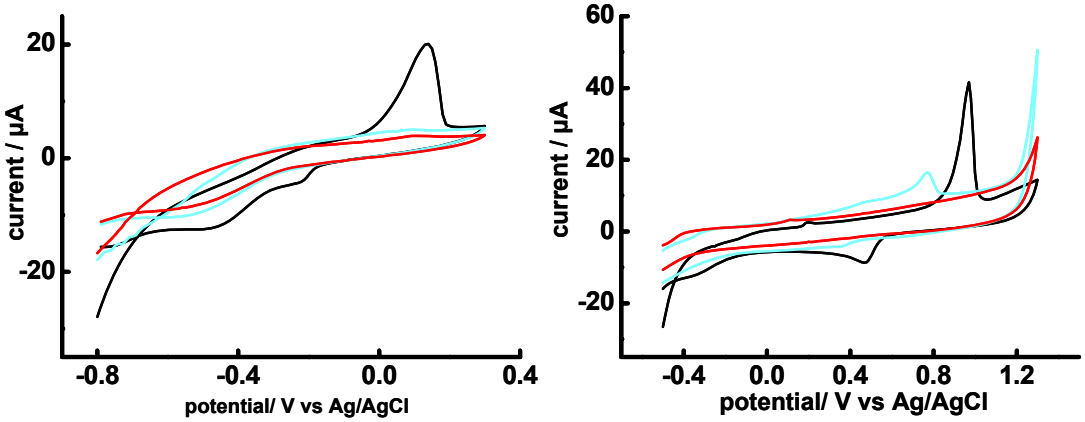

Figure 3.14 (Right) CV recorded in 0.1 M HCl from - 0.80 V to +1.30 V, for a 50 µM AuNPs solution (black), the supernatant solution after centrifugation (blue) and for the electrolyte solution (red). Deposition/conditioning potential: -0.8 V; deposition/conditioning time: 240 s; scan rate: 50 mV/s. (Left) Cyclic voltammograms recorded in 1 M NH_3, from -0.80 V to +0.30 V, for a 25 µM AgNPs solution (black), the supernatant solution after centrifugation (blue) and for the electrolyte solution (red). Deposition/conditioning potential: -0.8 V; deposition/conditioning time: 60 s; scan rate: 50 mV/s.

In the case of the AuNPs, cyclic voltammograms were registered in 0.1 M HCl, for a 50 μM AuNPs solution (black curve), the supernatant solution after centrifugation (grey curve) and for the electrolyte (blank-dot line), as it is shown in figure 3.14 right peak at approximately +0.95 V is observed for the AuNPs solution, which corresponds to the oxidation process of gold (see figure 3.15 left), the oxidation mechanism implicates the complex formation:

$$AuNP + 4Cl^- \rightarrow AuCl_4^- + 3e \qquad (3.6)$$

A smaller peak for the supernatant solution also appears. Two facts could explain this behaviour. The centrifugation step is not efficient due to the smaller size of the NPs that stay in the supernatant solution (the solution remains slightly coloured). On the other hand, the peak could be, due to the presence of an excess of gold ions from the synthesis solution.

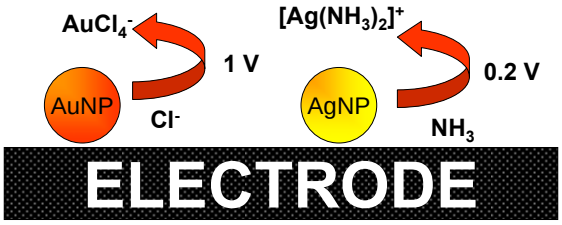

Figure 3.15. Schematic of the mechanisms for the electrochemical detections of AuNP and AgNPs.

3.2.10 Conclusions

Four kinds of water-soluble nanoparticles: AgNP, AuNP, Ag–AuNP and Au–AgNP have been synthesized and characterized using transmission electronic microscopy (TEM), UV-Vis absorption spectroscopy and cyclic voltammetry. The reported nanoparticles show stability in water suspensions up to several months of storage, indicating that no nanoparticle aggregation occurred.

An important point we observe here is that the morphologies of the obtained nanoparticles are determined by the order of addition of reactants beside the other experimental conditions such as the metal ion concentration, and other appropriate parameters, as was seen by the TEM and UV studies.

The CVs obtained for both nanoparticles show that it is possible to use these nanoparticles for future applications in biosensing. For the biosensing applications the synthesised metal nanoparticles have to be conjugated to biomolecule, such as DNA and proteins in a similar way as reported recently by our group[19,27 ,28].

3.3 References

[1] Trindade T., O'Brien P., Pickett N. L. *"Nanocrystalline Semiconductors: Synthesis, Properties, and Perspectives"* **2001** *Chem. Mater.* 13, 3843-3858.

[2] Kairdolf B. A., Smith A. M., Nie S. *"One-Pot Synthesis, Encapsulation, and Solubilization of Size-Tuned Quantum Dots with Amphiphilic Multidentate Ligands"* **2008** *J. Am. Chem. Soc.* 130, 12866-12867.

[3] Willner I., Patolsky F., Wasserman J. *"Photoelectrochemistry with Controlled DNA-Cross-Linked CdS Nanoparticle Arrays"* **2001** *Angew. Chem. Int. Ed.* 40, 1861-1864.

[4] Haram S. K., Quinn B. M., Bard A. J. *"Electrochemistry of CdS Nanoparticles: A Correlation between Optical and Electrochemical Band Gaps"* **2001** *J. Am. Chem. Soc.* 123, 8860-8861.

[5] Wang J., Liu G., Merkoçi A. *"Electrochemical Coding Technology for Simultaneous Detection of Multiple DNA Targets"* **2003** *J. Am. Chem. Soc.* 125, 3214-3215.

[6] Castañeda M. T., Perez B., Pumera M., Del Valle M., Merkoçi A., Alegret S. *"Sensitive stripping voltammetry of heavy metals by using a composite sensor based on a built-in bismuth precursor"* **2005** *Analyst* 130, 971-976.

[7] Steigerwald M. L., Alivisatos A. P., Gobson J. M., Harris T. D., Kortan R., Muller A. J., Thayer A. M., Duncan T. M., Douglass D. C., Brus L. E. *"Surface Derivatization and Isolation of Semiconductor Cluster Molecules"* **1988** *J. Am. Chem. Soc.* 110, 3046-3050.

[8] Barglik-Chory Ch., Buchold D., Schmitt M., Kiefer W., Heske C., Kumpf C., Fuchs O., Weinhardt L., Stahl A., Umbach E., Lentze M., Geurts J., Müller G. *"Synthesis, structure and spectroscopic characterization of water-soluble CdS nanoparticles"* **2003** *Chem. Phys. Lett.* 379, 443-451.

[9] Pumera M., Aldavert M., Mills C., Merkoçi A., Alegret S. *"Direct voltammetric determination of gold nanoparticles using graphite-epoxy composite electrode"* **2005** *Electrochim. Acta* 50, 3702-3707.

[10] Merkoçi A., Marín S., Castañeda M. T., Pumera M., Ros J., Alegret S. *"Crystal and electrochemical properties of water dispersed CdS nanocrystals obtained via reverse micelles and arrested precipitation"* **2006** *Nanotechnology* 17, 2553-2559.

[11] Cushing B. L., Kolesnichenko V. L., O'Connor C. J. *"Recent Advances in the Liquid-Phase Syntheses of Inorganic Nanoparticles"* **2004** *Chem. Rev.* 104, 3893-3946.

[12] Chen X., Samia A. C. S., Lou Y., Burda C. *"Investigation of the Crystallization Process in 2 nm CdSe Quantum Dots"* **2005** *J. Am. Chem. Soc.* 127, 4372-4375.

[13] Kadirgan F., Mao D., Song W., Ohno T., McCandles B. *"Properties of Electrodeposited Cadmium Sulfide Films for Photovoltaic Devices With Comparison to CdS Films Prepared by Other Methods"* **2000** *Turk. J. Chem.* 24, 21-33.

[14] Kolny J., Kornowski A., Weller H. *"Self-Organization of Cadmium Sulfide and Gold Nanoparticles by Electrostatic Interaction"* **2002** *Nano Lett.* 2, 361-364.

[15] Malik M. A., Revaprasadu N., O'Brien P. *"Air-Stable Single-Source Precursors for the Synthesis of Chalcogenide Semiconductor Nanoparticles"* **2001** *Chem. Mater.* 13, 913-920.

[16] Malik M. A., O'Brien P., Revaprasadu N. *"A Simple Route to the Synthesis of Core/Shell Nanoparticles of Chalcogenides"* **2002** *Chem. Mater.* 14, 2004-2010.

[17] Vossmeyer T., Katsikas M., Giersig M., Popovic I. G., Diesner K., Chemseddine A., Eychmüller A., Weller H. *"CdS Nanoclusters: Synthesis, Characterization, Size Dependent Oscillator Strength, Temperature Shift of the Excitonic Transition Energy, and Reversible Absorbance Shift"* **1994** *J. Phys. Chem.* 98, 7665-7673.

[18] Chen S., Truax L. A., Sommers J. M. *"Alkanethiolate-Protected PbS Nanoclusters: Synthesis, Spectroscopic and Electrochemical Studies"* **2000** *Chem. Mater.* 12, 3864-3870.

[19] Pumera M., Castañeda M. T., Pividori M. I., Eritja R., Merkoçi A., Alegret S. *"Magnetically Trigged Direct Electrochemical Detection of DNA Hybridization Using Au_{67} Quantum Dot as Electrical Tracer"* **2005** *Langmuir* 21, 9625-9629.

[20] Schmid G. *"Large clusters and colloids. Metals in the embryonic state"* **1992** *Chem. Rev.* 92, 1709-1727.

[21] Mulvaney P. *"Surface plasmon spectroscopy of nanosized metal particles"* **1996** *Langmuir* 12, 788-800.

[22] Ozin G. A. *"Nanochemistry: synthesis in diminishing dimensions"* **1992** *Adv. Mater.* 4, 612-649.

[23] Toshima N., Harada M., Yamazaki Y., Asakura K. *"Catalytic activity and structural analysis of polymer-protected Au–Pd bimetallic clusters prepared by the simultaneous reduction of $HAuCl_4$ and $PdCl_2$"*. **1992** *J. Phys. Chem.* 96, 9927-9933.

[24] Merkoçi A., Aldavert M., Tarrasón G., Eritja R., Alegret S. *"Toward an ICPMS-Linked DNA Assay Based on Gold Nanoparticles Immunoconnected through Peptide Sequences"* **2005** *Anal. Chem.* 77, 6500-6503.

[25] Elghanian R., Storhoff J. J., Mucic R. C., Letsinger R. L., Mirkin C. A. *"Selective colorimetric detection of polynucleotides based on the distance-dependent optical properties of gold nanoparticles"* **1997** *Science* 277, 1078-1081.

[26] Merkoçi A. *"Electrochemical biosensing with nanoparticles"* **2007** *FEBS J.* 274, 310-316.

[27] Castañeda M. T., Merkoçi A., Pumera M., Alegret S. *"Electrochemical genosensors for biomedical applications based on gold nanoparticles"* **2007** *Biosensors and Bioelectronics* 22, 1961-1967.

[28] Ambrosi A., Castañeda M. T., Killard A. J., Smyth M. R., Alegret S., Merkoçi A. *"Double-codified gold nanolabels for enhanced immunoanalysis"* **2007** *Anal. Chem.* 79, 5232-5240.

[29] Wang H. Y., Li Y. F., Huang C. Z. "*Detection of ferulic acid based on the plasmon resonance light scattering of silver nanoparticles"* **2007** *Talanta* 72, 1698-1703.

[30] Tarimala S., Kothari N., Abidi N., Hequet E., Fralick J., Dai L. L. *"New approach to antibacterial treatment of cotton fabric with silver nanoparticle-doped silica using a sol-gel process"* **2006** *J. Appl. Polym. Sci.* 101, 2938-2943.

[31] Nomiya K., Yoshizawa A., Tsukagoshi K., Kasuga N. C., Hirakawa S., Watanabe S. J. *"Synthesis and structural characterization of silver(I), aluminium(III) and cobalt(II) complexes with 4-isopropyltropolone (hinokitiol) showing noteworthy biological activities. Action of silver(I)-oxygen bonding complexes on the antimicrobial activities"* **2004** *J Inorg Biochem* 98, 46-60.

[32] Dirk L., Hyning V., Zukoski C. F. *"Formation mechanisms and aggregation behavior of borohydride reduced silver particles"* **1998** *Langmuir* 14, 7034-7046.

[33] Douglas F., Yañez R., Ros J., Marín S., de la Escosura-Muñiz A., Alegret S., Merkoçi A. *"Silver, gold and the corresponding core shell nanoparticles: synthesis and characterization"* **2008** *J. Nanopart. Res.* 10, 9374-9384.

[34] Solomon S. D., Bahadory M., Jeyarajasingam A. V., Rutkowsky S. A. *"Synthesis and study of silver nanoparticles"* **2007**. *J Chem Educ* 84, 322-325.

[35] Davis R. E., Swain C. G. *"General acid catalysis of the hydrolysis of sodium borohydride"* **1960** *J. Am. Chem. Soc.* 82, 5949-5950.

[36] Davis R. E., Bromels E., Kibby C. L. *"Hydrolysis of sodium borohydride in aqueous solution"* **1962** *J. Am. Chem. Soc.* 84, 885-892.

[37] Lu X., Tuan H. Y., Chen J., Li Z. Y., Korgel B. A., Xia Y. *"Mechanistic Studies on the galvanic replacement reaction between multiply twinned particles of Ag and $HAuCl_4$ in an organic medium"* **2007** *J. Am. Chem. Soc.* 129, 1733-1742.

[38] Schwartzberg A. M., Olson T. Y., Talley C. E., Zhang J. Z. *"Synthesis, characterization, and tunable optical properties of hollow gold nanospheres"* **2006** *J. Phys. Chem. B* 110, 19935-19944.

[39] Kim D., Park J., An K., Yang N. K., Park J. G., Hyeon T. *"Synthesis of hollow iron nanoframes"* **2007** *J. Am. Chem. Soc.* 129, 5812-5813.

[40] Grace A. N., Pandian K. *"One pot synthesis of polymer protected gold nanoparticles and nanoprisims in glycerol"* **2006** *Colloid Surf A: Physicochem Eng Aspect* 290, 138-142.

[41] Sun L., Wei G., Song Y., Liu Z., Wang L., Li Z. *"Solution phase synthesis of Au@ZnO core-shell composites"* **2006** *Mater. Lett.* 60, 1291-1295.

Chapter 4

Electrochemical analysis of QDs

Chapter 4 Electrochemical analysis of QDs

4.1 Introduction

Several works on DNA or immunoanalysis based on gold nanoparticle[1-4] or quantum dot[5] detection by using stripping techniques have been reported. The majority of electrochemical methods have used chemical solutions of gold nanoparticles (in a hydrobromic acid/bromine mixture) or quantum dots (with nitric acid) followed by accumulation and stripping analysis of the resulting metal ion solutions. The HBr/Br_2 solution is highly toxic and therefore methods based on direct electrochemical detection of gold nanoparticle tags have been developed[6,7] and even applied for DNA analysis[8]. Regarding the direct electrochemical detection of quantum dots so as to achieve a full integration of DNA electrochemical sensors, there is still much work to be done.

The following chapter shows the development of a simple method for the direct detection of cadmium sulphide quantum dots in neutral solution medium (pH 7.0) without the need for chemical dissolution. It is based on dropping a few microlitres of CdS QD suspension on the surface of a screen-printed electrode and the subsequent square wave voltammetry detection based on the reduced cadmium formation and stripping, giving a well shaped and sensitive analytical signal. The proposed method can be easily extended for other quantum dots based on other heavy metals, offering new opportunities for applications in electrochemical DNA genosensors.

4.2 Reagents and materials

Synthesis of CdS QDs (by arrested precipitation method) was explained in chapter 3 section 3.1.5.

Potassium dihydrogenphosphate, phosphoric acid, and sodium hydroxide were purchased from Sigma-Aldrich; hydrochloric acid (37% m/m) was purchased from Panreac (Barcelona, Spain).

All solutions were prepared in doubly distilled water. Appropriate dilutions from this stock solution were also prepared in 0.1 mol l^{-1} phosphate buffer solution (pH 7.0) prior to each set of measurements.

4.3 Equipment

All voltammetric experiments were performed using a PalmSens (Palm Instrument BV, Houten, The Netherlands) that consists of a portable potentiostat interfaced with a palmtop PC (155 mm × 85 mm × 35 mm) (see figure 4.1, left). Electrochemical experiments were carried out using a screen printed electrode (SPE) (Palm Instrument BV, Houten, The Netherlands). The screen printing electrochemical cell (see figure 4.1, right) consists of a graphite working (W) electrode (diameter 3 mm), a graphite counter-electrode (C) and a silver pseudo-reference (R) electrode.

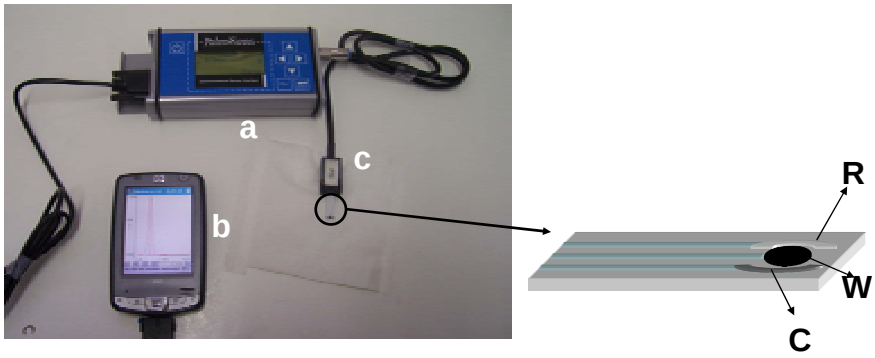

Figure 4.1 (Left) Image of the hand held device system used for CdS QD detection. The principal components are the potentiostat (a), the palm PC (b) and the screen printed electrode (SPE) (c). (Right) Schematic of screen-printed electrode formed by the reference (R), working (W) and counter (C) electrodes.

4.4 Electrochemical detection

The measurements were performed suspending a volume of 20 µl under the sensor stripped in the horizontal position, to ensure electrical contact (complete circuit).

Each SPE was pretreated, before using, by applying −1.1 V for 300 s and then square wave voltammetric (SWV) scans were carried out until a low and stable background was obtained[9].

SWV experiments were performed to evaluate the electrochemical behaviour of the SPE for CdS QD detection. The proposed protocol (figure 4.2) involves the introduction of CdS QDs onto the surface of the SPE (figure 4.2 A). During this step a drop of 20 µl containing an appropriate concentration of CdS QDs (ranging from 0.5 to 14.0 * 10^{16} QDs ml^{-1}) was suspended onto the SPE for 60 s and a potential of 0 V was applied. The second step was the accumulation step. In this step (figure 4.2 B) a deposition potential of −1.1 V for 120 s was applied to promote the electrochemical reduction of Cd^{2+} ions contained in the CdS QD structure to Cd^0. After the accumulation step, SWV was performed. During this step (figure 4.2 C) the potential was scanned from −1.1 to −0.7 V (step potential 10 mV, modulation amplitude 30 mV and frequency 15 Hz), resulting in an analytical signal due to the oxidation of Cd^0. After the SWV measurement, the SPE was manually cleaned (figure 4.2 D) with a 0.1 mol l^{-1} phosphate buffer solution (pH 7.0).

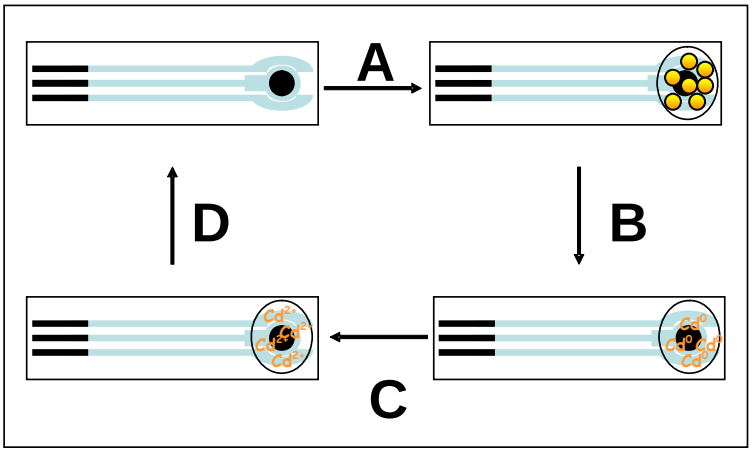

Figure 4.2 Schematic diagram of the direct voltammetric detection of the CdS QDs using an SPE. See description in the text.

Blank subtraction method was performed[10]. The blank was measured using a separate blank solution (0.1 mol l^{-1} phosphate buffer solution, pH 7.0). After this measure, using the same sensor, a determined volume of the QD suspension was added and measurements (SWV) were performed by using the 'sample' option. In this way, the subtracted curve was obtained.

No special activation of the electrode surface was used for further experiments with the same sensor (up to six or seven measurements).

4.5 Results and discussion

A detailed description of the obtained results is given in the published article[11].

In brief, the results are described and discussed in the following sections:

First of all, the system was checked so as to verify its response for the cadmium solution (see article supporting information figure 1s)

During the deposition time, applying a potential of −1.1 V, the reduced cadmium, necessary for further stripping, could have been obtained via two mechanisms:

1^{st} Mechanism: $(CdS)Cd^{2+} + 2e \rightarrow (CdS)Cd^{0}$ (4.1)

The cadmium ions in equilibrium with CdS nanoparticles can be directly reduced according to:

2^{nd} Mechanims: $CdS + 2H^{+} + 2e \rightarrow Cd^{0} + H_2S$ (4.2)

The direct reduction of CdS nanoparticles: in analogy with the cathodic reduction of PbS nanoparticles in water solution[12], that depends on pH solution. This effect of pH was studied (see figure 4.3 A) and the results show that even at pH 7.0 the SWV signal was around half of that obtained at pH 3.0 and so sufficient for further analytical use. Moreover, the use of pH 7.0 is of interest, taking into consideration future applications in DNA sensing, being the usual pH medium in hybridization procedures.

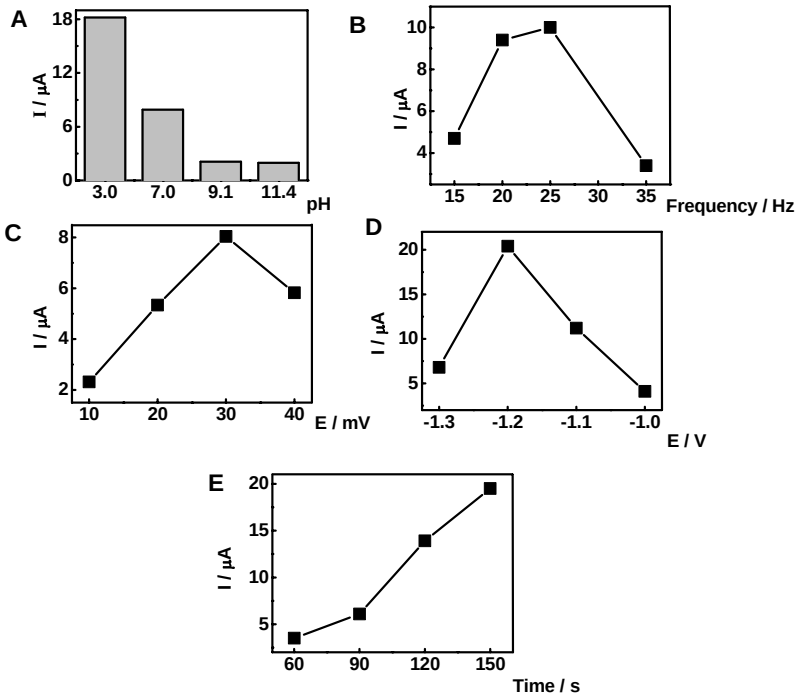

Figure 4.3 (A) Effect of pH; (B) SW frequency; (C) modulation amplitude; (D) deposition potential; (E) deposition time to the SPE response for CdS QDs (4.65 * 10^{17} mol l^{-1}) in a solution of 0.1 mol l^{-1} phosphate buffer (pH 7.0). Square-wave voltammetric scan with frequency of 25 Hz, step potential 10 mV and amplitude of 30 mV. Deposition potential of -1.1 V during 120 s.

The CdS QDs are reduced in this way to Cd^0 while applying a potential of −1.1 V for 120 s. After this 'preconcentration' the redissolution of the Cd^0 formed occurs, giving the SWV response that depends on the number of CdS QDs.

Also the response mechanism of CdS QD detection was studied (see figure 4.4). The mechanism is a mixed phenomenon between adsorption of QDs and diffusion control.

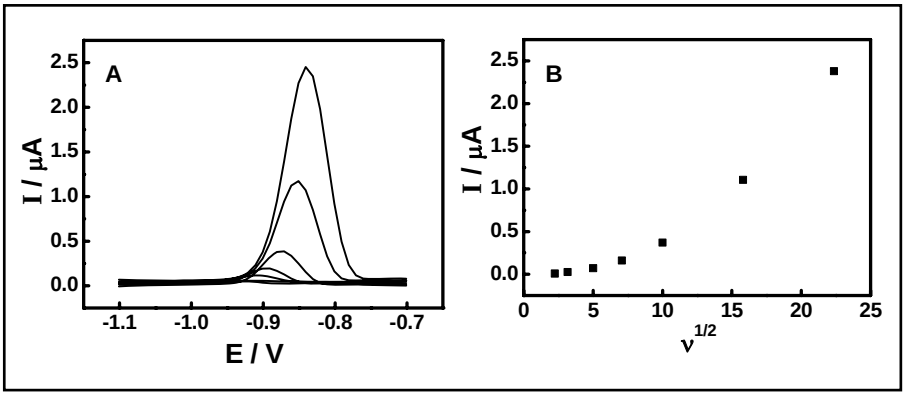

Figure 4.4 Linear sweep voltammograms using the SPE (A) and a plot of the peak current vs. the square root of potential sweep rate (B). Scan rate of 10 to 500 mV s^{-1}. Conditions: supporting electrolyte 0.1 mol l^{-1} phosphate buffer (pH 7.0); accumulation time: 60 s; electrochemical reduction time: 120 s; reduction potential: -1.1 V; start potential: -1.1 V.

The SWV parameters were optimized so as to obtain the highest peak signal for CdS QD detection using a 20 µl drop of QD suspension at pH 7.0 phosphate buffer. A maximum response was obtained at 25 Hz of frequency, 30 mV of modulation amplitude, -1.1 V of deposition potential and 120 s of deposition time. (see figure 4.3) (Results were shown in the article section 3.2 Detection of CdS QDs).The reproducibility of SPEs was studied using ten different sensors to detect the same concentration of CdS QDs (14 * 10^{16} QDs ml^{-1}) (see figure 4.5) obtaining a 6.73 % of RSD. The stability of the response for the same SPE was also studied. For this case, an RSD of 11.8% was obtained for up to six measurements and it was almost doubled (22.2%) for four consecutive measurements. These results show that better responses are obtained by using one SPE for each measurement.

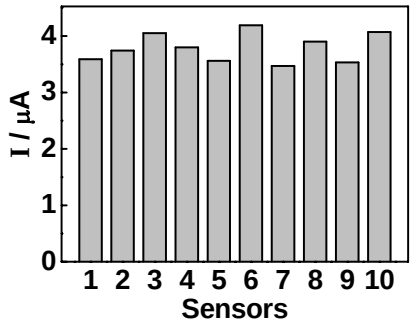

Figure 4.5 Performance of ten different sensors during measurements with a 14 * 10^{16} QDs ml^{-1} concentration suspension. Others experimental conditions as in the figure 4.3.

Figure 4.6 shows typical square wave stripping voltammograms after the blank subtraction for increasing concentration of CdS QDs up to 10^{16} QDs ml^{-1}. The corresponding calibration plot including the error bars for a set of three parallel measurements is also shown. CdS QDs as low as 10^{16} ml^{-1} have been possible to detect. Taking into consideration the CdS QD drop volume introduced (20 µl), it corresponds to a detection limit of around 2 * 10^{14} CdS QDs.

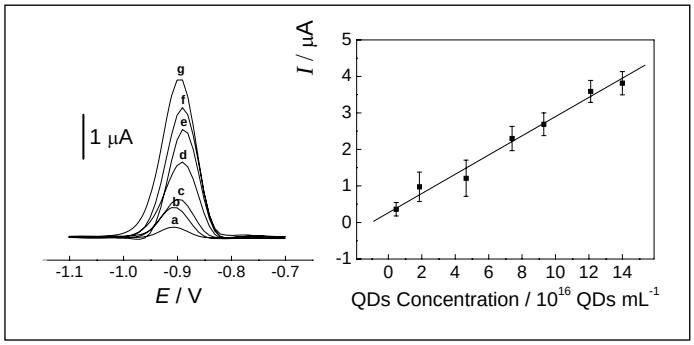

Figure 4.6 Square-wave stripping voltammograms after blank subtraction for increasing concentration of QDs: (a) 0.5, (b) 2.0, (c) 4.7, (d) 7.4, (e) 9.3, (f) 12.1 and (g) 14.0 * 10^{16} QDs ml^{-1}. The corresponding calibration plot (right) over the range 0.5-14.0 * 10^{16} QDs ml^{-1} is also shown. The measuring solution was 0.1 mol l^{-1} phosphate buffer, pH 7.0. Square-wave voltammetric scan with frequency of 25 Hz, step potential 10 mV and amplitude of 30 mV. Deposition potential of −1.1 V for 120 s.

4.6 Conclusions

A direct detection technique for CdS QDs, which can be extended for other similar QDs, that avoids the chemical dissolving as in the previously reported electrochemical detection methods is achieved[5]. The hypothesis for the detection is explained in the light of the experimental results obtained. Moreover, the optimization of the detection procedure is achieved which will be of interest for further applications of the proposed techniques in the developing electrochemical biosensors.

The detection of CdS QDs is simple, low cost, and based on a sensitive electrochemical method. It is based on the square wave voltammetry of the CdS QD suspension dropped onto the surface of a SPE. In the first step, a drop of 20 µl containing an

appropriate concentration of CdS QDs is introduced onto the surface of the SPE and maintained for 60 s while applying a potential of 0 V. In the second step a deposition potential of −1.1 V for 120 s was applied, during which the electrochemical reduction of CdS QDs to Cd^0 occurs. After the accumulation step, SWV was performed by scanning from −1.1 to −0.7 V, resulting in an analytical signal due to the oxidation of Cd^0.

The analytical signal used for the CdS QDs quantification comes from a mixed phenomenon detection that depends on the medium pH. The analytical protocols have been optimized to give results which display a wide, linear response range as well as a CdS QD detection limit that is of interest for various applications ranging from DNA analysis to immunoassays. The proposed technique represents a lower cost alternative to optical methods and will be of interest for fast screening as well as in field analysis.

4.7 References

[1] Wang J., Xu D. A., Kawde N., Polsky R. *"Metal Nanoparticle-Based Electrochemical Stripping Potentiometric Detection of DNA Hybridization"* **2001** *Anal. Chem.* 73, 5576-5581.

[2] Hernandez-Santos D., Gonzales-Garcia M. B., Costa Garcia A. C. *"Metal-Nanoparticles Based Electroanalysis"* **2002** *Electroanalysis* 14, 1225-1235.

[3] Wang J. "Nanoparticle-based electrochemical DNA detection" 2003 Anal. Chim. Acta 500, 247-257.

[4] Dequaire M., Degrand C., Limoges B. *"An Electrochemical Metalloimmunoassay Based on a Colloidal Gold Label"* **2000** *Anal. Chem.* 72, 5521-5528.

[5] Wang J., Liu G., Merkoçi A. *"Electrochemical Coding Technology for Simultaneous Detection of Multiple DNA Targets"* **2003** *J. Am. Chem. Soc. Communications* 125, 3214-3215.

[6] González-García M. B., Costa-García A. *"Adsorptive stripping voltammetric behaviour of colloidal gold and immunogold on carbon paste electrode"* **1995** *Bioelectrochemistry and Bioenergetics* 38, 389-395.

[7] Hernández-Santos D., González-García M. B., Costa-García A. *"Electrochemical determination of gold nanoparticles in colloidal Solutions"* **2000** *Electrochim. Acta* 46, 607-615.

[8] Pumera M., Castañeda M. T., Pividori M. I., Eritja R., Merkoçi A., Alegret S. *"Magnetically Trigged Direct Electrochemical Detection of DNA Hybridization Using Au_{67} Quantum Dot as Electrical Tracer"* **2005** *Langmuir* 21, 9625-9629.

[9] Palchetti I., Majid S., Kicela A., Marraza G., Mascini M. *"Polymer-mercury coated screen printed sensors for electrochemical stripping analysis of heavy metals"* **2003** *Intern. J. Environ. Anal. Chem.* 83, 701-711.

[10] Palchetti I., Laschi S., Mascini M. *"Miniaturised stripping-based carbon modified sensor for in field analysis of heavy metals*" **2005** *Analytica Chimica Acta* 530, 61-67.

[11] Merkoçi A., Marcolino-Junior L. H., Marín S., Fatibello-Filho O., Alegret S. *"Detection of cadmium sulphide nanoparticles by using screen-printed electrodes and a handheld device"* **2007** *Nanotechnology* 18, 035502 (1-6).

[12] Chen S., Truax L. A., Sommers J. M. *"Alkanethiolate-Protected PbS Nanoclusters: Synthesis, Spectroscopic and Electrochemical Studies"* **2000** *Chem. Mater.* 12, 3864-3870.

Chapter 5

DNA analysis based on electrochemical stripping of QDs

Chapter 5 DNA analysis based on electrochemical stripping

5.1 Introduction

The enormous amount of information generated in the Human Genome Project has prompted the development of DNA sensors and high-density DNA arrays[1]. DNA hybridization has gained importance as a detection system due to interest in the diagnosis and treatment of genetic diseases, the detection of infectious agents, and reliable forensic analysis. Recent activity has focused on the development of hybridization assays that permit simultaneous determination of multiple DNA targets[2,3].

Conventional and highly sensitive detection methods for DNA are based on labeling techniques using fluorescent dyes[4-6], enzymes[7,8] or radiolabels[9,10]. However, since those techniques involve some problems related to stability, a broader range of more reliable and more robust labels, that can enable high-throughput bioanalysis and determination of multiple-molecule types present in a sample are now required.

Electrochemical systems for the detection of DNA hybridization based on the use of nanoparticles as tracers have been developed[11-13]. Most of the reported systems are based on stripping voltammetric detection of the dissolved tags[14]. The proposed electrochemical systems are highly promising of rapid, simple, and low cost decentralized detection of specific nucleic acid sequences by DNA hybridization. In addition to the aforementioned advantages, the use of nanoparticles offers "bar-code" DNA and protein detection[15]. There is a possibility of developing a large number of smart nanostructures with different electrochemical properties that have molecular-recognition abilities and built-in codes for rapid target identification.

The use of QDs as electrochemical labels[16] for DNA offers several advantages upon optical properties. In comparison with optical methods, electrochemical techniques are cheaper, faster and easier to use in field analysis. Nanoparticles offer excellent prospects for DNA analysis, owing to their many attractive properties.

Although a nanoparticle based detection system for DNA hybridization based on magnetically induced electrochemical detection of the cadmium sulphide quantum dot tag linked to the target DNA was reported by Wang et al.[17], herein we report for the first time a sandwich assay that can directly be detected by using a screen printed electrode.

The proposed method employs lower sample volumes than those reported earlier along with the high sensitivity and fast detection mode.

As far as we know, this is the first time that such a direct electrochemical detection of drop solutions of CdS DNA sandwich in connection to magnetic microparticles has been presented. Moreover, important aspects related to the avoidance of nonspecific adsorption have been clarified better and the results obtained have been successfully employed in a model biosensor with an interest in future applications, obtaining a portable, automated, multiplexed system for the detection of DNA that could be used in medical consulting.

5.2 Reagents and materials

All stock solutions were prepared using deionized and autoclaved water. Tris(hydroxymethyl)methylamine (Tris), sodium chloride, sodium citrate, ethylenediamine tetraacetic acid disodium salt (EDTA), lithium chloride and Tween 20 were purchased from Sigma-Aldrich. Hydrochloridric acid (37 %) was purchased from Panreac. Streptavidin coated paramagnetic beads Dynabeads M-280 Streptavidin (diameter 2.8 μm) were purchased from Dynal Biotech. DNA oligonucleotides were received from Alpha DNA and their sequences are shown in Table 5.1. The CdS-quantum dots glutathione was described in chapter 3 section 3.1.5.

PROBE	SEQUENCE[a]
Capture DNA (CF-A)	5'TGC TGC TAT ATA TAT-biotin-3'
Signaling DNA (CF-B)	Thiol-5'GAG AGT CGT CGT CGT3'
Target DNA (CF-T) [b]	5' ATA TAT ATA GCA GCA GCA GCA GCA GCA GCA GAC GAC GAC GAC TCT C3'
One base mismatch (CF-MX1)	5' ATA TAT AAA GCA GCA GCA GCA GCA GCA GCA GAC GAC GAC GAC TCT C3'
Three base mismatch (CF-MX3)	5' ATA TAT CCC GCA GCA GCA GCA GCA GCA GCA GAC GAC GAC GAC TCT C3'
Non complementary (CF-NC)	5'GGT CAG GTG GGG GGT ACG CCA GG3'

Table 5.1 DNA sequences used.

[a] Underlined nucleotides correspond to the mismatches.

[b] Target related to cystic fibrosis gene.

The buffers and hybridization solution were composed as follows:

- TTL buffer: 100 mM Tris-HCl, pH 8.0; 0.1 % Tween 20; and 1 M LiCl.
- TT buffer: 250 mM Tris-HCl, pH 8.0; and 0.1% Tween 20.
- TTE buffer: 250 mM Tris-HCl, pH 8.0; 0.1% Tween 20; and 20 mM Na_2EDTA.
- Hybridization solution: 750 mmol/L NaCl, 75 mmol/L sodium citrate.

5.3 Equipment

All voltammetric experiments were performed using a PalmSens (Palm Instrument BV) that consists of a portable potentiostat interfaced with a palmtop PC (155 mm × 85 mm × 35 mm) (see figure 4.1, left section). Electrochemical experiments were carried out using a screen-printed electrode (SPE) (Palm Instrument BV, Houten) (see schematic, not to scale, figure 4.1, right section). The SPE sensors (From the University of Florence - Available from Palm Instruments, http://www.palmsens.com) consisted of a screen-printing electrochemical cell with three electrodes in one single strip: a graphite working (W) electrode modified with a plasticizer mixed with mercury acetate, a graphite counter (A) electrode and a silver pseudo-reference electrode (R).

The binding of streptavidin coated paramagnetic beads (MB) with biotinylated probe and hybridization events were carried out on a TS-100 Thermo Shaker (Spain). Magnetic

separation was carried out on an MCB 1200 biomagnetic processing platform (Sigris) (figure 5.1). A neodymium magnet (diameter 3 mm, height 1.5 mm, Halde Gac Sdad) was used.

Figure 5.1 MCB 1200 biomagnetic processing platform (Sigris)

5.4 Sandwich assay

Figure 5.2 is a schematic representation, not to scale, of the MB modification and the hybridization procedures employed for this assay.

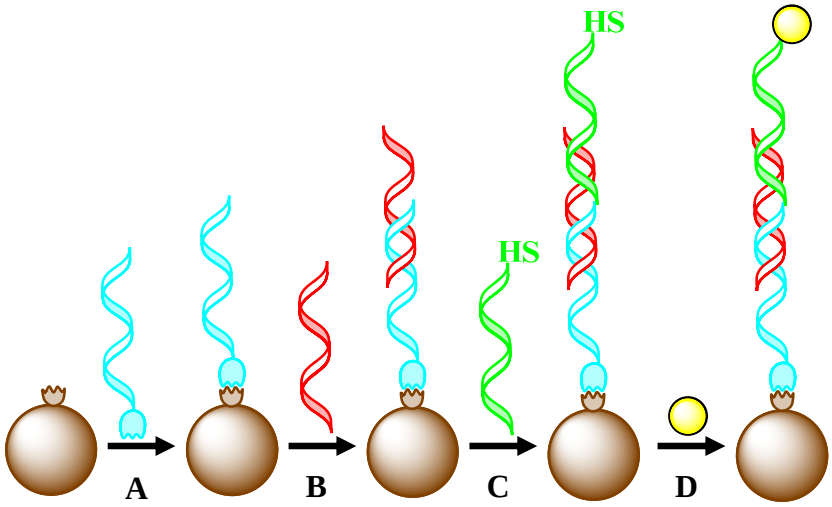

Figure 5.2 Schematic representation of sandwich protocol (not to scale): (A) immobilization of the biotinylated CF-A probe onto the streptavidin-coated magnetic beads; (B) first hybridization between CF-T and CF-A; (C) second hybridization between CF-T and CF-B modified thiol; (D) addition and capture of the CdS-quantum dots.

Immobilization of the capture DNA probe (CF-A) onto paramagnetic beads. The binding of the biotinylated probe (CF-A) with streptavidin-coated paramagnetic beads (Figure 5.2 A) was carried out using a modified procedure recommended by Bangs

Laboratories [18] using the MCB 1200 biomagnetic processing platform. Briefly, 10 μg of MB were transferred into a 0.5 mL Eppendorf tube. The MB were washed once with 100 μl of TTL buffer and then separated, decanted and resuspended in 20 μl TTL buffer and the desired amount of CF-A (8 μg) added. The resulting solution was incubated for 15 min at a temperature of 25ºC with gentle mixing (400 rpm) in a TS-100 Thermo Shaker. The MB immobilized CF-A were then separated from the incubation solution and washed sequentially with 100 μl of TT buffer, 100 μl of TTE buffer and 100 μl of TT buffer and then resuspended in 50 μl of hybridization solution, whereupon it was ready for the first hybridization.

First hybridization procedure. The desired amount of CF-T (1.36 μg; 300 pmol of target) was added to the solution (50 μl) of MB/CF-A conjugate obtained in the previous step (Figure 5.2 B). The first hybridization reaction was carried out at 25 º C for 15 min in a TS-100 Thermo Shaker (800 rpm) (if not stated otherwise). The MB/CF-A/CF-T conjugate was separated, washed twice with 100 μl of TT buffer, decanted and resuspended in 50 μl of hybridization solution, whereupon it was ready for the second hybridization.

Second hybridization procedure. The desired amount of CF-B (1.36 μg) was added to the solution (50 μl) of MB/CF-A/CF-T conjugate obtained previously (Figure 5.2 C). This second hybridization reaction was also carried out at 25 º C for 15 min in a TS-100 Thermo Shaker (800 rpm) (if not stated otherwise). The resulting MB/CF-A/CF-T/CF-B conjugate was then washed twice with 100 μl of TT buffer and resuspended in 20 μl of TTL buffer, whereupon it was ready for adding CdS-QDs-Glutathione label.

Binding of CdS-QDs-Glutathione. The desired amount of CdS-QDs-Glutathione was added to the solution (80 μl) of MB/CF-A/CF-T/CF-B conjugate obtained previously (Figure 5.2 D). Then the solution was incubated with gentle mixing (400 rpm) for 15 min at 25 º C in a TS-100 Thermo Shaker. The resulting MB/CF-A/CF-T/CF-B/CdS-QDs-Glutathione conjugate was washed twice with 100 μl of TT buffer separated, decanted and resuspended in 20 μl of hybridization solution and transferred onto the screen-printed electrode for electrochemical measurements.

5.5 Electrochemical detection

SWV measurements were performed to evaluate the electrochemical behavior of the CdS QDs conjugate. The measurement principle is based on the direct detection of CdS Quantum Dots using the procedure previously described (chapter 4, section 4.4)[19] with the only difference being that the CdS QDs in this case are modified with DNA and linked through hybridization steps with paramagnetic microparticles. The measurements were performed suspending a volume of 20 µl of sample (i.e. MB/CF-A/CF-T/CF-B/CdS-QDs-Glutathione conjugate suspension) onto the SPE surface held in the horizontal position covering the three electrodes (W, A and R electrodes) to ensure electrical contact (complete circuit). Each SPE was pretreated, before using, by applying −1.1 V for 300 s as recommended by the SPE supplier[20]. Figure 5.3 is a schematic of the electrochemical cycles steps applied for each measurement. During the first step (Figure 5.3 A) a drop of 20 µl CdS QD suspension (CdS QDs DNA conjugate) of known concentration was suspended onto the top of the SPE surface. The conjugate was then concentrated onto the working electrode surface using the neodymium magnet (Figure 5.3 B). During this step a conditioning potential of 0 V was applied for 60 s. The next step (Figure 5.3 C) was accumulation. In this step a deposition potential of -1.1 V for 120 s was applied to promote the electrochemical reduction of Cd^{2+} ions contained in the CdS QD structure to Cd^{0}. After the accumulation step, SWV was performed. During this step (Figure 5.3 D) the potential was scanned from −1.1 to −0.6 V (step potential 10 mV, modulation amplitude 30 mV and frequency 25 Hz), during each an analytical signal due to the oxidation of Cd^{0} to Cd^{2+} was obtained After the SWV measurement the SPE was manually cleaned using the hybridization solution.

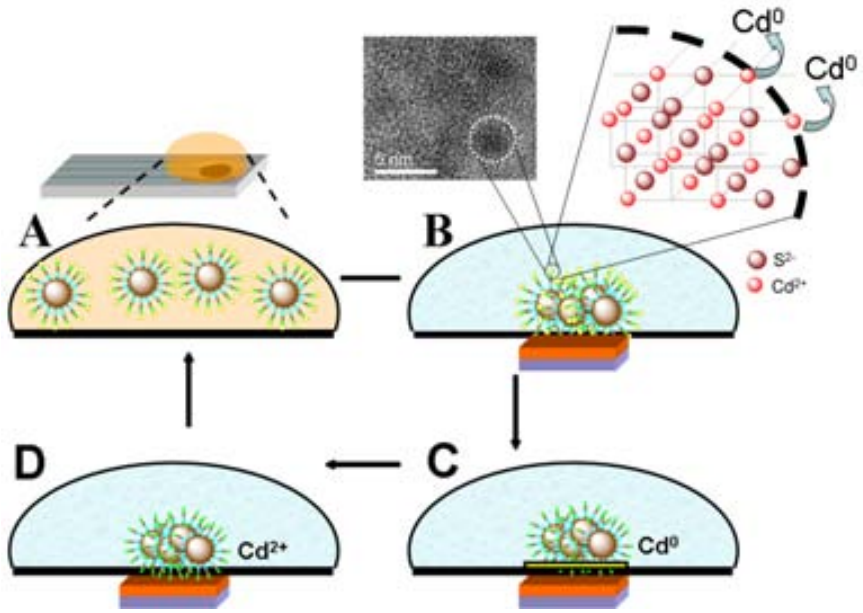

Figure 5.3 Schematic representation of electrochemical detection of DNA sandwich complex labeled with CdS QDs. A). Introduction of a drop of 20 µl CdS QD suspension (CdS QDs DNA conjugate) onto the top of the SPE surface. B). The conjugate is concentrated onto the working electrode surface using the neodymium magnet. A conditioning potential of 0 V was applied for 60 s. C). A deposition potential of -1.1 V for 120 s was applied during which the cadmium ions are reduced. D) The reduced cadmium is oxidized back to cadmium ions by SWV scanning from −1.1 to −0.6 V (step potential 10 mV, modulation amplitude 30 mV and frequency 25 Hz).

The blank subtraction method was performed[21]. The measurement of the blank was performed using the same procedure but using a blank solution (hybridization solution) instead of the CdS QDs DNA conjugate. After this step, using the same sensor, a determined volume of the QD –conjugate suspension is added and measurements (SWV) performed using the 'sample' option. Thus the subtracted curve was obtained for each QD sample.

The non specific adsorption of quantum dots onto MB surface was also studied. The effect of BSA added during the binding step between CdS QDs-Glutathione and CF-T was studied. In addition the effect of the CdS QDs concentration upon the non specific adsorption was also evaluated.

5.6 Results and discussion

A detailed description of the obtained results is given in the published article[22]. In brief, the results are described and discussed in the following sections.

Optimizations of the assay parameters. The detection method uses the same conditions as those applied for the direct detection of CdS QDs (chapter 4, section 4.4). To achieve the analytical signal a deposition potential of -1.1 V for 120 s was applied to promote the electrochemical reduction of Cd^{2+} ions (accessible from the surface of CdS QDs crystal) (see schematic in figure 5.3) to Cd^{0}.

Several parameters regarding the assay procedure have been used on the basis of the previous results or new optimizations performed. The amont of magnetic particles deposited onto the surface of the SPE is deduced from a previously developed procedure based on the same sandwich DNA using the same magnetic particles but gold nanoparticles instead of quantum dots. Hybridization time (15 min) and temperature (25 ºC) were the same as for AuNP based assay.

The assay using 1 $*10^{21}$ QDs ml^{-1} for labeling step shows that when not using CF-T (blank 1) or CF-B (blank 2) the signals obtained were too high due to the nonspecific adsorptions of QDs onto the surface of the magnetic beads. To avoid this, nonspecific adsorptions BSA as a blocking agent [23] and lower QDs quantities have been checked. BSA is commonly employed as an effective blocking solution in preventing non specific binding of non-complementary DNA[24] . It is also used during the preparation of DNA microarrays on a silanised support[25], to block gold surface[26] or even magnetic beads[27].

The optimal concentration obtained was 5 % of BSA and 1.1 * 10^{19} QDs ml^{-1}, obtaining the minimum SWV peak current of blank assay (without CF-B). (See more details in section 3.1. Optimizations of the assay parameters, figure 1SB of article).

Figure 5.4 summarizes the typical responses obtained for the positive assay (A) and the control assays (B, C) studied. Well-shaped SWV curves were obtained when the optimized parameters had been applied while the control assays gave non-significant peaks. Curve A corresponds to the assay with 34 μg ml^{-1} CF-T using DNA probes and other parameters as mentioned before. The oxidation peak of Cd at around -0.72 V, which corresponds to CdS

QDs linked to magnetic particles via DNA hybridization, is shifted by 170 mV toward negative potentials in comparison to CdS QDs (-0.89 V) without DNA and magnetic particles as reported earlier. This is probably related to the easier reduction of the magnetically collected CdS QDs modified with DNA in comparison to the reduction of CdS without DNA and in the absence of magnetic field. The presence of magnetic particles better induces the stripping of cadmium ions coming from CdS QDs making possible for them to be stripped at almost the same potential as that for the case of the free cadmium ion – cadmium ion solutions (-0.71 V). (See supporting information of reference 19)

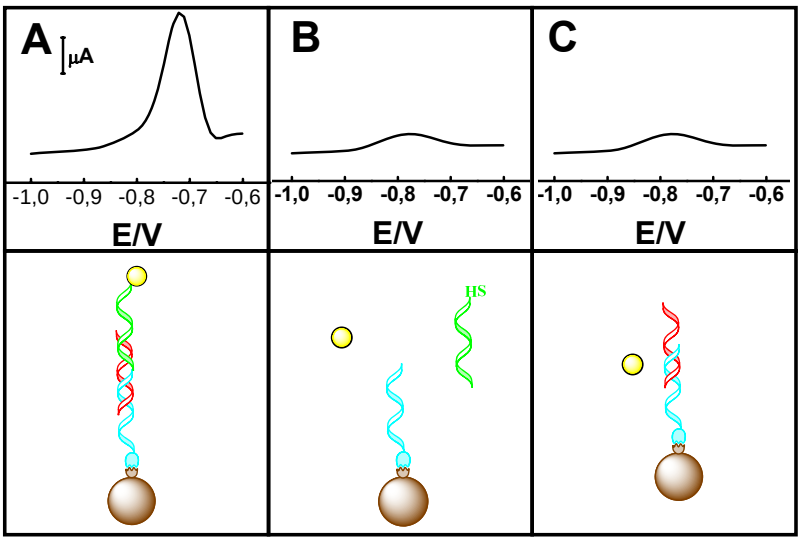

Figure 5.4 Square wave voltammograms of (A) the normal assay (34 µg ml-1of CF-T); (B) The blank does not contain the CF-B (C) blank does not contain the CF-T.

*Hybridizing assay***.** Figure 5.5 (left) shows the square wave voltammograms that demonstrate the efficacy of the genomagnetic assay using CF-T as target. Three typical calibration curves obtained with three different sensors have been shown. The peak current shows a good linear relationship (Figure 5.5, right) with the concentration of the QDs modified CF-T in the range from 6.8 to 68 µg ml^{-1}, with a correlation coefficient of 0.9998, according to the following equation: Ip (µA) = 0.0087[CF-T] (µg ml^{-1}) + 0.258 (n = 4).

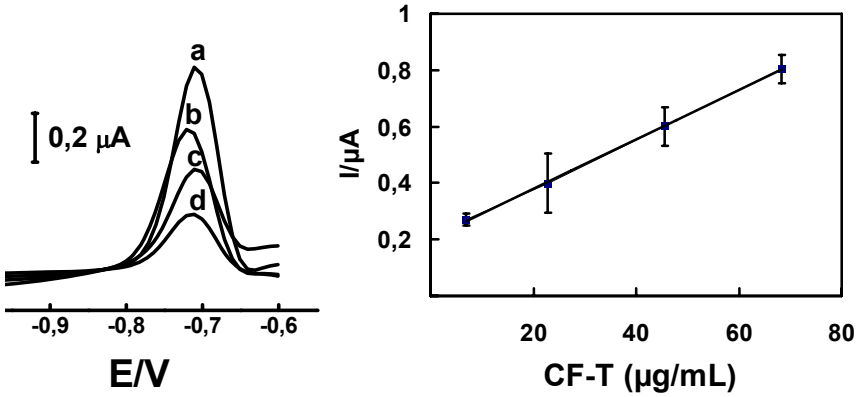

Figure 5.5 Square-wave stripping voltammograms after blank subtraction to increase concentrations of CF-T: (a) 68, (b) 45, (c) 23, (d) 6.8 μg ml^{-1}. Also shown is the corresponding calibration plot (right) over the range 6.8- 68 μg ml^{-1} of CF-T. The measuring solution was hybridization solution. Square-wave voltammetric scan with frequency of 25 Hz, step potential 10 mV and amplitude of 30 mV was performed. The deposition potential of −1.1 V for 120 s was applied. Other experimental conditions as explained in the text.

The lowest specific signal recorded for the target strand was 6.83 μg ml^{-1} (30 pmol in 20 μl or 1.5 μM). The limit of detection (LOD) is also calculated as 3σ where σ is the standard deviation obtained for the noncomplementary DNA (CF-NC). In our case LOD=1.82 μg ml-1 (for a 8 pmol CF-T).

The lowest specific signal recorded is almost the same as that obtained using gold nanoparticles (33 pmol in the 50 μl) reported earlier by our group. However, the advantage lays on the detection at a lower sample volume (20 μl instead of 50 μl) in connection to low cost, miniaturized and user friendly sensors and detection system.

The response of the developed sensor to non complementary DNA (CF-NC), one (CF-MX1) and three (CF-MX3) mismatch DNA were also checked. Figure 5.6 shows a well-defined signal for 150 pmol CF-T (around 0.8 μA) along with a good discrimination of CF-NC, CF-MX1 and CF-MX3 (all less than 0.1 μA).

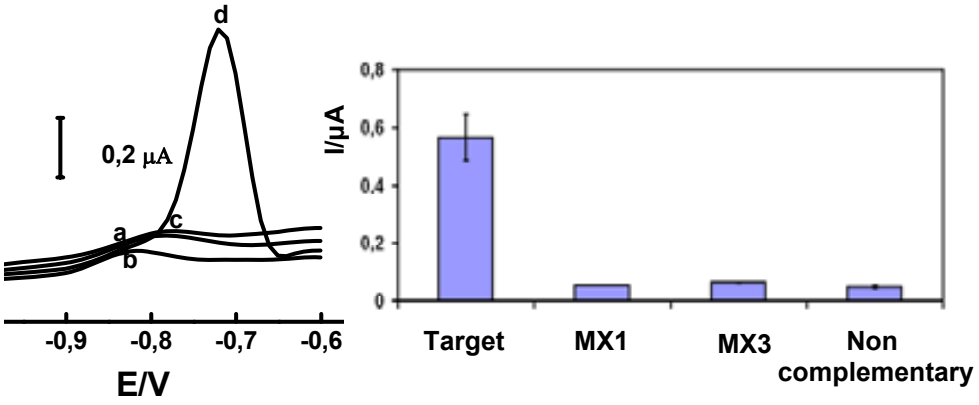

Figure 5.6 Square-wave stripping voltammograms after blank subtraction for assays performed with: (a) Non complementary sequence, (b) three mismatch basis, (c) one mismatch basis, (d) target. The concentrations of each DNA were 7.5 μM (left). Also shown is the corresponding diagram of the current peak heights (right).

The developed assay provides better discrimination of the DNA mismatches avoiding the use of stringent conditions (i.e. formamide) used for such a purpose[28].

5.7 Conclusions

An electrochemical genomagnetic hybridization assay that takes advantage of an efficient magnetic separation/mixing process and the use of cadmium sulphide nanoparticles tracers for DNA detection has been developed. It combines the magnetic isolation of DNA hybridization sandwich with the efficient, direct and sensitive electrochemical detection of electroactive nanoparticles. The developed assay employs paramagnetic microparticles modified with streptavidin and linked through a sandwich hybridized DNA target and probes and the use of CdS QDs as electrochemical tag. The detection method is simple and based on the use of screen-printed electrodes as a detection platform and a handheld potentiostatic device as a measuring system. The detection is based on the stripping of electrochemical reduced cadmium at hybridization solution using square wave voltammetry. The nonspecific signal was eliminated using BSA to block the magnetic bead surface making it possible to discriminate the target from mismatched and noncomplementary DNA strands.

The proposed method allows the simultaneous detection of quantum dots modified DNA in a similar way to that reported earlier but with the difference of direct detection onto the surface of the electrode rather than the previous method of dissolving quantum dots. In addition to this, there is a possibility of applying the same detection methodology to an array composed of several electrodes and using the same quantum dot but allowing for the simultaneous and independent detection of each tag connected with the corresponding DNA target.

The technology reported here offers various advantages, such as simplicity, sensitivity and effective discrimination against mismatched and noncomplementary oligomers. Moreover, using a handheld device and screen printed electrodes the detection methodology is compatible with the possibility of rapid analysis even in a doctor's surgery with the minimum waste of reagents and low cost.

5.8 References

[1] Vo-Dinh T., Isola N., Alarie J. P., Landis D., Griffin G.D., Allison S. *"Development of a multiarray biosensor for DNA diagnostics"* **1998** *Instrumentation Science & Technology* 26, 503-514.

[2] Cao Y. W., Jin R., Mirkin C.A. "Nanoparticles with Raman Spectroscopic Fingerprints for DNA and RNA Detection" 2002 Science 297, 1536-1540.

[3] Taton T. A., Lu G., Mirkin C. A. *"Two-Color Labeling of Oligonucleotide Arrays via Size-Selective Scattering of Nanoparticle Probes"* **2001** *J. Am. Chem. Soc.* 123, 5164-5165.

[4] Brinkley M. *"A Brief Survey of Methods for Preparing Protein Conjugates with Dyes, Haptens, and Cross-Linking Reagents"* **1992** *Bioconjugate Chem.* 3, 2-13.

[5] Takalo H., Mukkala V., Mikola H., Liitti P., Hemmilä I. *"Synthesis of Europium(111) Chelates Suitable for Labeling of Bioactive Molecules"* **1994** *Bioconjugate Chem.* 5, 278-282.

[6] Hakala H., Mäki E., Lönnberg H. *"Detection of Oligonucleotide Hybridization on a Single Microparticle by Time-Resolved Fluorometry: Quantitation and Optimization of a Sandwich Type Assay"* **1998** *Bioconjugate Chem.* 9, 316-321.

[7] Prieto H., Utz D., Castro A., Aguirre C., González-Agüero M., Valdés H., Cifuentes N., Defilippi B. G., Zamora P., Zúñiga G., Campos-Vargas R. *"Browning in Annona cherimola Fruit: Role of Polyphenol Oxidase and Characterization of a Coding Sequence of the Enzyme*" **2007** *J. Agric. Food Chem.* 55, 9208.

[8] Pividori M. I., Merkoçi A., Alegret S. *"Graphite-epoxy composites as a new transducing material for electrochemical genosensing"* **2003** *Biosensors and Bioelectronics* 19, 473-484.

[9] Reed M. W., Panyutin I. G., Hamlin D., Lucas D. D., Wilbur D. S. *"Synthesis of 125I-Labeled Oligonucleotides from Tributylstannylbenzamide Conjugates"* **1997** *Bioconjugat Chem.* 8, 238-243.

[10] Kuijpers W. H. A., Bos E. S., Kaspersen F. M., Veeneman G. H., Van Boeckel C. A. A. *"Specific Recognition of Antibody-Oligonucleotide Conjugates by Radiolabeled Antisense Nucleotides: A Novel Approach for Two-step Radioimmunotherapy of Cancer"* **1993** *Bioconjugate Chem.* 4, 94-102.

[11] Wang J., Liu G., Zhu Q. *"Indium Microrod Tags for Electrochemical Detection of DNA Hybridization"* **2003** *Anal. Chem.* 75, 6218-6222.

[12] Castañeda M. T., Merkoçi A., Pumera M., Alegret S. *"Electrochemical genosensors for biomedical applications based on gold nanoparticles"* **2007** *Biosensors and Bioelectronics* 22, 1961-1967.

[13] Merkoçi A., Aldavert M., Marín S., Alegret S. *"New materials for electrochemical sensing V: Nanoparticles for DNA labeling"* 2005 *Trends in Analytical Chemistry* 24, 341-349.

[14] Wang J., Xu D. A., Kawde N., Polsky R. *"Metal Nanoparticle-Based Electrochemical Stripping Potentiometric Detection of DNA Hybridization"* **2001** *Anal. Chem.* 73, 5576-5581.

[15] Niu L., Knoll W. *"Electrochemically Addressable Functionalization and Parallel Readout of a DNA Biosensor Array"* **2007** *Anal. Chem.* 79, 2695-2702.

[16] Merkoçi A., Marín S., Castañeda M. T., Pumera M., Ros J., Alegret S. *"Crystal and electrochemical properties of water dispersed CdS nanocrystals obtained via reverse micelles and arrested precipitation"* **2006** *Nanotechnology* 17, 2553-2559.

[17] Wang J., Liu G., Merkoçi A. *"Electrochemical Coding Technology for Simultaneous Detection of Multiple DNA Targets"* **2003** *J. Am. Chem. Soc.* 125, 3214-3215.

[18] Bangs Laboratories Inc. **1999** *Technote 101* 1-8.

[19] Merkoçi A., Marcolino-Junior L. H., Marín S., Fatibello-Filho O., Alegret S. *"Detection of cadmium sulphide nanoparticles by using screen-printed electrodes and a handheld device"* **2007** *Nanotechnology* 18, 035502 (1-6).

[20] Palchetti I., Majid S., Kicela A., Marraza G., Mascini M. *"Polymer-mercury coated screen printed sensors for electrochemical stripping analysis of heavy metals"* **2003** *Intern. J. Environ. Anal. Chem.* 83, 701-711.

[21] Palchetti I., Laschi S., Mascini M. *"Miniaturised stripping-based carbon modified sensor for in field analysis of heavy metals*" **2005** *Analytica Chimica Acta* 530, 61-67.

[22] Marín S., Merkoçi A. *"Direct electrochemical stripping detection of cystic fibrosis related DNA linked through cadmium sulphide quantum dots"* **2009** *Nanotechnology* 20, 055101(1-6).

[23] Steinitz M. *"Quantitation of the Blocking Effect of Tween 20 and Bovine Serum Albumin in ELISA Microwells"* **2000** *Analytical Biochemistry* 282, 232-238.

[24] Taylor S., Smith S., Windle B., Guiseppi-Elie A. *"Impact of surface chemistry and blocking strategies on DNA microarrays"* **2003** *Nucleic Acid Res.* 31, e 87 (1-19).

[25] Lillis B., Manning M.,. Berney H, Hurley E., Mathewson A., Sheehan M. *"Dual polarisation interferometry characterisation of DNA immobilisation and hybridisation detection on a silanised support"* **2006** *Biosensors and Bioelectronics* 21, 1459-1467.

[26] Zhi Z., Powell A. K., Turnbull J. E. *"Fabrication of Carbohydrate Microarrays on Gold Surfaces: Direct Attachment of Nonderivatized Oligosaccharides to Hydrazide-Modified Self-Assembled Monolayers"* **2006** *Anal. Chem.* 78, 4786-4793.

[27] Morozova T. Y., Morozov V. N. *"Force differentiation in recognition of cross-reactive antigens by magnetic beads"* **2008** *Analytical Biochemistry* 374, 263-271.

[28] De la Escosura-Muñiz A., González-García M. B., Costa-García A. *"DNA hybridization sensor based on aurothiomalate electroactive label on glassy carbon electrodes"* **2007** *Biosensors and Bioelectronics 22, 1048-1054.*